Title

Global change in brain state during spontaneous and forced walk in *Drosophila* is composed of combined activity patterns of different neuron classes

Authors

Sophie Aimon[1†]*, Karen Y. Cheng[1,3], Julijana Gjorgjieva[1,2], Ilona C. Grunwald Kadow[1,3]*

Affiliations

1 Technical University of Munich, School of Life Sciences, 85354 Freising, Germany
2 Max Planck Institute for Brain Research, Computation in Neural Circuits, 60438 Frankfurt, Germany
3 University of Bonn, Medical Faculty (UKB), Institute of Physiology II, 53115 Bonn, Germany
† new address: Max Planck Institute for Biological Cybernetics, 72076 Tübingen, Germany

Sophie Aimon, sophie.aimon@gmail.com
Ilona C. Grunwald Kadow, ilona.grunwald@uni-bonn.de

Abstract

Movement-correlated brain activity has been found across species and brain regions. Here, we used fast whole-brain lightfield imaging in adult *Drosophila* to investigate the relationship between walk and brain-wide neuronal activity. We observed a global change in activity that tightly correlated with spontaneous bouts of walk. While imaging specific sets of excitatory, inhibitory, and neuromodulatory neurons highlighted their joint contribution, spatial heterogeneity in walk- and turning-induced activity allowed parsing unique responses from subregions and sometimes individual candidate neurons. For example, previously uncharacterized serotonergic neurons were inhibited during walk. While activity onset in some areas preceded walk onset exclusively in spontaneously walking animals, spontaneous and forced walk elicited similar activity in most brain regions. These data suggest a major contribution of walk and walk-related sensory or proprioceptive information to global activity of all major neuronal classes.

Introduction

Growing evidence from nematodes to mammals shows that ongoing behavior affects brain activity globally (Kaplan and Zimmer, 2020; Parker et al., 2020). Using a combination of imaging and neuropixel recordings in awake, behaving mice, recent work showed that multiple dimensions of (spontaneous) behavior, including facial or body movements, are represented brainwide, allowing the integration of external or internal stimuli with the current behavioral state (Mace et al., 2018; Musall et al., 2019; Stringer et al., 2019). Brainwide imaging at single cell-resolution of calcium activity in *C. elegans* and larval zebrafish indicated that as in mammals, multiple aspects of behavior and motor activity are represented across the brain including areas thought to be dedicated to primary sensory information processing (Kato et al., 2015; Marques et al., 2020; Vladimirov et al., 2014). Importantly, such brainwide representations of motor states are observed independently of visual or olfactory inputs.

Previous studies suggested a similar phenomenon in insects. For example, in *Drosophila melanogaster*, active flight modulates visual motion processing (Maimon et al., 2010). Similarly, visual horizontal system cells encode quantitative information about the fly's walking behavior independently of visual input (Fujiwara et al., 2017). Beyond primary sensory brain areas, several types of dopaminergic neurons innervating the fly's higher brain center, the mushroom body (MB), show activity highly correlated with bouts of walking (Siju et al., 2020; Zolin et al., 2021). Importantly, wholebrain imaging revealed that behavior-related activity occurred in most brain regions and was independent of visual or olfactory input (Aimon et al., 2019; Mann et al., 2021; Schaffer et al., 2021).

These and other studies provide convincing evidence for brainwide signatures of behavior across species. However, the identity of the specific neuron types and neurotransmitters involved as well as where and how behavior-related information is relayed to the brain remain largely unanswered questions. Complementary to other animal models, the fly provides opportunities to study adult, global brain states associated with behavior at high temporal and spatial resolution due to its small brain size (Aimon and Grunwald Kadow, 2019). In addition, recent electron microscopy (EM) connectomics highlighted that neural networks spread across the entire brain with many pathways unrevealed by traditional single neuron manipulation experiments (Scheffer et al., 2020). Adult *Drosophila* behavior has been studied in detail for many years (Berman et al., 2016; Calhoun et al., 2019; DeAngelis et al., 2019; Geurten et al., 2014; Katsov et al., 2017; Mendes et al., 2014; Mueller et al., 2019; Tao et al., 2019; Tsai and Chou, 2019), but the resulting or underlying brain-wide activity for even just roughly defined behavioral states such as resting or walking remains mostly unknown.

Movement in adult *Drosophila* is thought to be controlled by descending neurons connecting the brain to the ventral nerve cord (VNC), which contains local pattern generators responsible for movement (Bidaye et al., 2020, 2014; Emanuel et al., 2020; von Philipsborn et al., 2011; Zacarias et al., 2018). This top-down view is challenged by other studies suggesting that behavioral control is decentralized with feedback loops involving the brain (Schilling and Cruse, 2020; Sims et al., 2019), or even that many behaviors could be locally controlled by neurons in the VNC without involving the brain (e.g., decapitated grooming (Hirsh, 1997)).

Here, we build on our previous work (Aimon et al., 2019) using fast whole brain imaging during ongoing behavior to more comprehensively unravel the spatial and temporal relationship between movement, brain state, and neural network activity across multiple brain structures and neuronal subtypes. We first look at which regions and neurons expressing different neuromodulators are correlated to walk and turn. We next characterize the timing of activation at behavior transitions between rest and walk and find that walk-related activity in most brain regions starts at or after the transition. Nevertheless, several activity components, e.g., in the posterior slope, show increased activity before walk onset. This is consistent with the hypothesis that brain activity in most regions originates primarily from efferent or proprioceptive feedback, and that few brain regions are directly involved in top-down movement control. To test this hypothesis, we compare global brain activity during forced and spontaneous walk and find them to be similar in most brain regions with select areas preceding exclusively spontaneous walk. Our results suggest that walk elicits a global change in brain state composed of the activity of all brain regions and major neuron types.

Results

Whole brain imaging reveals broad activation during walk

To image whole brain activity during spontaneous behavior, we fixed the fly's head to a holder, opened the posterior head capsule for optical access while leaving the legs free to move (Woller et al., 2021) (Fig. 1A), and used a ball as a walkable surface (Seelig et al., 2010) (Fig. 1A). We expressed GCaMP pan-neuronally and imaged calcium transients in the neuropil as a proxy of neuronal activity in the whole brain using fast light field microscopy (LFM) as described previously (Aimon et al., 2019). Briefly, a multilens array captures an image of the entire brain. These raw images were subsequently processed to reconstruct the brain volume, corrected for movement artifacts, and aligned to a template to identify the brain regions or activity components with behavior-correlated calcium changes (Fig. 1A). This resulted in recordings of neuropil at a typical scale of 5 microns (Aimon et al., 2019). To characterize the relationship between neuropil activity and behavior, we used linear models ($\frac{\Delta F}{F} = f(behavior)$), generating a coefficient and R^2, which have complementary properties. The R^2, representing the fraction of variance explained by the behavior, will decrease with noisier signals (such as those from flies with low GCaMP expression levels). By contrast, the coefficient, representing the intensity and sign of the relationship between activity and behavior, will not have the same dependance to noise (its value will be less precise with higher noise). While LFM allows for very fast imaging frame rates (up to 200 Hz for the whole brain), signal-to-noise ratio decreases with imaging speed. We used a variety of GCaMP sensors (*UAS-GCaMP6s/6m/6f/7s/7f*) and frame rates to capture both high speed and low signal to noise transients. With our data (N=12 flies), we found no significant difference between the R^2 at different frame rates (5 – 98 Hz) for flies expressing GCaMP pan-neuronally (Figure 1-figure supplement 1A), and thus pooled these data for the analysis below regarding global brain state.

We observed a strong increase in neuronal activity across the brain during bouts of walking compared to during resting or grooming (Movie 1, Fig. 1B, C). Accordingly, in experiments where the fly was both walking and resting, the first principal component (PC1) of the whole brain activity data was strongly correlated to walk (Fig. 1D). By aligning whole brain imaging data to the JFR2018 fly brain template using landmark registration, and by averaging

activity in each large anatomically defined region (see Methods), we also found that the global activity of individual brain regions correlated with walk (Fig. 1B and C). Neuronal activation followed movement bouts at high temporal precision (limited by the temporal resolution of the calcium reporter) inconsistent with activity generated by slower general arousal such as wake and sleep (Fig. 1B, C). However, the calcium responses were still a little slower than some of the fast changes in walking, even after convolution of walking with the GCaMP impulse response, which suggests that faster probes could capture finer dynamics in further studies (Fig. 1C). Nevertheless, using walking behavior we were able to explain ~ 20 % of all variances observed in the experiments (R^2 median = 0.194, Fig. 1E). Moreover, the global activity correlated primarily with walk and not with the start or end of walk (Fig. 1F).

We next mapped the differences in activity during different behaviors to smaller brain regions to understand their spatial organization. Strikingly, unlike grooming, which resulted in local activation of ventral brain areas consistent with (Hampel et al., 2015), all brain regions were significantly positively correlated with walking (Fig. 1E and G). To compare walk-related vs. flailing-related neural activity, we also carried out experiments without a walking substrate, so that the fly moves its legs freely in the air. While we still observed an increase in activity during bouts of flailing, the brain was not as consistently globally activated as during walking in our hands (Fig. 1E and G, see also (Schaffer et al, 2021)). We used one linear model to characterize the correlation of brain activity with walking ($\frac{\Delta F}{F} = f(walk)$), generating a coefficient and R^2) and an additional linear model to determine how this correlation depended on the brain region ($R^2 = f(region)$, and $Coefficient = f(region)$). To ensure our results were not biased by heterogeneous expression in the pan-neuronal transgenic driver line, we used two different pan-neuronal lines (*nsyb-Gal4* and *GMR57C10-Gal4*). The linear model (Table 1) showed that there was no significant effect of the Gal4-driver. We found a small but significant effect of the GCaMP version used, likely reflecting the higher signal to noise ratio for GCaMP6s and GCaMP7s, and thus kept using the model to take this effect into account for the rest of the study. Using this model, we quantified the effect of the distinct brain regions on both the normalized coefficient and the R^2 of the regression of regionally averaged activity with the behavior regressor (Fig. 1G, Figure 1-figure supplement 1C-G,J,K). While all brain areas were significantly activated during walk (Fig. 1G, H, Figure 1-figure supplement 1C), only the ventral regions (AMMC, GNG, IPS, IVLP, and SAD; see Table 2 and Ito et al., 2014 for meaning of acronyms) showed significant correlation with grooming (Figure 1-figure supplement 1E,G). Flailing represents an intermediate state with many brain regions activated but less consistently as compared to walk (Fig. 1G, Figure 1-figure supplement 1D,F).

To test whether part of the observed global brain activity could be due to visual input coupled to behavior, e.g., by the fly seeing the optic flow from the ball (Borst et al., 2020; Suver et al., 2016), or unexpectedly fixed reflections from the environment (Creamer et al., 2018), and to use an acute approach complementary to developmentally blind norpA mutant flies (Aimon et al., 2019), we performed the same experiments but covered the fly's eyes with black nail polish to prevent outside light from activating its photoreceptor neurons. With this strongly limited visual input, we still observed a similar, global activity pattern indicating that visual input is at best a minor contributor to our observed wide brain activity (Figure 1-figure supplement 1B). This result also suggests that the global increase in activity during walk is not due to a mismatch between an actual and a predicted visual stimulus.

Given that air-supported balls can show erratic movements due to air turbulences that could cue the fly to change its behavior (DeAngelis et al., 2019; Sen et al., 2019), or impose constraints on the animal's posture, we performed parallel experiments with an unsupported styrofoam ball held by the fly (see Methods). The comparison of the two datasets revealed a significant difference in R^2 for global brain activity (Figure 1-figure supplement 1H), possibly reflecting differences in surface material, or erratic movements of the air supported ball unrelated to the fly's movements confounding the walk regressor. While the R^2 was globally different, distribution across brain regions was similar between the two substrate types (cosine similarity = 0.98, Figure 1-figure supplement 1I). We thus combined the datasets for most analysis below.

Together these data confirm that walking behavior induces a change in global brain activity (Aimon et al., 2019) with most brain regions showing highly temporally correlated activity during bouts of spontaneous walk.

Inhibitory and excitatory neurons, as well as aminergic neurons are recruited during walk

We next asked what major neuron types underly this global change. We expressed GCaMP6 exclusively in GABAergic inhibitory neurons (*GAD1-Gal4; UAS-GCaMP6m*), glutamatergic neurons (*Vglut-gal4;UAS-GCaMP6m*), and excitatory cholinergic neurons (*Cha-gal4;UAS-GCaMP6m or f*). Using the same approach and analysis as described above, we detected an increase in global brain activity for excitatory and inhibitory types of neurons (Fig. 2A, D), closely following individual walk bouts (Fig. 2D). As in pan-neuronal data, we mapped neural activity to brain regions using a linear model of regional average activity as a function of walk (Fig. 2B,C). All regions significantly responded to walk for all genotypes (Fig. 2B,C Figure 2-figure supplement 1), with high similarity in the distribution across regions (cosine similarity: Cha vs Vglut: 0.98, Cha vs Gad: 0.99, Vglut vs Gad: 0.98). (Fig. 2E, Figure 2-figure supplement 1A-C). Together these data show that both inhibitory neurons and excitatory neurons are activated in most brain regions during walk. Future work will be necessary to determine whether such patterns are driven by all neurons expressing a specific neurotransmitter or a subset of neurons in each region.

We also assessed the role of aminergic neurons in walk, specifically focusing on dopaminergic, octopaminergic and serotonergic neurons. While we observed an increase in activity for all neuromodulatory neuron types, serotonergic neurons (*Trh-GAL4;UAS-GCaMP6*) were significantly less globally activated than dopaminergic (*TH, DDC or GMR58E04-GAL4; GCaMP*) and octopaminergic (*Tdc-GAL4; UAS-GCaMP6*) neurons during spontaneous bouts of walk (Fig. 3A and D, Movie 2-4). When we mapped activity to brain regions (Fig. 3B), we found that contrary to the pan-neuronal and broad neurotransmitter line results, maps for individual aminergic lines were distinctly patterned (cosine similarity: TH-DDC vs Trh: 0.69, Tdc vs Trh: 0.69, Tdc vs TH-DDC: 0.93, Fig. 3B,C). Nevertheless, most regions were significantly correlated with walk for all three aminergic types (Fig. 3F and Figure 3-figure supplement 1). Interestingly, the strongest correlation for serotoninergic neurons was negative and mapped to the anterior ventrolateral protocerebrum (AVLP) region (Fig. 3B (blue area), 3E,F).

Unsupervised method extracts functional maps matching anatomical structures

We used global brain activity to generate functional maps of the brain and matched their specific shape and location to anatomical maps of subregions and in some cases to single candidate neuron types (Chiang et al., 2011; Ito et al., 2014) (Table 2). To this end, we extracted

functional components using PCA followed by ICA to spatially separate PCA maps (see Methods) (Fig. 4A, Figure 4-figure supplement 1A-C). We grouped smaller functional components within a larger brain region (e.g., different antennal and protocerebral bridge glomeruli), if the precision of the alignment of the template did not allow for a clear assignment of individual regions. Interestingly, almost all functional components derived from recorded neuronal activity matched anatomical structures without further subdivisions or blurring of anatomical boundaries. This suggested that the activity within brain regions was more homogenous as compared to the activity in neighboring regions. In one exception, our functional data separated a larger region in the lateral neuropil, the AVLP, into smaller subregions (Figure 4-figure supplement 1A,B, orange box) suggesting that subregions of the AVLP had different activity signatures. Of note, some components also identified more than one brain region (i.e., PENP-SLP) indicating a strong functional connection between these regions. For example, among the components correlating with spontaneous walk, the PENP-SLP (periesophageal neuropils and superior lateral protocerebrum) and PENP-CL (periesophageal neuropils and clamp) and WPNb-like (bilateral wedge projection neuron-like (Coates et al., 2020)) components connected ventral neuropils (e.g., GNG) to higher areas or vice versa.

As some of the data used to extract maps were from flies expressing GCaMP specifically in inhibitory, excitatory and neuromodulatory neurons (Fig. 4A), components could be matched to candidate neurons of the same types (Table 2). For dopaminergic neurons, walk-correlated neuronal activity was found, for instance, for components in and around the MB (i.e. γ3-compartment as previously observed; (Cohn et al., 2015; Siju et al., 2020; Zolin et al., 2021)), in the central complex (protocerebral bridge (PB-DA) and ellipsoid body (EB-DA-like (Kong et al., 2010))), but also in ventral neuropil such as the wedge (WE-DA-like (Liu et al., 2017)) and neuropil connecting central regions to the optic lobes (Fig. 4A). For octopamine, one particular component connecting the optic lobe and the periesophageal neuropil (OL-PENP) was strongly correlated with walk, while for serotoninergic neurons the highest R^2 was detected for the AVLP and components within (Fig. 4A). Most components with significant R^2 were positively correlated with walk (Fig. 4B,C), with few exceptions: a specific component within the AVLP mostly detected in the experiment using Trh-Gal4, which we named the AVLPshell due to its shape, was negatively correlated (i.e. inhibited) with walk (Fig. 4B, Figure 4-figure supplement 1A-C).

Turning modulates activity in specific brain regions and potential neurons

Some functional components activated during walk were mirrored by components in the other half of the brain (Fig. 5A). We next asked whether these components had differential activity when turning left or right (Figure 5-figure supplement 1). To quantify turning, we extracted rotational ball movements (left and right) using its optic flow. The components that were differentially activated during turning were reproducibly found across different flies based on similar position and morphology (Fig. 5 A,B). These included the IPS-Y (inverse Y shape in the posterior slope) and LAL-PS (lateral accessory lobe and posterior slope) as previously mentioned in (Aimon et al., 2019). For dopaminergic neurons, the components most correlated with turning had a shape closely matching the dopaminergic neuron type known to project to the LAL and WED areas: neurons of the PPM2 cluster, i.e., PPM2-LW (PPM2-LAL-WED: PPM2-lateral accessory lobe-wedge (Mao and Davis, 2009))(Fig. 5A, right panels; Movie 5).

Brain dynamics at transitions between rest and walk

Thus far, we have analyzed neuronal activity during walk, turn, flail, groom, or rest. Next, we analyzed whole brain activity at the transition between rest and walk. Importantly, different GCaMP versions showed similar onset dynamics under our experimental conditions. For improved temporal resolution, we only included datasets recorded at 30 Hz (with a maximum of +/- 30 ms error between behavior and brain activity) or faster for the entire brain in Fig. 6 (see all individual trials including data recorded at less than 30 Hz in Figure 6-figure supplement 1). We normalized activity at the onset of walk and averaged trials. This analysis revealed a more complex picture of neuronal activity with some components being activated before walk onset (Fig. 6). In particular, we found that regions around the esophagus such as the posterior slope (IPS-Y, SPS) and the dopaminergic M-Omega component (corresponding to two posterior neuropil regions), as well as the WE-DA-like component showed activity that began to increase significantly before walk onset. In addition, several compartments of the MB and regions in the superior neuropil regions (e.g. SMP and SLP) showed trials with some increase preceding walk (Fig. 6, Figure 6-figure supplement 1). The OL-PLP-WED component was also activated significantly before walk. Most components that mapped to the central complex (comprising the protocerebral bridge (PB), fan-shaped body (FB), ellipsoid body (EB), and noduli (NO)) were activated at walk onset but not before (Fig. 6, Figure 6-figure supplement 1A). In particular, the components PB-EB (connecting the PB and the EB), and EB-DA (comprising neurons in the EB and the lateral accessory lobe) became activated once the fly started to walk (Fig. 6, Figure 6-figure supplement 1A), consistent with an increase at walk onset of dopaminergic activity in the EB and LAL (Figure 6-figure supplement 2). Distinct components mapped to the AVLP displayed very different activities related to walk. While anterior and medial components of AVLP increased in activity at walk onset, the AVLP component that resembled the shape of a shell (AVLPshell) displayed a very clear decrease in neuronal activity as soon as the fly started to walk (Fig. 6, Figure 6-figure supplement 1, Figure 1-figure supplement 2). Several other components displayed more variable, and at times too variable dynamics between flies to detect a clear direction (i.e. FBlayv in Figure 6-figure supplement 1).

Forced walk recapitulates most activity while forced turning reveals differences

Our data suggest that walking induces a change of activity in most of the brain. But where does this activity come from? We hypothesized that in the extreme case, activity could originate from two opposite sites. First, the activity could arise initially in superior decision-making areas and then spread across the brain (top-down) or, second, activity is initiated by motor activity and proprioception (bottom-up) and then distributes to higher brain areas. In the latter case, activity would originate in the VNC and move to the basal regions of the brain, i.e., the GNG, via ascending neurons (AN) (Chen et al., 2023; Tsubouchi et al., 2017). While our component analysis of data recorded at 30 Hz identified several putative ‘top-down’ components active before walk onset, most activity was more consistent with a ‘bottom-up’ scenario (Fig. 1, 6 and S6). In some trials, we observed that the activity detected during walk appeared to progress from areas at the base of the brain, i.e. GNG to more dorsal areas (Figure 7-figure supplement 1D, see Movie 6 for an example trial).

We thus asked whether walk-induced activity could be contributed by axon terminals of ANs. To this end, we expressed a synaptically-tethered GCaMP, syt-GCaMP6, under the control of a pan-neuronal driver and imaged whole brain activity during walk (Fig. 7A). Compared to

cellular-GCaMP, syt-GCaMP activity was very strong in the GNG, AMMC and AVLP, regions receiving input from the VNC (Fig. 7A) (Tsubouchi et al., 2017).

Since such axonal activity, or a fraction of it, could also originate from top-down projections, we performed another experiment to compare neural activity from spontaneous, self-induced walk to that of forced walk. We argued that if global neural activation indeed comes from proprioception of walking or related sensory input from the legs, then we should also observe similar global activation when the fly is forced to walk, without having the possibility to decide to do so as in spontaneous walk. To test this idea, we placed a walking substrate controlled by a motor under the fly legs (see Movie 7 and methods). We forced the flies to walk by turning this motor on and off at a speed range between 1.5 to 6 mm/s. Similarly to spontaneous walk (Fig. 7B,D), forced walk induced a change in brain state, with brain wide activity increases across regions (Fig. 7C,D, Movie 7, cosine similarity: 0.993 for R^2 and 0.985 for the coefficients), and across components (Fig. 7E, cosine similarity: 0.87 for R^2 and 0.85 for the coefficients). In addition, flies with a surgically severed connection between brain and VNC walked on the treadmill while showing hardly any activity in the brain (Fig. 7D, Movie 8), consistent with the hypothesis that the brain is not necessary for forced walk and walking signals driving whole brain state change originate in the VNC. Importantly, these observations were not only true for pan-neuronal data but also for dopaminergic, octopaminergic and serotonergic neuronal subsets (Figure 7-figure supplement 1A-C). While we did observe some variation between forced and spontaneous walk in the R^2 for regression of activity traces with walk, confidence intervals were overlapping for all the brain regions (Figure 7-figure supplement 1A-C) and cosine similarity was high (TH-DDC: 0.985 for R^2, 0.978 for coefficients, Tdc: 0.96 for R^2, 0.93 for coefficients, Trh: 0.84 for R^2, 0.62 for coefficients) further suggesting that walking, whether spontaneous or forced, elicits a similar global state change of the brain.

By contrast, forced turns elicited different activity signatures than spontaneous turns (Fig. 7F). We subtracted the R^2 for turn of the contralateral side of the brain from the corresponding value of the ipsilateral side and compared these values for individual components. We found that some components switched sign (i.e., IPS-Y) while other components that showed little lateralization during spontaneous turns showed differences for forced turns (i.e., PPM2-VI, GNGm, FBcol) (Fig. 7F). The PPM2-LW component that showed lateralized activity during spontaneous walk was not lateralized during forced walk.

Given our observation that certain brain regions appear to be activated shortly before walk onset (Fig. 6), we next compared the activity around walk onset in spontaneous and forced walk more carefully (Fig. 7G, Figure 7-figure supplement 1E). Most components detected in both types of experiments appeared very similar as expected based on the analysis above (Fig. 7E). Importantly, components with activity prior to spontaneous walk were either activated after walk had been triggered and/or their activity before walk was significantly different between spontaneous and forced walk (e.g. in areas around the esophagus, and in dorsal areas such as the γ3 compartment of the mushroom body and the superior medial neuropil Fig. 7G, Figure 7-figure supplement 1G).

Discussion

Work over recent years has revealed that locomotion and movement influence neural activity in many brain areas and many organisms (Busse et al., 2017; Kaplan and Zimmer, 2020). Importantly, motor activity modulates not only local activity in specific brain regions, but also the global state of the brain. Which neurons and neurotransmitters and neuromodulators underly this activity, how it spreads, and what it means for the animal are still largely unknown (Kaplan and Zimmer, 2020). Using fast *in vivo* whole brain calcium imaging in head-tethered behaving flies, we show that movement elicits a global change in brain activity during spontaneous as well as forced walk. Walk activates several classes of neurons including excitatory, inhibitory and aminergic, modulatory neurons. Except for serotonergic neurons which are inhibited during walk in some brain areas, we observed neuronal activation across all brain regions at the start of and during walking, but not during grooming or resting. Using PCA/ICA, we mapped neuronal activities to discrete functional components, which we assigned to specific smaller subregions and in some cases even to single candidate neuron types by aligning the activity maps to anatomical data. For instance, we found that maps of dopaminergic activity during turning matched the spatial distribution of specific dopaminergic neurons. Based on the timing of activation and similarity between spontaneous and forced walk induced brain activity, we propose that locomotion activates the brain by sending movement and proprioceptive information to specific regions (e.g. GNG) from where it activates all brain regions and neuron classes.

Advantages and limitation of the method

Our approach, using light field microscopy (Levoy et al., 2006) to image neuropile activity, has several advantages and limitations, which complement other existing methods. First, the light field speed –significantly higher temporal resolution as compared to sequential scanning methods– allowed us to record whole brain activity at the same time as fast behavior such as walk. Even though GCaMP dynamics and limitations in signal-to-noise ratio rarely permitted us to resolve single action potentials, it helped us detect differences in temporal dynamics and pinpoint brain areas potentially involved in triggering spontaneous walk as opposed to merely responding to it. Second, the spatial resolution of light field imaging is inferior to that of confocal or volumetric multiphoton imaging. Although these methods also do not allow resolving single neurites with pan-neuronally expressed sensors, light field could in principle make it even more difficult to detect their activity. On the other hand, capturing the whole volume simultaneously makes it easier to unmix signals as we showed with our PCA/ICA approach, which partially compensates for the lower spatial resolution. Importantly, however, averaging the activity in neuropile regions could hide information, and reflect different activity patterns across single neurons. Third, our data is based on observations without genetic or functional manipulation of neurons or circuits. Excitation and inhibition of single neurons or neuron groups are performed frequently in *Drosophila* thanks to its unique genetic tools. We believe that our data complements previous and future functional studies as imaging or manipulation of individual neurons provides only limited insights into the role and effect of a neuron in the complex and brain-wide dynamic neural network in which they are embedded. In the future, a combination of single neuron manipulation and whole-brain imaging will likely lead to unexpected insights into the relationship between a neuron, global brain state, and a specific behavior. Fourth, we have observed subtler differences between flies that are obvious from individual experiments but difficult to capture quantitatively across a population of animals.

These differences might be resolvable by greatly increasing the number of experiments. Given the technical difficulty of the preparation method, reaching high animal numbers will be extremely challenging but perhaps possible in the future. Finally, together with the now available whole brain EM connectome, our data provides a timely resource for the community of fly neuroscientists interested in linking neuronal activity to behavior.

Using PCA/ICA as an unsupervised approach gave us insights into the organization of whole brain activity underlying brain states. This technique groups voxels that are correlated and thus misses more complex relationships. Furthermore, our method would not detect signals strongly corrupted by noise or different signals with the same spatial patterns. Nevertheless, it allowed us to extract components and compare their shape and localization to known structures. Based on these, we were able to propose a correspondence with specific candidate neurons (Table 2). Although some of these correspondences are very speculative, some components matched precisely the shape of known neurons (e.g. Fig. 5), or reproduced the shape of the only neuron types present in the same region for specific Gal4 lines (e.g. mushroom body compartments for dopamine). Several of these neurons were previously implicated in walking or its modulation. For instance, EB-DA, found in data from dopaminergic neurons, shows among the strongest and most reliable activity during walk. These neurons were shown to be involved in ethanol-induced locomotion (Kong et al., 2010), are involved in sleep regulation (Liang et al., 2016), and were shown more recently to be involved in walk (Fisher et al. 2022), with a timing relative to walk onset consistent with Fig. 6. Dopaminergic components in the MB also recapitulate previous studies (Cohn et al., 2015; Siju et al., 2020). Some correspondences between component and neurons are more speculative, such as IPS-Y and LAL-PS matching the shape of DNb02 and DNb01 neurons (Table 2). These neurons were found to project to the VNC (Namiki et al., 2018), and optogenetic activation of DNb01 induced twitching of the fly's front legs consistent with a role in turning (Cande et al., 2018). The component PB-EB is consistent with neurons in the previously described head direction cells circuit shown to receive movement-related information during navigation (Lu et al., 2022; Lyu et al., 2022; Seelig and Jayaraman, 2015). Among patterns not yet reported, the AVLP-shell might be generated by a serotonergic neuron type of unknown function (e.g. Trh-F-100082 (Chiang et al., 2011)). Additional patterns such as the M-Omega pattern in data sets from dopaminergic cells might correspond to unknown neurons or a combination of tightly coupled neurons. Although most components were correlated with walk, others had an R^2 indistinguishable from zero thus likely representing ongoing activity unrelated to walk (Schaffer et al., 2021) or not captured by a linear model with a binary regressor for walk.

Our data provides an entry point to relate anatomical connectivity to brain states and activity in brain-wide neural networks (Aimon and Grunwald Kadow, 2019). Whole brain connectomics in several small organisms including *Drosophila* has shown that neural networks extend across the entire brain with many pathways not predicted by single neuron or small motif imaging or manipulation of individual neurons (Li et al., 2020; Scheffer et al., 2020; Zheng et al., 2018). Whole-brain imaging, as previously demonstrated in other model animals such as larval zebrafish, is a powerful method for observing these brainwide networks to study their contribution to behavior and ultimately to local activities within specific neurons or brain regions. Whole brain data can be used to build functional connectomes allowing speculations about how information underpinning behavior travels throughout a whole brain. While such data can be generated for other animals including humans, the fly (along with C. elegans and in the near future zebrafish) currently provides the important advantage of being able to combine such

activity maps with highly detailed anatomical maps from light microscopy with cellular resolution and whole brain EM connectomics with synaptic resolution. Ultimately, such data could be used to generate precise models of how recorded neural activity spreads through a brain. For instance, DNs receive input from regions of the brain that are innervated by outputs from higher brain regions such as the MB and central complex (CC) (Hsu and Bhandawat, 2016). DN and AN innervation of the GNG is consistent with an important role of the GNG in motor control and motor feedback integration (Chen et al., 2023; Tsubouchi et al., 2017). How anatomical connectivity relates to activity in widespread neural networks is not clear. Our method and data complement some of the ongoing efforts to fill this significant gap in our knowledge.

Walk elicits differential activities in neuromodulatory neurons

Perhaps not surprisingly, neuromodulatory systems participate and show signatures of ongoing behavior in the adult fly brain (see Fig. 3). Dopaminergic and octopaminergic neurons are broadly activated when the fly walks compared to rest or groom (see Fig. 3 (Aimon et al., 2019; Siju et al., 2020)), while serotonergic neurons show more complex activation patterns and timing with areas such as the AVLP being inhibited during walk (see Fig. 3 and S6).

Our data is consistent with data from other species and suggest that relationships between the activity of neuromodulatory neurons and locomotion are broadly conserved across species. Dopaminergic neurons are activated during locomotion in mammals, with some neurons reporting ongoing behavior (Howe and Dombeck, 2016) while others show activity increase preceding behavior onset (Coddington and Dudman, 2019). We find that although the majority of fly dopamine neurons are activated during ongoing behavior, some dopaminergic neurons are activated hundreds of milliseconds before the onset of walk in some trials (e.g. WE-DA, M-Omega pattern and γ1-3 compartments of the mushroom body in some trials, Fig. 6). Norepinephrine/octopamine is also a key neuromodulatory system involved in arousal in a variety of species (Berridge, 2008), with reports of an increase in activity of these neurons during locomotion in mammals (Gray et al., 2021; Kaufman et al., 2020; Xiang et al., 2019). In vertebrates, basal ganglia and brainstem aminergic neurons affect the cortico-basal ganglia-thalamic loops. A disruption of these loops can result in a loss of motor control (Vicente et al., 2020). Such loops likely exist in insects, too. For example, several octopaminergic neurons in the SEZ connect lower brain regions to the MB (Busch et al., 2009).. Interestingly, serotonergic neurons show mixed roles in the control of motor behavior in different vertebrate species (Dayan and Huys, 2015; Flaive et al., 2020; Vitrac and Benoit-Marand, 2017), as well as in insect, where it regulates various types of motor behaviors including feeding, aggression and larval locomotion (e.g., (Aonuma, 2020; Helfrich-Förster, 2018; Ngai et al., 2019; Schoofs et al., 2018, 2014)). In particular, serotonin has been implicated in behavioral inhibition (e.g. patience (Doya et al., 2021)) and as an opposing system to dopamine (Dayan, 2012). This is consistent with our observation that serotonergic neurons in some brain regions such as the AVLP are inhibited during walk. The AVLP receives input from ascending neurons from the VNC conveying somatosensory information from the legs (Tsubouchi et al., 2017). Furthermore, calcium imaging revealed a spatial map for the AVLP and WED with neurons responding primarily to movement of fore-, mid- or hindlegs (Chen et al., 2023; Tsubouchi et al., 2017), and the AVLP contains several descending neurons projecting toward the VNC (Namiki et al., 2022, 2018). Serotonin inhibition in the AVLP could thus also be affecting a sensorimotor loop. However, we also found some serotoninergic neurons activated during walk, suggesting that, as for mammals, serotonin

neurons are strongly heterogeneous (Dayan and Huys, 2015). Our study thus suggests that key aspects of activity of neuromodulatory neurons during locomotion are conserved between mammals and insects despite their evolutionary distance.

Origin of broad activation during ongoing behavior

Our results are most consistent with a model where proprioceptive, walking and leg sensory information are sent from the VNC into the GNG at the base of the fly's brain. Then, how is walk-related information relayed to the brain? Tuthill and colleagues recently identified some of the presumably many neural substrates in the VNC that receive, process and relay proprioceptive sensory information from the legs to the CNS (Agrawal et al., 2020; Mamiya et al., 2018). Their findings provide strong support for an important role of proprioception in movement and locomotion control in the adult fly. This information is transmitted by ascending neurons from the VNC to the central brain. Less was known regarding the type, connectivity and function of the likely dozens or more ascending neurons (AN) in *Drosophila*, but screening approaches and advanced imaging techniques have shed light on some of them (Allen et al., 2020; Sen et al., 2019). In particular, a very recent study analyzed behavior-related activity of dozens of ANs labeled with specific Gal4 lines (Chen et al., 2023) and came to the complementary conclusion that ANs innervating regions such as the AVLP and GNG are poised to convey behavioral state and self-motion to several brain regions.

While grooming or forced walk on a treadmill does not require an active brain, lesions of the neck connectives as we have carried out dramatically decrease spontaneous walking in locusts (Kien, 1990a, 1990b), indicating that at least initiation of walk can be dependent on the brain. On the other hand, a cat with a severed spinal cord, like our fly with a severed VNC, maintains a highly coordinated walk pattern when forced to walk on a treadmill (Afelt, 1974). Thus, coordinated walk appears to mainly depend on central pattern generators in the spinal cord or VNC and is largely independent of brain input. Surprisingly, whole brain activity induced by spontaneous walking was similar to the activity we observed by forcing the animal to walk on a rotating rod (Fig. 7). This result and our finding that the activity induced by walk in the GNG stems from axons are consistent with the interpretation that walk itself and not top-down motor control is responsible for the majority of activity observed in actively moving animals' brains. In the future, imaging whole brain activity while activating or silencing specific leg proprioceptive neurons or other ANswould confirm these findings and help dissect their contributions.

Once the walk signals reach the brain, neurons connecting lower to higher areas (e.g. neurons underlying the PENP-CL, GNG-SLP and WPNb components, as well as octopaminergic neurons) could relay this information to higher areas. Interestingly, our data that inhibitory neurons are also broadly activated is inconsistent with the idea that broad brain activation arises due to a global disinhibition during periods of walking (Benjamin, 2010), although additional experiments will be necessary to ensure that activity in individual regions is not dominated by a small subset of activated neurons in a sea of inhibited neurons.

Importantly, however, we identified several brain components and small subregions, for instance in the posterior slope, that were activated hundreds of milliseconds before the fly started to walk (see Fig. 7). This activity was delayed in forced walk and started only when the fly had started to move. This suggests a potential role of these areas in initiating walk. Activity before walk onset could also be due to preparatory movements that were not detected as walk (Ache et al., 2019), or represent the activity of neurons downstream of neurons responsible for triggering walk.

Role of broad activation during ongoing behavior

One important concept to explain the role of behavioral state-dependent neural modulation is "active sensation" (Busse et al., 2017). Essentially, ongoing movement can shape how neurons respond to visual, somatosensory and possibly other sensory stimuli (Chapman et al., 2018; Cruz et al., 2021; Fenk et al., 2021; Henschke et al., 2021; Wolpert et al., 2011). For example, extracellular recordings from mouse V1 neurons walking on a ball showed that evoked visual responses differ in neurons of moving animals and those of still animals (Dadarlat and Stryker, 2017). Similarly, fly visual neurons respond more strongly to stimuli during walk or flight (Chiappe et al., 2010; Maimon et al., 2010; Suver et al., 2012). Our data indicate that the increase whole brain activity is elicited at walk onset and maintained afterwards (Fig. 6). Since the overall increase in brain activity is not larger during forced walk as compared to spontaneous walk, our data also suggest that global brain activity does not generally represent a mismatch, or error signal, between actual and predicted proprioceptive feedback during walk. These observations support the conclusion that movement specific information reach the brain and modulate brain activity widely. Such information could serve multiple purposes from uncoupling of sensory-to-motor information, i.e. own movement *vs.* movement of environment, to learning of complex movements (Lu et al., 2022).

Conclusions

We provide an overview of global brain activity during simple behaviors in *Drosophila*. As for other animals, *Drosophila* brain activity is globally correlated with locomotion leading to global change in brain state. However, our results challenge the assumption that most of the activity is related to decision-making, top-down motor control, or prediction error detection from sensory feedback and instead suggest that walk itself and somatosensory bottom-up stimuli are largely responsible. By using a combination of pan-neuronal and specific neuron subtype imaging, we shed light on the nature of neurons and their location in the brain that respond so strongly to behavior. Altogether, our data provide a novel resource for generating new hypotheses regarding the brain-behavior-loop and for dissecting the neural circuits and computations underpinning it.

Materials and Methods

Key resources table

Experimental models: Organisms/strains		
UAS-GCaMP6s	Bloomington Drosophila Stock Center	BDSC_42749
UAS-GCaMP6m	Bloomington Drosophila Stock Center	BDSC_42750

UAS-GCaMP7s	Bloomington Drosophila Stock Center	BDSC_79032
UAS-GCaMP6f	Bloomington Drosophila Stock Center	BDSC_42747
UAS-GCaMP7f	Bloomington Drosophila Stock Center	BDSC_79031
UAS-syt-GCaMP6s	Vanessa Ruta	N/A
GMR58E04-Gal4	Bloomington Drosophila Stock Center	BDSC_41347
Th-Gal4	Bloomington Drosophila Stock Center	BDSC_8848
Tdc2-Gal4	Bloomington Drosophila Stock Center	BDSC_9313
Trh-Gal4	Bloomington Drosophila Stock Center	BDSC_38388
Ddc-Gal4	Bloomington Drosophila Stock Center	BDSC_7009
TH, 58E02-Gal4	Siju et al.	N/A
TH, DDC-Gal4	This paper	N/A
Vglut-Gal4	Bloomington Drosophila Stock Center	BDSC_24635
Cha-Gal4	Bloomington Drosophila Stock Center	BDSC_6798
Nsyb-Gal4	Bloomington Drosophila Stock Center	BDSC_51635
GMR57C10-Gal4	Bloomington Drosophila Stock Center	BDSC_39171
Gad1-Gal4	Bloomington Drosophila Stock Center	BDSC_51630
Software and algorithms		
Python 3	Python Software Foundation	https://www.python.org

ImageJ	Schneider et al., 2012	https://imagej.nih.gov/ij/
Fiji	MPI-CBG	https://fiji.sc/
MATLAB	MATLAB	mathworks.com
Analysis code	GitHub	https://github.com/sophie63/Aimon2022

Fly preparation for imaging

We used one to four days old female flies raised at 25 °C. Most flies were starved 24 or 48h with a water only environment, and we clipped their wings at least one day in advance. Experiments were performed in the evening peak of circadian activity (ZT0 or ZT11) and we heated the room to ~28 °C during the experiment. In total, we recorded brain activity and behavior from 84 adult female flies.

We prepared the flies as described in detail in (Woller et al., 2021). Briefly, we fixed a fly to a custom-designed 3D printed holder, so as to allow access to the whole posterior side of the head while the legs were free to move. We added saline (103 mM NaCl, 3 mM KCl, 5 mM TES, 8 mM trehalose 2 H_2O, 10 mM glucose, 26 mM $NaHCO_3$, 1 mM NaH_2PO_4, 2.5 mM $CaCl_2 \cdot 2\ H_2O$, 4 mM $MgCl_2 \cdot 6\ H_2O$) and dissected the cuticle, muscles, and air sacks at the back of the head to expose the brain. Note that the intact esophagus partially obscured the subesophageal zone, decreasing the intensity and resolution in this area. The signal was nevertheless sufficient to identify several subregions with the component analysis (see below).

Walk substrates

For studying spontaneous walk, we used two types of small balls. One was an air-supported ball as previously described (Sayin et al., 2019). As we wanted to make sure the walk was initiated by the fly rather than erratic movement of the ball, we also used small styrofoam balls that were held by the fly. The speed of the rotational flow, which is proportional to the degree of turning, was 0.4 - 2 radian/s.

As treadmill for studying forced walk and turn, we used small motors (DC 6V gear motor with long M3 x 55mm lead screw thread output shaft speed reducer Walfront Store, www.amazon.de), covered with self-curing rubber (from Sugru) to provide a smoother surface. The speed for forced walk was between 1.5 and 6 mm/s. The rotation speed for forced turn was 0.3 to 2 rad/s.

In vivo light field imaging

Fast volumetric imaging was performed using light field imaging – in which a microlens array separates rays from different angles to give information on depth – and was carried out as previously described in detail by (Aimon et al., 2019). A few datasets were previously published in Aimon et al. (Aimon et al., 2019) and source data (http://dx.doi.org/10.6080/K01J97ZN), with a microscope equipped with a 20x NA1.0 objective. Most data were obtained with a light field microscope constituted of a Thorlabs Cerna system with a Leica HC FLUOTAR L 25x/0.95 objective and an MLA-S125-f12 microlens array (Viavi). The microlens array was placed on the

image plane, while the camera imaged the microlens array through 50 mm f/1.4 NIKKOR-S Nikon relay lenses. The light field images were recorded with a scientific CMOS camera (Hamamatsu ORCA-Flash 4.0). The volumes were reconstructed offline, using a python program developed by (Broxton et al., 2013) and available on github: https://github.com/sophie63/FlyLFM.

Given that the maximum recording speed depended on the expression of the Gal4-line, the UAS-reporter, and each individual fly preparation, i.e. the limiting factor was the signal-to-noise ratio for lines with low expression, we started recording at 2 or 5 Hz for the first experiment. If the quality of recording suggested that higher speeds were possible, we increased recording speed to a maximum of 98 Hz. If the viability of the fly allowed for it, we recorded experiments on air-supported and Styrofoam balls in the same fly.

Gal4	**UAS - GCaMP**	**# of flies, spontaneous Walk (flail, groom)**	**flailing**	**grooming**	**frame rate in Hz (# of experiments)**	**Walking Substrate (# of experiments)**	**# flies of flies forced walk**
total	**total**	**58**	9	6	98(8), 50(21), 20(11), 10(9), 5(30), 2(2)	Air-supported ball (33), styrofoam ball (54)	**26**
Nsyb	7f	1	1	1	50(1)	Air-supported ball	
	7s	1	1		5(1)	styrofoam ball	1
	6m	6	5	2	50(8), 20(5), 10(3), 5(4)	Air-supported ball (16), styrofoam ball (5)	3
	6f	3		1	98(2), 50(1)	Air-supported ball (2), styrofoam ball (1)	
	6s	1	1		50(1)	styrofoam ball(1)	2
	total	12	8	4	98(2), 50(11), 20(5), 10(3), 5(5)	Air-supported ball (19), styrofoam ball (8)	6
R57C10	7s	1		1	98(2)	styrofoam ball(2)	
	6s	3	1	1	50(1), 5(1), 20(1)	styrofoam ball(3)	3
	total	4	1	2	98(2), 50(1), 20(1), 5(1)	Air-supported ball (0), styrofoam ball (5)	3
Cha	6m	4			5(4)	styrofoam ball (4)	
	6f	1			98(1)	Air-supported ball (1)	
	total	5			98(1), 5(4)	Air-supported ball	0

						(1), styrofoam ball (4)	
Vglut	6m	5			20(2), 10(3), 5(4)	Air-supported ball (3), styrofoam ball (6)	
	total	5			20(2), 10(3), 5(4)	Air-supported ball (3), styrofoam ball (6)	0
Gad	6m	5			98(2), 20(1), 5(5), 2(1)	styrofoam ball (9)	
	total	5			98(2), 20(1), 5(5), 2(1)	Air-supported ball (0), styrofoam ball (9)	0
TH/DDC	6m	5			50(2), 5(1), 10(1)	Air supported ball (3), styrofoam ball (2)	4
	6f	6			50(5), 98(1)	Air supported ball (2), styrofoam ball (3)	1
	total	11			98(1), 50(7), 10(1), 5(1)	Air-supported ball (5), styrofoam ball (5)	5
Trh	6m	3			50(3), 5(3)	Air supported ball (1), styrofoam ball (6)	
	6f	3			10(2)	Air supported ball (2), styrofoam ball (1)	
	6s	3			5(3)	styrofoam ball(4)	6
	total	9			50(3), 10(2), 5(6)	Air-supported ball (3), styrofoam ball (11)	6
Tdc2	6s	7			20(2), 5(4), 2(1)	Air supported ball (2), styrofoam ball (6)	6
	total	7			20(2), 5(4), 2(1)	Air-supported ball (2), styrofoam ball (6)	6

Behavior recording and scoring

We imaged the fly and substrate movements using infra-red illumination and two small cameras FFMV-03M2M from Point Grey triggered by the fluorescence recording camera to ensure time alignment between fluorescence and behavior.

Walking, flailing, and grooming were obtained by measuring the optic flow from the Movies of the ball or by analyzing the movement of the fly's legs using the "optic flow" plugin in FIJI. For turning or rotational speed (rad/s), the sum of left or right optic flows was not binarized. For

regression of neuronal time series with behavior, all behavioral time series were then convolved with the single spike response of the GCaMP version used for the experiment and subjected to the same deltaF/F procedure as the fluorescence time series (see below).

Pre-processing

Reconstructed volumetric fluorescence data was pre-processed by first correcting for movement using 3Dvolreg from AFNI (https://github.com/afni/afni). In Matlab, we then calculated the deltaF/F for each voxel by subtracting and dividing by the signal averaged for 4000 time points. We finally decreased noise with a Kalman filter (from https://www.mathworks.com/matlabcentral/fileexchange/26334-kalman-filter-for-noisy-movies) with a gain of 0.5.

We generated summary movies by maximum projecting the ΔF/F volumes and combining these to the behavior.

Alignment to template

We aligned the functional data to the anatomical template JRC2018 (https://www.janelia.org/open-science/jrc-2018-brain-templates) using the landmarks registration plugin with ImageJ (as described in http://imagej.net/Name_Landmarks_and_Register), with the landmarks found in https://github.com/sophie63/Aimon2022/blob/main/Registration/SmallJRC2018Template.points. allowed finding the anatomically defined regions covered by the functional regions (see Table 2) and find candidate neurons using Flycircuit (http://www.flycircuit.tw/) or Virtual Fly Brain https://v2.virtualflybrain.org data bases.

STATISTICAL ANALYSIS

Sample size determination: As we expected large effects (Aimon et al. 2019), we chose to focus on those and planned for a minimum of 5 flies per condition satisfying quality criteria. Low quality flies were flies in which no spontaneous activity was detected, or which front legs were not touching the substrate for walking experiments.

Statistics were performed in python with code freely available on https://github.com/sophie63/Aimon2022. To compare fluorescence time series (normalized by the absolute maximum value per fly) and behavioral time series, we used a simple regression model: $\frac{\Delta F}{F} = f(behavior\ regressor)$, solved with the ordinary least square fit function of the python statsmodels package. For each time series (either regional averaged intensity or the PCA/ICA component), this provided a fraction of variance explained by the behavior (R^2), and the sign and strength of the correlation (coefficient). We compared these values with pair-wise tests using two-sided Mann-Whitney non-parametric tests with a Bonferroni multiple comparison correction. We used a more complex linear model to evaluate the effect of variables of interest (behavior, brain region, neural type) while explaining away confounds (GCaMP version, exact pan neuronal Gal4): R^2 ~ Behavior+RegionNames+Gal4+UAS and Coef ~ Behavior+RegionNames+Gal4+UAS. We then plotted the coefficients + intercept, and 95% interval of coefficient + 95% interval of the intercept to compare the effect of the variables to zero. We also compared these values with zero with a t-test and corrected for multiple comparison using the Benjamini-Hochberg method. For detection of activation before walk, we

integrated activity from -0.5 s before to walk onset minus level at -0.5 s before onset. We used a Wilcoxon test to compare these values to zero and corrected for multiple comparison using the Benjamini-Hochberg method. Flies were recorded over prolonged periods of times at different imaging speeds and during different behaviors. See table above for details on number of individual flies and types of experiments per fly.

PCA/ICA

To obtain functional maps of the fly brain, we performed PCA and ICA as described previously (Aimon et al., 2019; Beckmann and Smith, 2004). Briefly, SVD (singular value decomposition) was used a first time to find the level of noise and normalize voxels by their noise variance. SVD was performed a second time on this normalized data resulting in maps and time series for principal components. The principal component maps were unmixed using ICA to obtain localized regions. The same matrix was used to unmix the time series.

References

Ache JM, Namiki S, Lee A, Branson K, Card GM. 2019. State-dependent decoupling of sensory and motor circuits underlies behavioral flexibility in Drosophila. *Nat Neurosci* **22**:1132–1139. doi:10.1038/s41593-019-0413-4

Afelt Z. 1974. Functional significance of ventral descending tracts of the spinal cord in the cat. *Acta Neurobiol Exp (Wars)* **34**:393–407.

Agrawal S, Dickinson ES, Sustar A, Gurung P, Shepherd D, Truman JW, Tuthill JC. 2020. Central processing of leg proprioception in Drosophila. *Elife* **9**. doi:10.7554/eLife.60299

Aimon S, Grunwald Kadow IC. 2019. Studying complex brain dynamics using Drosophila. *J Neurogenet* 1–7. doi:10.1080/01677063.2019.1706092

Aimon S, Katsuki T, Jia T, Grosenick L, Broxton M, Deisseroth K, Sejnowski TJ, Greenspan RJ. 2019. Fast near-whole-brain imaging in adult Drosophila during responses to stimuli and behavior. *PLoS Biol* **17**:e2006732. doi:10.1371/journal.pbio.2006732

Allen AM, Neville MC, Birtles S, Croset V, Treiber CD, Waddell S, Goodwin SF. 2020. A single-cell transcriptomic atlas of the adult Drosophila ventral nerve cord. *Elife* **9**. doi:10.7554/eLife.54074

Aonuma H. 2020. Serotonergic control in initiating defensive responses to unexpected tactile stimuli in the trap-jaw ant Odontomachus kuroiwae. *J Exp Biol* **223**. doi:10.1242/jeb.228874

Yoshinori Aso, Divya Sitaraman, Toshiharu Ichinose, Karla R Kaun, Katrin Vogt, Ghislain Belliart-Guérin, Pierre-Yves Plaçais, Alice A Robie, Nobuhiro Yamagata, Christopher Schnaitmann, William J Rowell, Rebecca M Johnston, Teri-T B Ngo, Nan Chen, Wyatt Korff, Michael N Nitabach, Ulrike Heberlein, Thomas Preat, Kristin M Branson, Hiromu Tanimoto, Gerald M Rubin (2014) Mushroom body output neurons encode valence and guide memory-based action selection in Drosophila eLife 3:e04580

Beckmann CF, Smith SM. 2004. Probabilistic independent component analysis for functional magnetic resonance imaging. *IEEE Trans Med Imaging* **23**:137–52. doi:10.1109/TMI.2003.822821

Benjamin. 2010. What roles do tonic inhibition and disinhibition play in the control of motor programs? *Front Behav Neurosci*. doi:10.3389/fnbeh.2010.00030

Berman GJ, Bialek W, Shaevitz JW. 2016. Predictability and hierarchy in Drosophila behavior. *Proc Natl Acad Sci U S A* **113**:11943–11948. doi:10.1073/pnas.1607601113

Berridge CW. 2008. Noradrenergic modulation of arousal. *Brain Res Rev* **58**:1–17. doi:10.1016/j.brainresrev.2007.10.013

Berry JA, Cervantes-Sandoval I, Chakraborty M, Davis RL. 2015. Sleep Facilitates Memory by Blocking Dopamine Neuron-Mediated Forgetting. *Cell* **161**:1656–1667. doi:10.1016/j.cell.2015.05.027

Bidaye SS, Laturney M, Chang AK, Liu Y, Bockemuhl T, Buschges A, Scott K. 2020. Two Brain Pathways Initiate Distinct Forward Walking Programs in Drosophila. *Neuron* **108**:469-485 e8. doi:10.1016/j.neuron.2020.07.032

Bidaye SS, Machacek C, Wu Y, Dickson BJ. 2014. Neuronal control of Drosophila walking direction. *Science (1979)* **344**:97–101. doi:10.1126/science.1249964

Borst A, Haag J, Mauss AS. 2020. How fly neurons compute the direction of visual motion. *J Comp Physiol A Neuroethol Sens Neural Behav Physiol* **206**:109–124. doi:10.1007/s00359-019-01375-9

Broxton M, Grosenick L, Yang S, Cohen N, Andalman A, Deisseroth K, Levoy M. 2013. Wave optics theory and 3-D deconvolution for the light field microscope. *Opt Express* **21**:25418–25439. doi:10.1364/OE.21.025418

Busch S, Selcho M, Ito K, Tanimoto H. 2009. A map of octopaminergic neurons in the Drosophila brain. *J Comp Neurol* **513**:643–667. doi:10.1002/cne.21966

Busse L, Cardin JA, Chiappe ME, Halassa MM, McGinley MJ, Yamashita T, Saleem AB. 2017. Sensation during Active Behaviors. *J Neurosci* **37**:10826–10834. doi:10.1523/JNEUROSCI.1828-17.2017

Calhoun AJ, Pillow JW, Murthy M. 2019. Unsupervised identification of the internal states that shape natural behavior. *Nat Neurosci*. doi:10.1038/s41593-019-0533-x

Cande J, Namiki S, Qiu J, Korff W, Card GM, Shaevitz JW, Stern DL, Berman GJ. 2018. Optogenetic dissection of descending behavioral control in Drosophila. *Elife* **7**. doi:10.7554/eLife.34275

Chapman PD, Burkland R, Bradley SP, Houot B, Bullman V, Dacks AM, Daly KC. 2018. Flight motor networks modulate primary olfactory processing in the moth Manduca sexta. *Proc Natl Acad Sci U S A* **115**:5588–5593. doi:10.1073/pnas.1722379115

Chen, CL., Aymanns, F., Minegishi, R. *et al*. Ascending neurons convey behavioral state to integrative sensory and action selection brain regions. *Nat Neurosci* (2023). https://doi.org/10.1038/s41593-023-01281-z

Chen CL, Hermans L, Viswanathan MC, Fortun D, Aymanns F, Unser M, Cammarato A, Dickinson MH, Ramdya P. 2018. Imaging neural activity in the ventral nerve cord of behaving adult Drosophila. *Nat Commun* **9**:4390. doi:10.1038/s41467-018-06857-z

Chiang AS, Lin CY, Chuang CC, Chang HM, Hsieh CH, Yeh CW, Shih CT, Wu JJ, Wang GT, Chen YC, Wu CC, Chen GY, Ching YT, Lee PC, Lin CY, Lin HH, Wu CC, Hsu HW, Huang YA, Chen JY, Chiang HJ, Lu CF, Ni RF, Yeh CY, Hwang JK. 2011. Three-dimensional reconstruction of brain-wide wiring networks in Drosophila at single-cell resolution. *Curr Biol* **21**:1–11. doi:10.1016/j.cub.2010.11.056

Chiappe ME, Seelig JD, Reiser MB, Jayaraman V. 2010. Walking modulates speed sensitivity in Drosophila motion vision. *Curr Biol* **20**:1470–1475. doi:10.1016/j.cub.2010.06.072

Coates KE, Calle-Schuler SA, Helmick LM, Knotts VL, Martik BN, Salman F, Warner LT, Valla S v, Bock DD, Dacks AM. 2020. The Wiring Logic of an Identified Serotonergic Neuron That Spans Sensory Networks. *J Neurosci* **40**:6309–6327. doi:10.1523/JNEUROSCI.0552-20.2020

Coddington LT, Dudman JT. 2019. Learning from Action: Reconsidering Movement Signaling in Midbrain Dopamine Neuron Activity. *Neuron* **104**:63–77. doi:10.1016/j.neuron.2019.08.036

Cohn R, Morantte I, Ruta V. 2015. Coordinated and Compartmentalized Neuromodulation Shapes Sensory Processing in Drosophila. *Cell* **163**:1742–1755. doi:10.1016/j.cell.2015.11.019

Creamer MS, Mano O, Clark DA. 2018. Visual Control of Walking Speed in Drosophila. *Neuron* **100**:1460-1473 e6. doi:10.1016/j.neuron.2018.10.028

Cruz TL, Perez SM, Chiappe ME. 2021. Fast tuning of posture control by visual feedback underlies gaze stabilization in walking Drosophila. *Curr Biol*. doi:10.1016/j.cub.2021.08.041

Dadarlat MC, Stryker MP. 2017. Locomotion enhances neural encoding of visual stimuli in mouse V1. *Journal of Neuroscience* **37**. doi:10.1523/JNEUROSCI.2728-16.2017

Dayan P. 2012. Twenty-Five Lessons from Computational Neuromodulation. *Neuron* **76**:240–256. doi:10.1016/j.neuron.2012.09.027

Dayan P, Huys Q. 2015. Serotonin's many meanings elude simple theories. *Elife* **4**. doi:10.7554/eLife.07390

DeAngelis BD, Zavatone-Veth JA, Clark DA. 2019. The manifold structure of limb coordination in walking Drosophila. *Elife* **8**. doi:10.7554/eLife.46409

Donlea JM, Pimentel D, Miesenbock G. 2014. Neuronal Machinery of Sleep Homeostasis in Drosophila. *Neuron* **81**:1442. doi:10.1016/j.neuron.2014.03.008

Doya K, Miyazaki KW, Miyazaki K. 2021. Serotonergic modulation of cognitive computations. *Curr Opin Behav Sci*. doi:10.1016/j.cobeha.2021.02.003

Emanuel S, Kaiser M, Pflueger HJ, Libersat F. 2020. On the Role of the Head Ganglia in Posture and Walking in Insects. *Front Physiol* **11**:135. doi:10.3389/fphys.2020.00135

Fenk LM, Kim AJ, Maimon G. 2021. Suppression of motion vision during course-changing, but not course-stabilizing, navigational turns. *Curr Biol*. doi:10.1016/j.cub.2021.09.068

Fisher, Y. E., Marquis, M., D'Alessandro, I., & Wilson, R. I. (2022). Dopamine promotes head direction plasticity during orienting movements. *Nature 2022 612:7939*, *612*(7939), 316–322. https://doi.org/10.1038/s41586-022-05485-4

Flaive A, Fougere M, van der Zouwen CI, Ryczko D. 2020. Serotonergic Modulation of Locomotor Activity From Basal Vertebrates to Mammals. *Front Neural Circuits* **14**:590299. doi:10.3389/fncir.2020.590299

Fujiwara T, Cruz TL, Bohnslav JP, Chiappe ME. 2017. A faithful internal representation of walking movements in the Drosophila visual system. *Nat Neurosci* **20**:72–81. doi:10.1038/nn.4435

Geurten BR, Jahde P, Corthals K, Gopfert MC. 2014. Saccadic body turns in walking Drosophila. *Front Behav Neurosci* **8**:365. doi:10.3389/fnbeh.2014.00365

Gray SR, Ye L, Ye JY, Paukert M. 2021. Noradrenergic terminal short-term potentiation enables modality-selective integration of sensory input and vigilance state. *Sci Adv* **7**:eabk1378. doi:10.1126/sciadv.abk1378

Hampel S, Franconville R, Simpson JH, Seeds AM. 2015. A neural command circuit for grooming movement control. *Elife* **4**:e08758. doi:10.7554/eLife.08758

Helfrich-Förster C. 2018. Sleep in Insects. *Annu Rev Entomol* **63**:69–86. doi:10.1146/annurev-ento-020117-043201

Henschke JU, Price AT, Pakan JMP. 2021. Enhanced modulation of cell-type specific neuronal responses in mouse dorsal auditory field during locomotion. *Cell Calcium* **96**:102390. doi:10.1016/j.ceca.2021.102390

Hirsh J. 1997. Decapitated Drosophila: A Novel System for the Study of Biogenic Amines. *Adv Pharmacol* **42**. doi:10.1016/S1054-3589(08)60903-5

Howard CE, Chen CL, Tabachnik T, Hormigo R, Ramdya P, Mann RS. 2019. Serotonergic Modulation of Walking in Drosophila. *Curr Biol* **29**:4218-4230 e8. doi:10.1016/j.cub.2019.10.042

Howe MW, Dombeck DA. 2016. Rapid signalling in distinct dopaminergic axons during locomotion and reward. *Nature* **535**. doi:10.1038/nature18942

Hsu CT, Bhandawat V. 2016. Organization of descending neurons in Drosophila melanogaster. *Sci Rep* **6**:20259. doi:10.1038/srep20259

Ito K, Shinomiya K, Ito M, Armstrong JD, Boyan G, Hartenstein V, Harzsch S, Heisenberg M, Homberg U, Jenett A, Keshishian H, Restifo LL, R??ssler W, Simpson JH, Strausfeld NJ, Strauss R, Vosshall LB. 2014. A systematic nomenclature for the insect brain. *Neuron* **81**:755–765. doi:10.1016/j.neuron.2013.12.017

Kaplan HS, Zimmer M. 2020. Brain-wide representations of ongoing behavior: a universal principle? *Curr Opin Neurobiol* **64**:60–69. doi:10.1016/j.conb.2020.02.008

Kato S, Kaplan HS, Schrödel T, Skora S, Lindsay TH, Yemini E, Lockery S, Zimmer M. 2015. Global Brain Dynamics Embed the Motor Command Sequence of Caenorhabditis elegans. *Cell* **163**. doi:10.1016/j.cell.2015.09.034

Katsov AY, Freifeld L, Horowitz M, Kuehn S, Clandinin TR. 2017. Dynamic structure of locomotor behavior in walking fruit flies. *Elife* **6**. doi:10.7554/eLife.26410

Kaufman AM, Geiller T, Losonczy A. 2020. A Role for the Locus Coeruleus in Hippocampal CA1 Place Cell Reorganization during Spatial Reward Learning. *Neuron* **105**:1018-1026 e4. doi:10.1016/j.neuron.2019.12.029

Kien J. 1990a. Neuronal activity during spontaneous walking--I. Starting and stopping. *Comp Biochem Physiol A Comp Physiol* **95**:607–621. doi:10.1016/0300-9629(90)90747-g

Kien J. 1990b. Neuronal activity during spontaneous walking--II. Correlation with stepping. *Comp Biochem Physiol A Comp Physiol* **95**:623–638. doi:10.1016/0300-9629(90)90748-h

Kong EC, Woo K, Li H, Lebestky T, Mayer N, Sniffen MR, Heberlein U, Bainton RJ, Hirsh J, Wolf FW. 2010. A pair of dopamine neurons target the D1-like dopamine receptor DopR in the central complex to promote ethanol-stimulated locomotion in Drosophila. *PLoS One* **5**:e9954. doi:10.1371/journal.pone.0009954

Lee YJ, Yang CP, Miyares RL, Huang YF, He Y, Ren Q, Chen HM, Kawase T, Ito M, Otsuna H, Sugino K, Aso Y, Ito K, Lee T. 2020. Conservation and divergence of related neuronal lineages in the Drosophila central brain. *Elife* **9**. doi:10.7554/eLife.53518

Levoy M, Ng R, Adams A, Footer M, Horowitz M. 2006. Light field microscopy. *ACM Trans Graph* **25**:924. doi:10.1145/1141911.1141976

Li F, Lindsey JW, Marin EC, Otto N, Dreher M, Dempsey G, Stark I, Bates AS, Pleijzier MW, Schlegel P, Nern A, Takemura SY, Eckstein N, Yang T, Francis A, Braun A, Parekh R, Costa M, Scheffer LK, Aso Y, Jefferis GS, Abbott LF, Litwin-Kumar A, Waddell S, Rubin GM. 2020. The connectome of the adult Drosophila mushroom body provides insights into function. *Elife* **9**. doi:10.7554/eLife.62576

Liang X, Holy TE, Taghert PH. 2016. Synchronous Drosophila circadian pacemakers display nonsynchronous Ca2+ rhythms in vivo. *Science (1979)* **351**:976–981. doi:10.1126/science.aad3997

Liu Q, Tabuchi M, Liu S, Kodama L, Horiuchi W, Daniels J, Chiu L, Baldoni D, Wu MN. 2017. Branch-specific plasticity of a bifunctional dopamine circuit encodes protein hunger. *Science (1979)* **356**. doi:10.1126/science.aal3245

Lu J, Behbahani AH, Hamburg L, Westeinde EA, Dawson PM, Lyu C, Maimon G, Dickinson MH, Druckmann S, Wilson RI. 2022. Transforming representations of movement from body- to world-centric space. *Nature* **601**:98–104. doi:10.1038/s41586-021-04191-x

Lyu C, Abbott LF, Maimon G. 2022. Building an allocentric travelling direction signal via vector computation. *Nature* **601**:92–97. doi:10.1038/s41586-021-04067-0

Mace E, Montaldo G, Trenholm S, Cowan C, Brignall A, Urban A, Roska B. 2018. Whole-Brain Functional Ultrasound Imaging Reveals Brain Modules for Visuomotor Integration. *Neuron* **100**:1241-1251 e7. doi:10.1016/j.neuron.2018.11.031

Maimon G, Straw AD, Dickinson MH. 2010. Active flight increases the gain of visual motion processing in Drosophila. *Nat Neurosci* **13**:393–399. doi:10.1038/nn.2492

Mamiya A, Gurung P, Tuthill JC. 2018. Neural Coding of Leg Proprioception in Drosophila. *Neuron* **100**:636-650 e6. doi:10.1016/j.neuron.2018.09.009

Mann K, Deny S, Ganguli S, Clandinin TR. 2021. Coupling of activity, metabolism and behaviour across the Drosophila brain. *Nature* **593**:244–248. doi:10.1038/s41586-021-03497-0

Mao Z, Davis RL. 2009. Eight different types of dopaminergic neurons innervate the Drosophila mushroom body neuropil: anatomical and physiological heterogeneity. *Front Neural Circuits* **3**:5. doi:10.3389/neuro.04.005.2009

Marques JC, Li M, Schaak D, Robson DN, Li JM. 2020. Internal state dynamics shape brainwide activity and foraging behaviour. *Nature* **577**:239–243. doi:10.1038/s41586-019-1858-z

Mendes CS, Rajendren S v, Bartos I, Marka S, Mann RS. 2014. Kinematic responses to changes in walking orientation and gravitational load in Drosophila melanogaster. *PLoS One* **9**:e109204. doi:10.1371/journal.pone.0109204

Mu Y, Narayan S, Mensh BD, Ahrens MB. 2020. Brain-wide, scale-wide physiology underlying behavioral flexibility in zebrafish. *Curr Opin Neurobiol* **64**:151–160. doi:10.1016/j.conb.2020.08.013

Mueller JM, Ravbar P, Simpson JH, Carlson JM. 2019. Drosophila melanogaster grooming possesses syntax with distinct rules at different temporal scales. *PLoS Comput Biol* **15**:e1007105. doi:10.1371/journal.pcbi.1007105

Musall S, Kaufman MT, Juavinett AL, Gluf S, Churchland AK. 2019. Single-trial neural dynamics are dominated by richly varied movements. *Nat Neurosci* **22**:1677–1686. doi:10.1038/s41593-019-0502-4

Namiki S, Dickinson MH, Wong AM, Korff W, Card GM. 2018. The functional organization of descending sensory-motor pathways in Drosophila. *Elife* **7**. doi:10.7554/eLife.34272

Namiki S, Ros IG, Morrow C, Rowell WJ, Card GM, Korff W, Dickinson MH. 2022. A population of descending neurons that regulates the flight motor of Drosophila. *Curr Biol* **32**:1189-1196 e6. doi:10.1016/j.cub.2022.01.008

Ngai M, Shoue DA, Loh Z, McDowell MA. 2019. The pharmacological and functional characterization of the serotonergic system in Anopheles gambiae and Aedes aegypti: influences on flight and blood-feeding behavior. *Sci Rep* **9**:4421. doi:10.1038/s41598-019-38806-1

Parker PRL, Brown MA, Smear MC, Niell CM. 2020. Movement-Related Signals in Sensory Areas: Roles in Natural Behavior. *Trends Neurosci* **43**:581–595. doi:10.1016/j.tins.2020.05.005

Robie AA, Hirokawa J, Edwards AW, Umayam LA, Lee A, Phillips ML, Card GM, Korff W, Rubin GM, Simpson JH, Reiser MB, Branson K. 2017. Mapping the Neural Substrates of Behavior Resource Mapping the Neural Substrates of Behavior. *Cell* **170**:393-406.e28. doi:10.1016/j.cell.2017.06.032

Sayin S, de Backer JF, Siju KP, Wosniack ME, Lewis LP, Frisch LM, Gansen B, Schlegel P, Edmondson-Stait A, Sharifi N, Fisher CB, Calle-Schuler SA, Lauritzen JS, Bock DD, Costa M, Jefferis G, Gjorgjieva J, Grunwald Kadow IC. 2019. A Neural Circuit Arbitrates between Persistence and Withdrawal in Hungry Drosophila. *Neuron* **104**:544-558 e6. doi:10.1016/j.neuron.2019.07.028

Schaffer ES, Mishra N, Whiteway MR, Li W, Vancura MB, Freedman J, Patel KB, Voleti V, Paninski L, Hillman EMC, Abbott LF, Axel R. 2021. Flygenvectors: The spatial and temporal structure of neural activity across the fly brain. *bioRxiv* 2021.09.25.461804. doi:10.1101/2021.09.25.461804

Scheffer LK, Xu CS, Januszewski M, Lu Z, Takemura SY, Hayworth KJ, Huang GB, Shinomiya K, Maitin-Shepard J, Berg S, Clements J, Hubbard PM, Katz WT, Umayam L, Zhao T, Ackerman D, Blakely T, Bogovic J, Dolafi T, Kainmueller D, Kawase T, Khairy KA, Leavitt L, Li PH, Lindsey L, Neubarth N, Olbris DJ, Otsuna H, Trautman ET, Ito M, Bates AS, Goldammer J, Wolff T, Svirskas R, Schlegel P, Neace ER, Knecht CJ, Alvarado CX, Bailey DA, Ballinger S, Borycz JA, Canino BS, Cheatham N, Cook M, Dreher M, Duclos O, Eubanks B, Fairbanks K, Finley S, Forknall N, Francis A, Hopkins GP, Joyce EM, Kim S, Kirk NA, Kovalyak J, Lauchie SA, Lohff A, Maldonado C, Manley EA, McLin S, Mooney C, Ndama M, Ogundeyi O, Okeoma N, Ordish C, Padilla N, Patrick C, Paterson T, Phillips EE, Phillips EM, Rampally N, Ribeiro C, Robertson MK, Rymer JT, Ryan SM, Sammons M, Scott AK, Scott AL, Shinomiya A, Smith C, Smith K, Smith NL, Sobeski MA, Suleiman A, Swift J, Takemura S, Talebi I, Tarnogorska D, Tenshaw E, Tokhi T, Walsh JJ, Yang T, Horne JA, Li F, Parekh R, Rivlin PK, Jayaraman V, Costa M, Jefferis GSXE, Ito K, Saalfeld S, George R,

Meinertzhagen IA, Rubin GM, Hess HF, Jain V, Plaza SM. 2020. A connectome and analysis of the adult Drosophila central brain. *Elife* **9**:1--74. doi:10.7554/ELIFE.57443
Schilling M, Cruse H. 2020. Decentralized control of insect walking: A simple neural network explains a wide range of behavioral and neurophysiological results. *PLoS Comput Biol* **16**:e1007804. doi:10.1371/journal.pcbi.1007804
Schoofs A, Hckesfeld S, Schlegel P, Miroschnikow A, Peters M, Zeymer M, Spiess R, Chiang AS, Pankratz MJ. 2014. Selection of Motor Programs for Suppressing Food Intake and Inducing Locomotion in the Drosophila Brain. *PLoS Biol* **12**:e1001893. doi:10.1371/JOURNAL.PBIO.1001893
Schoofs A, Huckesfeld S, Pankratz MJ. 2018. Serotonergic network in the subesophageal zone modulates the motor pattern for food intake in Drosophila. *J Insect Physiol* **106**:36–46. doi:10.1016/j.jinsphys.2017.07.007
Seelig JD, Chiappe ME, Lott GK, Dutta A, Osborne JE, Reiser MB, Jayaraman V. 2010. Two-photon calcium imaging from head-fixed Drosophila during optomotor walking behavior. *Nat Methods* **7**:535–540. doi:10.1038/nmeth.1468
Seelig JD, Jayaraman V. 2015. Neural dynamics for landmark orientation and angular path integration. *Nature* **521**:186–191. doi:10.1038/nature14446
Seelig JD, Jayaraman V. 2013. Feature detection and orientation tuning in the Drosophila central complex. *Nature* **503**:262–266. doi:10.1038/nature12601
Sen R, Wang K, Dickson BJ. 2019. TwoLumps Ascending Neurons Mediate Touch-Evoked Reversal of Walking Direction in Drosophila. *Curr Biol* **29**:4337-4344 e5. doi:10.1016/j.cub.2019.11.004
Siju KP, Stih V, Aimon S, Gjorgjieva J, Portugues R, Grunwald Kadow IC. 2020. Valence and State-Dependent Population Coding in Dopaminergic Neurons in the Fly Mushroom Body. *Curr Biol* **30**:2104-2115 e4. doi:10.1016/j.cub.2020.04.037
Sims DW, Humphries NE, Hu N, Medan V, Berni J. 2019. Optimal searching behaviour generated intrinsically by the central pattern generator for locomotion. *Elife* **8**. doi:10.7554/eLife.50316
Stringer C, Pachitariu M, Steinmetz N, Reddy CB, Carandini M, Harris KD. 2019. Spontaneous behaviors drive multidimensional, brainwide activity. *Science (1979)* **364**:255. doi:10.1126/science.aav7893
Suver MP, Huda A, Iwasaki N, Safarik S, Dickinson MH. 2016. An Array of Descending Visual Interneurons Encoding Self-Motion in Drosophila. *J Neurosci* **36**:11768–11780. doi:10.1523/JNEUROSCI.2277-16.2016
Tao L, Ozarkar S, Beck JM, Bhandawat V. 2019. Statistical structure of locomotion and its modulation by odors. *Elife* **8**. doi:10.7554/eLife.41235
Tsai KT, Chou YH. 2019. Random Walk Revisited: Quantification and Comparative Analysis of Drosophila Walking Trajectories. *iScience* **19**:1145–1159. doi:10.1016/j.isci.2019.08.054
Tsubouchi A, Yano T, Yokoyama TK, Murtin C, Otsuna H, Ito K. 2017. Topological and modality-specific representation of somatosensory information in the fly brain. *Science (1979)* **358**:615–623. doi:10.1126/science.aan4428
van Damme S, de Fruyt N, Watteyne J, Kenis S, Peymen K, Schoofs L, Beets I. 2021. Neuromodulatory pathways in learning and memory: Lessons from invertebrates. *J Neuroendocrinol*. doi:10.1111/jne.12911
Vicente AM, Martins GJ, Costa RM. 2020. Cortico-basal ganglia circuits underlying dysfunctional control of motor behaviors in neuropsychiatric disorders. *Curr Opin Genet Dev* **65**:151–159. doi:10.1016/j.gde.2020.05.042
Vitrac C, Benoit-Marand M. 2017. Monoaminergic Modulation of Motor Cortex Function. *Front Neural Circuits* **11**:72. doi:10.3389/fncir.2017.00072
Vladimirov N, Mu Y, Kawashima T, Bennett D v., Yang CT, Looger LL, Keller PJ, Freeman J, Ahrens MB. 2014. Light-sheet functional imaging in fictively behaving zebrafish. *Nat Methods*. doi:10.1038/nmeth.3040
von Philipsborn AC, Liu T, Yu JY, Masser C, Bidaye SS, Dickson BJ. 2011. Neuronal control of Drosophila courtship song. *Neuron* **69**:509–522. doi:10.1016/j.neuron.2011.01.011
Woller A, Bandow P, Aimon S, Grunwald Kadow IC. 2021. Preparing Adult Drosophila melanogaster for Whole Brain Imaging during Behavior and Stimuli Responses. *J Vis Exp*. doi:10.3791/61876
Wolpert DM, Diedrichsen J, Flanagan JR. 2011. Principles of sensorimotor learning. *Nat Rev Neurosci* **12**:739–751. doi:10.1038/nrn3112
Xiang L, Harel A, Gao H, Pickering AE, Sara SJ, Wiener SI. 2019. Behavioral correlates of activity of optogenetically identified locus coeruleus noradrenergic neurons in rats performing T-maze tasks. *Sci Rep* **9**:1361. doi:10.1038/s41598-018-37227-w
Zacarias R, Namiki S, Card GM, Vasconcelos ML, Moita MA. 2018. Speed dependent descending control of freezing behavior in Drosophila melanogaster. *Nat Commun* **9**:3697. doi:10.1038/s41467-018-05875-1
Zheng Z, Lauritzen JS, Perlman E, Robinson CG, Nichols M, Milkie D, Torrens O, Price J, Fisher CB, Sharifi N, Calle-Schuler SA, Kmecova L, Ali IJ, Karsh B, Trautman ET, Bogovic JA, Hanslovsky P, Jefferis G, Kazhdan

M, Khairy K, Saalfeld S, Fetter RD, Bock DD. 2018. A Complete Electron Microscopy Volume of the Brain of Adult Drosophila melanogaster. *Cell* **174**:730-743 e22. doi:10.1016/j.cell.2018.06.019

Zolin A, Cohn R, Pang R, Siliciano AF, Fairhall AL, Ruta V. 2021. Context-dependent representations of movement in Drosophila dopaminergic reinforcement pathways. *Nat Neurosci* **24**:1555–1566. doi:10.1038/s41593-021-00929-y

Acknowledgments

We are very grateful to Marta Costa and Kei Ito for sharing data, images, and knowledge during the course of this study. We also thank Francisco Rodriguez-Jimenez, Paul Bandow, Subhadarshini Parhi and Kunhi Purayil Siju for help with data analysis.

We would like to acknowledge funding from the European research commission (ERCStG FlyContext to IGK, ERCStG NeuroDevo to JG).

Competing interests: The authors declare no conflict of interest.

Data and materials availability:

Deposited data		
Example dataset with raw data	CNCRS	https://crcns.org/data-sets/ia/fly-1/about-fly-1
Processed data for figures	GitHub	https://github.com/sophie63/Aimon2022
Regional time series	Dryad	https://doi.org/10.5061/dryad.3bk3j9kpb

All original code is publicly available on Github. Original large (>1Tb) datasets are available upon request (Ilona.grunwald@uni-bonn.de).

Figures and Tables

Figure 1: Global brain activation during walk.
(**A**) Schematic overview of the preparation and analysis method. Please see methods for details. (**B**) Raster plot of the activity of regions. Top panels depict walking bouts in green and rest or grooming in magenta. Lower panel shows calcium activity elicited throughout the experiment. The brighter the higher the calcium transients. Mean forward speed: 5.6 mm/s, mean angular velocity: 0.4 radian/s. (**C**) Sample traces (deltaF/F) for different brain regions relative to walk (green). (**D**) First two principal components from whole brain activity color-coded with behavior (see additional examples in Figure 1-figure supplement 1). (**E**) R^2 for regression of single regions with single behaviors (all regions were pooled, but p-values are obtained after averaging regions for each fly. Walk: N=16, Flail: N=7, Groom: N=6). Mann-Withney U-test Bonferroni adjusted p-values: Walk vs. Flail 0.085, Walk vs. Groom: 0.011, Flail vs. Groom: 0.26. Center line, median; box limits, upper and lower quartiles; whiskers, 1.5x interquartile range; points, outliers (**F**) R^2 of single region activity regression with walk, walk onset and walk offset (all regions were pooled, nsyb-Gal4: N=16, GMR57C10-Gal4: N=4). Regressors for walk onset or offset are Dirac functions convolved with the GCaMP response (see methods section). Box plots show: center line, median; box limits, upper and lower quartiles; whiskers, 1.5x interquartile range; points, outliers. Mann-Whitney U-test for the two genotypes grouped (comparison of fly-wise averages): walk vs walk onset: $p=3.10^{-5}$, walk vs walk offset: $p=6.10^{-5}$. (**G**) Z-stack map of R^2 median (Walk: N (flies) =16, Flail: N=7, Groom: N=6) for regression between single region activity and walk, flail or groom (see values in Figure 1-figure supplement 1 D-F). (**H**) Coefficient of single regions' activity regression with walk. All regions' 95% CI are above zero and all adjusted p-values < 0.001 (Benjamini Hochberg correction). N=16.

Video 1: Movie of pan-neuronal activation during walk and groom (accelerated).

Figure 1-figure supplement 1:
(A) R^2 during walk at different recording frequencies for pan-neuronally expressed GCaMP6f or GCaMP6m (all regions were pooled). No significant difference was found for walk between the different frequencies. Box plots show: center line, median; box limits, upper and lower quartiles; whiskers, 1.5x interquartile range; points, outliers.
(B) R^2 for walking with eyes free (not painted, N=5) and eyes covered (painted, N=5, p-value: 0.34). Box plots show: center line, median; box limits, upper and lower quartiles; whiskers, 1.5x interquartile range; points, outliers.
(C) Additional examples (2 different flies) of whole brain activity reduces to the two first principal component space.
(D) R^2 obtained with regressing activity of individual regions with walk (pan-Gal4;UAS-GCaMP). Adjusted p-values (Benjamini-Hochberg correction) were all <0.01.

(E) R^2 obtained with regressing activity of individual regions with flail (pan-Gal4;UAS-GCaMP). Empty markers correspond to adjusted (Benjamini-Hochberg correction) p-value>0.05 for comparison to 0.
(F) R^2 obtained with regressing activity of individual regions with groom (pan-Gal4;UAS-GCaMP)
(G) Correlation coefficient obtained with regressing activity of individual regions with flail(pan-Gal4;UAS-GCaMP)
(H) Correlation coefficient obtained with regressing activity of individual regions withr grooming behavior (pan-Gal4;UAS-GCaMP)
(I) R^2 obtained with regressing activity of individual regions with walking on an air-supported (N=19) vs. a Styrofoam ball (N=13), p-value=0.02. Box plots show: center line, median; box limits, upper and lower quartiles; whiskers, 1.5x interquartile range; points, outliers.
(J) R^2 obtained with regressing activity of individual regions with walking on an air-supported (N=19) vs. a Styrofoam ball (N=13). Box plots show: center line, median; box limits, upper and lower quartiles; whiskers, 1.5x interquartile range; points, outliers.
(K) Top: Examples of brain activity maps (R^2 as z-stacks) and names of individual brain regions
Bottom: Schematic showing brain regions in adult fly brain reproduced from (Ito et al., 2014).

Figure 2: Activity of neurons releasing the three major neurotransmitters, glutamate, GABA and acetylcholine during walk. N= 5 flies for each genotype. (**A**) R^2 for regression of single region activity with walk for different genotypes (all regions were pooled). No pairwise comparison of fly-wise averages is significantly different (Mann-Whitney U-test). Boxplot: center line, median; box limits, upper and lower quartiles; whiskers, 1.5x interquartile range; points, outliers. (**B**) Maps of activation during walk (regression coefficient of single region activity with walk) for Cha-Gal4, GAD-Gal4 and Vglut-Gal4 expressing neurons. See Figure 2-figure supplement 1 for values and statistical tests. Cosine similarity: Cha vs Vglut: 0.98, Vglut vs GAD: 0.98, Cha vs GAD: 0.99. (**C**) Sample traces (deltaF/F) for different brain regions relative to forward walk (green). See Figure 2-figure supplement 1 for values. (**D**) R^2 of regression of single region activity with walk for Cha-Gal4, GAD-Gal4 and Vglut-Gal4. 95% CI is shown. All values are significantly above zero (Benjamini-Hochberg adjusted t-test p-values<0.001).

Figure 2-figure supplement 1: Correlation coefficients for regression of single region activity with walk. N=5 flies for each genotype. Empty markers correspond to adjusted (Benjamini-Hochberg correction) p-value>0.05 for comparison to 0. Right, expression pattern for three example flies per genotype (baseline fluorescence at z = -60, -18, 24 and 66 microns.
(A) Cholinergic neurons (Cha-Gal4;UAS-GCaMP6)
(B) Glutamatergic neurons (Vglut-Gal4;UAS-GCaMP6)

(C) GABAergic neurons (GAD-Gal4;UAS-GCaMP6)

Figure 3: Neuromodulatory neurons are strongly and differentially activated during walk. TH/DDC-Gal4: N = 9, Tdc2-Gal4: N = 7, Trh-Gal4: N = 6 flies.
(**A**) R^2 for regression of single region activity with walk for different genotypes (all regions were pooled). Mann-Whitney U-test Bonferroni adjusted p-values: TH vs. Trh: 0.032, TH vs. TDC: ns, Trh vs. TDC: 0.040. Box plot: center line, median; box limits, upper and lower quartiles; whiskers, 1.5x interquartile range; points, outliers. (**B**) Maps of activation during walk (regression coefficient of single region activity with walk) for TH-Gal4 and DDC-Gal4 or GMR58E04-Gal4 (dopaminergic neurons), TDC2-Gal4 (octopaminergic neurons) and Trh-Gal4 (serotoninergic neurons) expressing neurons. Blue indicates inhibition. (**C**) Overlay of activity maps of two neuromodulators in each panel. Cosine similarity: TH vs Trh: 0.69, TH vs TDC: 0.93, TDC vs Trh: 0.69. (**D**) Sample traces (deltaF/F) for different brain regions relative to forward walk (green). (**E**) Coefficient during walk for different brain regions for Trh-Gal4 expressing serotonergic neurons. All regions are significantly correlated. (**F**) R^2 of regression of fluorescence vs. walk for TH/DDC(58E02)-Gal4, Tdc2-Gal4 and Trh-Gal4 expressing excitatory neurons.

Video 2: Movie of TH/DDC-neuronal activation during walk (accelerated).

Video 3: Movie of TDC2-neuronal activation during walk (accelerated).

Video 4: Movie of Trh-neuronal activation during walk (accelerated).

Figure 3-figure supplement 1: Correlation coefficients for regression of single region activity with walk. Empty markers correspond to adjusted (Benjamini-Hochberg correction) p-value>0.05 (null hypothesis is 0). TH/DDC-Gal4: N = 9, Tdc2-Gal4: N = 7
(A) Dopaminergic neurons (TH/DDC-Gal4 or GMR58E04-Gal4;UAS-GCaMP6)
(B) Octopaminergic neurons (Tdc2-Gal4;UAS-GCaMP6)
(C) Expression pattern for three example flies per genotype (baseline fluorescence at z = -60, -18, 24 and 66 microns.)

Figure 4: Whole brain analysis pinpoints specific subregions responding to walk.
(A) Images of example components that are significantly correlated with walk (Coefficient or R^2 95% CI above zero). Upper left: components derived from imaging with a pan-neuronal driver. Upper right: components derived with Tdc2-Gal4. Lower left: components derived with TH/DDC or GMR58E02-Gal4. Lower right: components derived with Trh-Gal4. (**B**) Correlation coefficient for components activity vs walk. N = 58 flies of different genotypes, see table in methods for details. Empty markers correspond to adjusted (Benjamini-Hochberg correction) p-value>0.05 for comparison to 0.

Figure 4-figure supplement 1:
(A) Z-stacks of functional components for walk mapped onto the adult fly brain

(B) Functional components for walk and their names or acronyms. See Table 2 for definition of acronyms.
(C) R^2 for regression of components activity with walk. See Table 2 for definition of acronyms.
N = 58 flies of different genotypes, see table in methods for details.

Figure 5: Turning activates specific components and candidate neurons.

(**A**) Examples of components present in both the left and right hemisphere labeled in different colors (magenta and green). Panels on the right present an example component that could be mapped to a single neuron. Upper right panel: Turning-correlated component, lower right panel: reconstruction of neuron that this functional component was mapped to. (**B**) Difference between the correlation coefficient (normalized $\Delta F/F$) for turning on the ipsilateral side and the coefficient on the contralateral side is displayed as a function of the identified components. Positive and negative correlations correspond to components being active more during turn on the ipsi-lateral side than the contra-lateral side and the reverse, respectively. See Table 2 for definition of acronyms. N = 58 flies of different genotypes, see table in methods for details. Empty markers correspond to adjusted (Benjamini-Hochberg correction) p-value>0.05 for comparison to 0.

Video 5: Video sequence showing activation of the PPM2-LW neurons during turning.

Figure 5-figure supplement 1: Turning activates specific components and candidate neurons.
(A) Examples of components present in both the left and right hemisphere labeled in different colors (magenta and green).
(B) R^2 of regression coefficients during turn for all genotypes. The value for the contralateral side was subtracted from the ipsilateral side and plotted for every component. N=58 flies of different genotypes, see table in methods for details. Empty markers correspond to adjusted (Benjamini-Hochberg correction) p-value>0.05 for comparison to 0.

Figure 6: Onset dynamics of walk induces activity in multiple functional components across the brain at start of walk.
Walk-onset triggered average activity for pan-neuronal data in individual active components at 30 Hz or higher temporal resolution. Trials were normalized individually before averaging (see Figure 6-figure supplement 1 for non-normalized traces and all recording frame rates). Red band indicates walk onset. Note that while most components are activated after walk onset, several components show activity before start of walk. Stars correspond to an above zero significance for integrated traces from -0.5s to start of walk (Wilcoxon one sided test). Multiple comparison adjusted p-values (Benjamini Hochberg): * $p<0.05$, ** $p<0.01$, *** $p<0.001$. See Table 2 for definition of acronyms. N=30 flies of different genotypes, see table in methods for details.

Figure 6-figure supplement 1:
Graphs show onset of walk trials for all flies and all transgenic lines at all recording speeds. The grey band represents the uncertainty of walk onset time due to lower temporal resolution in some recordings. A corrective factor based on regression coefficient with walk (Fluorescence response to walk = coeff x UAS-GCaMP version: GCaMP7f: 0.6, GCaMP6f: 1, GCaMP6M: 1.1, GCaMP7s 1.2, GCaMP6s: 1.4) was applied for direct comparison between experiments with different reporter versions. The average value for the first 50 ms was taken as baseline and subtracted. Grey shaded area represents walk onset.

Figure 6-figure supplement 2: Normalized trials ΔF/F GCaMP fluorescence in brain regions 1 s before to 1 s after walk onset for different anatomically defined brain regions: dopaminergic neurons (TH/DDC-Gal4;GCaMP) left, octopaminergic neurons (Tdc2-Gal4;GCaMP) middle and serotonergic neurons (Trh-Gal4;GCaMP) right. Grey shading corresponds to the standard deviation. Red band is the onset of walk.

Figure 7: Forced and spontaneous walk elicit highly similar global brain activity.
(**A**) Z-stacks of map of brain regions activated by walk in flies expressing cytosolic GCaMP (pan-Gal4;UAS-GCaMP6m) or synaptically tagged GCaMP (pan-Gal4;UAS-GCaMP6m). (R^2 of $\frac{\Delta F}{F} = f(walk)$) (**B**) Time series of components during spontaneous walk or rest (magenta vs. green). (**C**) Time series of active components during forced walk or forced rest (magenta vs. green). (**D**) R^2 for behavior regression at different conditions (all regions were pooled, spontaneous, forced, forced with severed connection between VNC and brain) (**E**) R^2 for behavior regression for different active components for forced vs. spontaneous walk. Empty markers correspond to adjusted (Benjamini-Hochberg correction) p-value>0.05 for comparison to 0. (**F**) R^2 difference between brain region activity during forced turn on the ipsilateral side and forced turn on the contralateral side (orange). Forced turning speeds were from 0.3 to 2 radian/s. Only data with N>=4 components were analyzed. Lilac shows the difference for spontaneous turns. N = 58 flies for spontaneous walk/turn of different genotypes and N = 26 flies for forced walk/turn, see table in methods for details. Box plots show: center line, median; box limits, upper and lower quartiles; whiskers, 1.5x interquartile range; points, outliers. Empty markers correspond to adjusted (Benjamini-Hochberg correction) p-value>0.05 for comparison to 0. Star corresponds to a significant difference between spontaneous and forced turns: Mann-Whitney U test adjusted p-value<0.05 (Benjamini-Hochberg correction). (**G**) Comparison between activity at walk onset for spontaneous (green) and forced (red) walk, for additional components. Individual trials were normalized and averaged for each component. Shaded regions represent the trail SEM, nf: number of flies, nt: total number of trials. Grey shaded area indicate walk onset. Stars show the significance of difference in the integral between -0.5 s to start of walk, and is corrected for multiple comparison (Benjamini-Hochberg): * p<0.05, ** p<0.01, ***p<0.001.

Video 6: Video showing neuronal activation moving from ventral to dorsal brain areas. Note that a clear progression of activation was observed only in a fraction of trials.

Video 7: Video showing whole brain activity of a fly being forced to walk on a rotating rod.

Video 8: Video showing whole brain activity of a fly with a severed connection between brain and VNC being forced to walk on a rotating rod. Note that the fly is still capable of walking on the rod when being forced. We did, however, not observe spontaneous walking activity.

Figure 7-figure supplement 1:

(A) Comparison of activity during walk for cytosolic and axonal GCaMP. Left: expression patterns (baseline fluorescence), Right: coefficient in linear models of regional activity as a function of walk.

(B) Regression coefficients with forced or spontaneous walk for components.

(C) R^2 of $\Delta F/F$ regression with forced and spontaneous walk for different brain regions for dopaminergic neurons.

(D) R^2 of $\Delta F/F$ regression with forced and spontaneous walk for different brain regions for octopaminergic neurons.

(E) R^2 of $\Delta F/F$ regression with forced and spontaneous walk for different brain regions for serotonergic neurons.
TH/DDC-Gal4: spontaneous, N=9, forced, N=5; Tdc2-Gal4: spontaneous, N=7, forced, N=6; Trh-Gal4: spontaneous, N=6, forced, N=6 flies.
(A) To (D): Empty markers correspond to adjusted (Benjamini-Hochberg correction) p-value>0.05 for comparison to 0.

(F) Panel showing GCaMP-fluorescence relative to onset of walk for pan-neuronally expressed GCaMPs in different regions relative to the GNG. Piece-wise linear curves were fitted to fluorescence traces 0.5 s before to 0.5 s after the onset of walk. The onset time was determined as the point of change from one linear piece to the next. Note that all medians are positive. Inset: Fit of activity onset. TH/DDC-Gal4: N=9, Tdc2-Gal4: N=7, Trh-Gal4: N=6 flies.

(G) Comparison between activity at walk onset for spontaneous (green) and forced (red) walk, for additional components. Individual trials were normalized and averaged for each component. Shaded regions represent the trail SEM, nf: number of flies, nt: total number of trials.
Stars show the significance of difference in the integral between -500ms to start of walk, and is corrected for multiple comparison (Benjamini Hochberg): * $p<0.05$, ** $p<0.01$, *** $p<0.01$.

Table 1: Summary statistics of R^2 dependence on different factors where R^2 is obtained from regressing a single regionally averaged brain activity with a single behavior.

	sum_sq	PR(>F)
GAL4	0.002197	7.58E-01
Behavior	12.215185	1.64E-106
RegionNames	10.372902	4.13E-65
UAS	2.083138	2.13E-18
Behavior:RegionNames	1.45213	9.17E-01
Residual	67.904784	NaN

Table 2: List of components with potential underlying candidate neurons. Most matches are speculative except those in bold that correspond to high confidence matches due to the lack of other Gal4-positive neurons in the region.

Short name	**Description**	**Examples of matching (Flycircuit) neurons**	**present in Gal4 line** (detected in ≥ 5 flies)
Antennal lobe and Mushroom body			
AL	Whole antennal lobe	Gad1-F-000394; Gad1-F-100601; Gad1-F-800129; VGlut-F-900126	Nsyb , GMR57C10 , Vglut , Gad
PN	antennal lobe projection neuron	VGlut-F-500486	Nsyb , GMR57C10 , Cha , Vglut , Gad
MultiGl	Whole antennal lobe and PN-like projections	Trh-F-600017	TH , Trh , TDC
PNv	antennal lobe projection neuron, ventral tract of the lateral horn	VFB_00101133	Nsyb , GMR57C10 , Cha , Vglut , Gad
PN-KC	Antennal lobe projection neuron and kenyon cell in the same component		Nsyb , GMR57C10 , Cha, Vglut
KCab	Alpha-Beta Kenyon cell	Cha-F-300226; Cha-F-100049; fru-F-000026; Vglut-F-100284; Gad1-F-100014;	Nsyb , GMR57C10
KCapbp	Alpha'-Beta'; Kenyon cell	Gad1-F-100024; Trh-F-200069;	Nsyb , GMR57C10
KCg	Gamma kenyon cells	fru-F-000006; Vglut-F-100359; Gad1-F-100021;	Nsyb , GMR57C10
Beta1Betap1	Beta1 and/or Beta'1 mushroom body compartment	PAM10(B1)_L (FlyEM-HB:1328522741) [VFB_jrchk385]	TH
Beta2Betap2	Beta2 and/or Beta'2 mushroom body compartment	PAM02(B'2a)_L (FlyEM-HB:1295566429)	Nsyb, Gad , TH
Gamma1	**Gamma1 mushroom body compartment**	**PPL1-gamma1-pedc**	**TH**
Gamma2	**Gamma2 mushroom body**	**PPL1-gamma2-alpha'1**	**TH**

	compartment		
Gamma3	**Gamma3 mushroom body compartment**	**MBON-γ3, PAM-γ3**	**Gad, TH**
Gamma4	**Gamma4 mushroom body compartment**	**PAM-γ4**	**TH**
Gamma5	**Gamma5 mushroom body compartment**	**PAM-γ5**	**TH**
SLP-Alpha	Alpha or Alpha' lobe with projection through the superior lateral neuropil	VGlut-F-500002	Vglut
Alpha1	**Alpha1 mushroom body compartment**	**PAM-alpha1**	**TH**
Alpha2	**Alpha2 mushroom body compartment**	**PPL1-alpha'2alpha2**	**TH**
Alpha3	**Alpha3 mushroom body compartment**	**PPL1-alpha3**	**TH**
Alphap3	**Alpha'3 mushroom body compartment**	**PPL1-alpha'3**	**TH**
Superior neuropil			
SCLtract	Tract linking both superior clamp	Trh-F-200082,Trh-F-100051	Trh
CLvert	Lateral part of the superior clamp	TH-F-000023	Nsyb, TH
CL?	Interrogation point surrounding the pedonculus,	Trh-F-300074,Trh-M-700081, DNp32	TH , Trh
CL-LH	Surrounds the lateral horn from the medial and ventral directions	Trh-F-200047	Trh , TDC
CL	Other shapes at the level of the clamp	Gad1-F-700550,Gad1-F-800055	Nsyb, GMR57C10 , Gad, TH, TDC
SMPm	Medial part of the superior medial protocerebrum	TH-F-000021; VGlut-F-700286, Cha-F-300251	Nsyb, GMR57C10, Cha, Vglut, Gad , TH, TDC
PPL-SMP	ventral lateral part of the superior medial protocerebrum, with tracts coming from a posterior lateral cell cluster	TH-F-000019,TH-F-000018,TH-F-000046	TH
SMPl-SIP	Superior intermediate protocerebrum and lateral part of the superior medial protocerebrum	Cha-F-000221,Cha-F-300154, TH-F-300056	Nsyb , GMR57C10 , Cha , Gad, TH , TDC
SIP-SMPd	Superior intermediate protocerebrum and dorsal part of the superior medial protocerebrum	fru-F-800063	Nsyb
SIP-FB	Superior intermediate protocerebrum and dorsal layer of the fan-shaped body	Trh-F-100015;	Nsyb, GMR57C10 , TH, Trh

FB-SN	Broad innervaion of the superior neuropil, and fan-shaped body	OA-VMP3, OA-VPM4	TDC
SLP-SMPproj	Large SMP neuron projecting to ventral regions	Trh-F-700011,Trh-F-000083	Nsyb , GMR57C10, TH , Trh
SLP-SMP	Superior lateral protocerebrum and superior medial protocerebrum	Trh-F-500176, DNp25	Trh
SLP	Superior lateral protocerebrum only	TH-F-100046	Nsyb, GMR57C10, TH , TDC
LH-SLP	Lateral horn and superior lateral protocerebrum	Gad1-F-900346,Gad1-F-600340	Nsyb , Gad
Central complex			
FBcol	Fan shaped body columns	Tdc2-F-100009; Tdc2-F-300026; Tdc2-F-300001; Tdc2-F-200011; Tdc2-F-100062; Tdc2-F-100016; Gad1-F-900245; Gad1-F-800329; Gad1-F-500513; Gad1-100157	Nsyb , GMR57C10, Vglut , Gad, TDC
FBlayv	Ventral layer of the fan-shaped body	TH-M-300065	Nsyb, TH
FBlaym	Medial layer of the fan-shaped body	TH-F-200055	Nsyb , TH
FBlayd	Dorsal layer of the fan-shaped body	TH-F-200054; Trh-F-300036; Trh-F-400062	Nsyb, TH , Trh
NO	Nodulus or noduli	Cha-F-100429	Nsyb
PB	Protocerebral bridge only	Vglut-F-800282; Vglut-F-600784; Vglut-F-600229; Gad1-F-600267; Gad1-F-100361; Gad1-F-100593; Vglut-F-000156; Vglut-F-100064	Nsyb , Vglut , Gad
PBfull	Components with full protocerebral bridge	Cha-F-900016, Cha-F-200148	Nsyb , GMR57C10 , Cha
PB-DA	**Protocerebral bridge and two dots (maybe cell bodies) at the top of the trachea**	**TH-F-000048**	**TH**
BU-PBl-EB	Bulb, ellipsoid body and lateral part of the protocerebral bridge	Gad1-F-900445	Nsyb , Gad
PB-EB	EB-radial and PB glomeruli	Cha-F-500009	Nsyb , GMR57C10 , Cha, Gad
EB	Ellipsoid body rings	Trh-F-300095; Cha-F-800146	Nsyb, GMR57C10, Cha, Vglut , Trh
EB-DA	**Ellipsoid body and lateral accessory lobe**	**TH-F-100001**	**TH**
AOTU-BU	Anterior optic tubercule and bulb	Gad1-F-200712, VGlut-F-400630	Nsyb , GMR57C10 , Cha, Vglut, Gad
Posterior neuropil			

IB	Inferior bridge		Nsyb, Gad
ATL	Antler	adult antler neuron 031	TH, Trh
M-Omega	Posterior ensemble forming an M dorsally and an omega ventrally	TH-F-300078	TH
SPS	Superior posterior slope	VGlut-F-900089, VGlut-F-800136,Cha-F-800003,Gad1-F-900039	Nsyb , GMR57C10, Cha , Vglut , Gad
IPS-Y	inverse Y shape in the posterior slope	DNb02?	Nsyb , GMR57C10 , Cha, Vglut, Gad
LAL-PS	lateral accessory lobe and posterior slope	DNb01?	Nsyb , GMR57C10 , Cha, Vglut , Gad
PPM2-LW	**PPM2-LAL-We L,R**	**TH-F-000000,TH-F-000015,TH-F-000016**	**TH**
PPM2-VI	**PPM2-VMNP-INP L,R**	**TH-F-000007,TH-F-300058**	**TH**
Lateral neuropil			
WPENb	antennal mechanosensory and motor center and/or Wedge, in the posterior lateral protocerebrum and posterior connection to opposite side	VGlut-F-200005,WPNb, WPNB3#5 (FAFB:4271367) [VFB_001011lp]	Vglut , Gad
AMMC-PLP	antennal mechanosensory and motor center and/or Wedge and branch in the posterior lateral protocerebrum	VGlut-F-400269	Nsyb , Cha , Vglut, Gad
AMMC-WE	antennal mechanosensory and motor center and/or Wedge	VGlut-F-000138, VGlut-F-400586	Nsyb , GMR57C10 , Vglut , Gad
WE-DA	**Wedge with two branches forming a large V**	**TH-F-200127,TH-F-000024**	**TH**
AVLPonlyproj	Lowest medial part of the anterior ventral lateral protocerebrum projecting ventrally	Cha-F-700097	
AVLPprojm	Lowest medial part of the anterior ventral lateral protocerebrum projecting ventrally	Gad1-F-500762, Cha-F-400059; Gad1-F-000013	Nsyb , GMR57C10, Gad
AVLPprojl	Lowest lateral part of the anterior ventral lateral protocerebrum projecting ventrally	Cha-F-800125	Cha
AVLPm	anterior ventral lateral protocerebrum medial part	Gad1-F-900529, Cha-F-800062,Trh-F-400039,Trh-F-400070; Vglut-F-200405*; Vglut-F-900122; Cha-F-400237; Cha-F-200299; Gad1-F-500279	Nsyb , GMR57C10 , Vglut, Gad , TH, Trh, TDC

AVLPd	anterior ventral lateral protocerebrum dorsal part	Cha-F-000424	Nsyb
AVLPshell	anterior ventral lateral protocerebrum surface	Trh-F-100082	TH, Trh
AVLPsmear	anterior ventral lateral protocerebrum anterior part		Nsyb
VLPl	Ventro-lateral protocerebrum most lateral part	Gad1-F-900096, Vglut-F-500616,Cha-F-800087	Nsyb , GMR57C10 , Cha , Vglut, Gad
PLP-LH	Posterior lateral protocerebrum to the basis of the lateral horn	Gad1-F-500325	Nsyb
PLP	Posterior lateral protocerebrum	Gad1-F-800092	Nsyb, Gad
Ventral neuropil			
PI	Pars intercerebralis	Trh-F-100040, Trh-M-000056	Nsyb , GMR57C10 , TH , Trh
PI-PRW	Pars intercerebralis connected to Prow	VGlut-F-600158	Nsyb , GMR57C10 , Gad
PRW	Prow	TH-M-000037	Nsyb , GMR57C10 , Vglut, Gad , TH
PRW-SLP	Prow and superior lateral protocerebrum	Gad1-F-600213, Cha-F-200258; fru-F-000133; Gad1-F-600213; Trh-F-100091	Nsyb , GMR57C10
PENP-CL	periesophageal neuropils and clamp	mALD3_L (FlyEM-HB:822708945)	Nsyb , GMR57C10, Cha , Gad
GNGvw	gnathal ganglia medial and lateral	Cha-F-400186	Cha
GNGm	gnathal ganglia medial	Cha-F-300235	Nsyb , GMR57C10
GNGml	gnathal ganglia medial-lateral	Cha-F-400159	Nsyb , GMR57C10, Cha, Gad
GNGl	gnathal ganglia lateral	Cha-F-400146	Nsyb, Cha
GNG-AMMC	gnathal ganglia and on the opposite side antennal mechanosensory and motor center and posterior lateral protocebrum	VGlut-F-600685	Nsyb, Vglut
GNGva	ventral anterior part of the gnathal ganglia		Nsyb
vaCells	ventral anterior cells	TH-F-100049	TH , Trh
Optic lobe			
OL	Optic lobe; mostly medulla and lobulla		Nsyb, GMR57C10 , Cha , Vglut , Gad
LOP	Lobulla plate	Cha-F-600161	Cha, TDC
OL-FB	Optic lobe to central regions including the fan-shaped body		TH
OL-PENP	Optic lobe and periesophageal neuropils	Tdc2-F-200056	Nsyb , Gad , Trh , TDC

OL-PLP	Optic lobe and posterior lateral protocerebrum	Cha-F-000316	Nsyb , Cha, Gad
OL-WE	Optic lobe and wedge	TH-F-300030	TH

1248
1249
1250

A

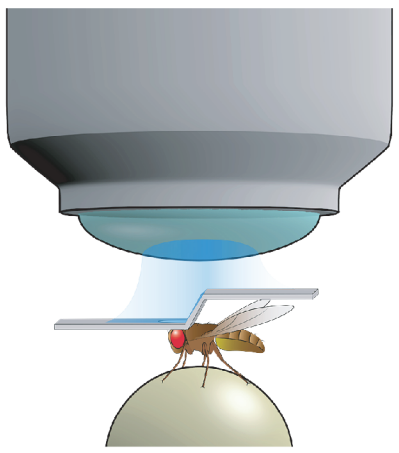

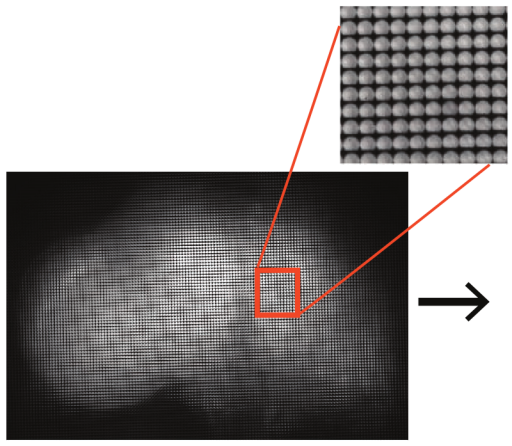

wholebrain image

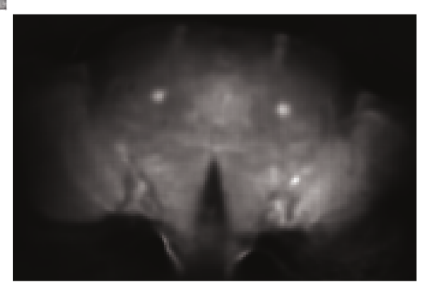

lightfield deconvolution

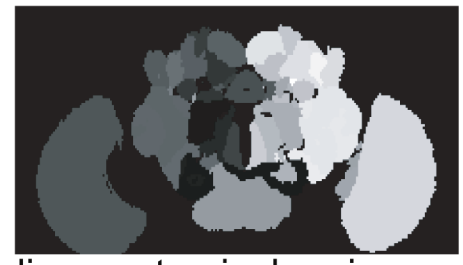

align anatomical regions

functional components

B

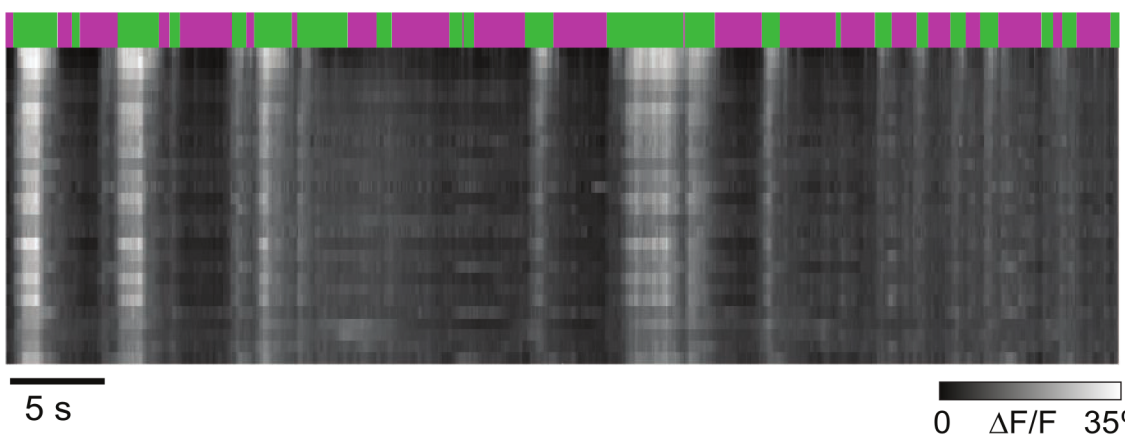

E

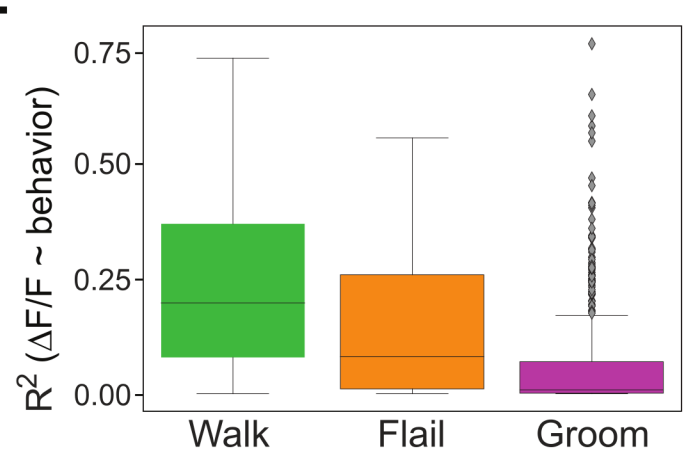

C

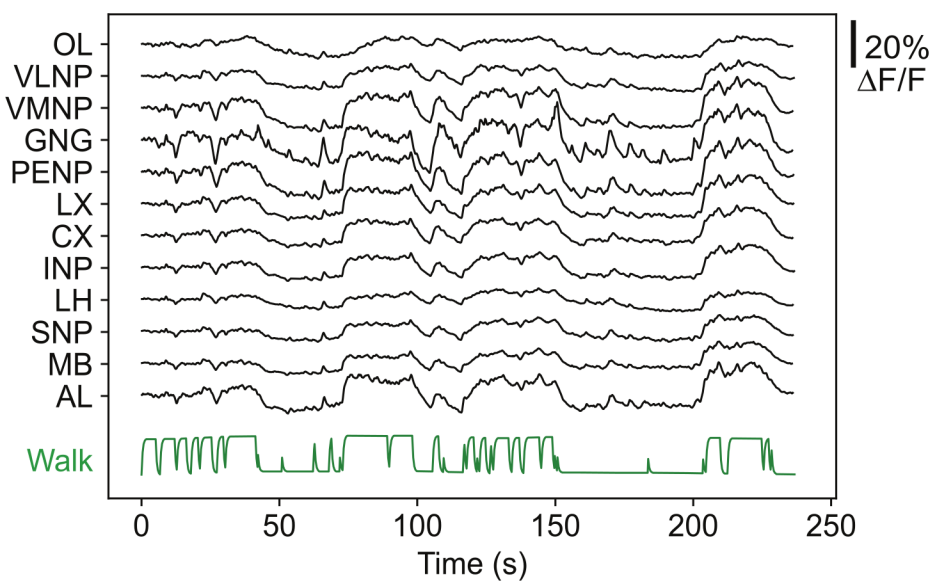

G

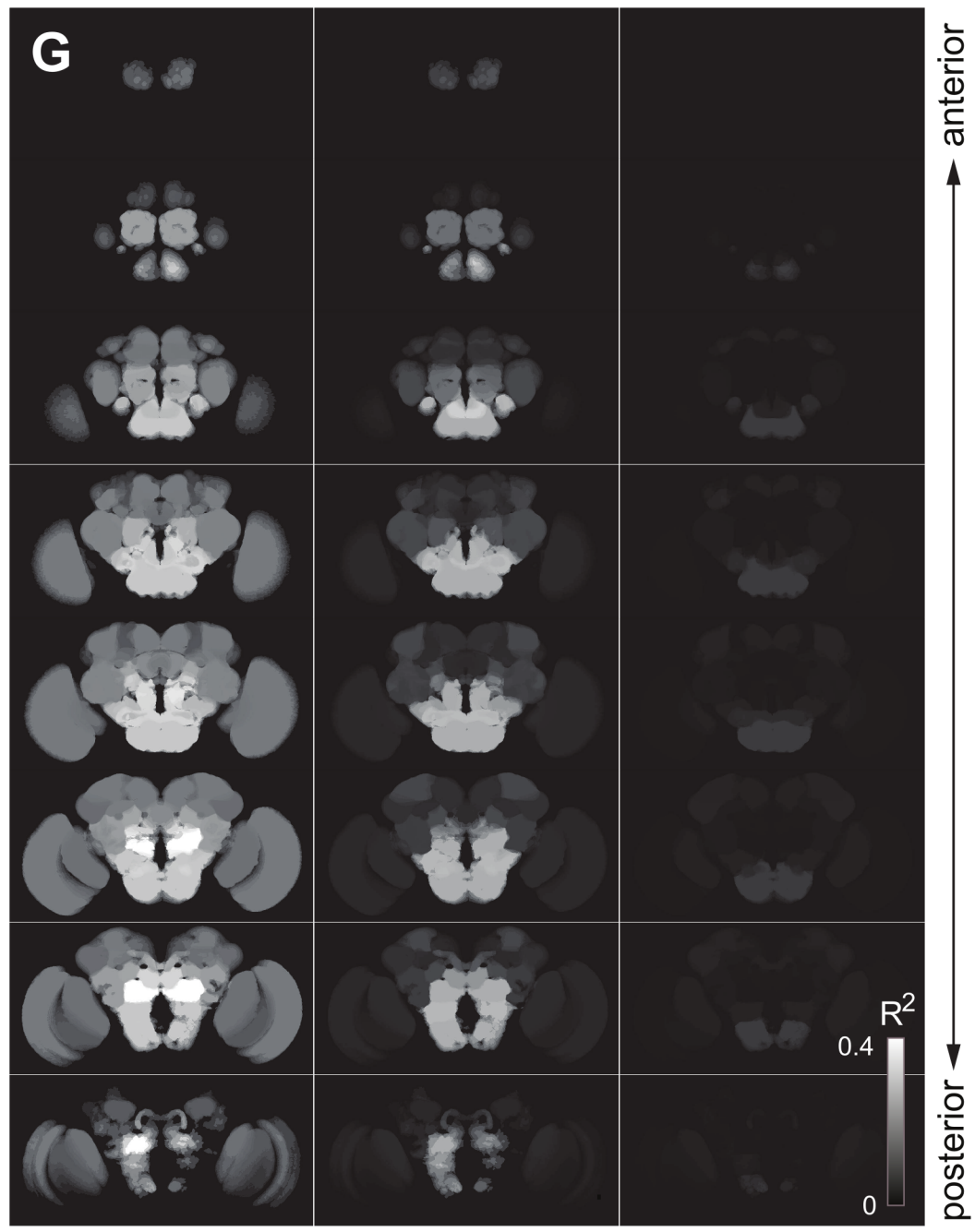

D

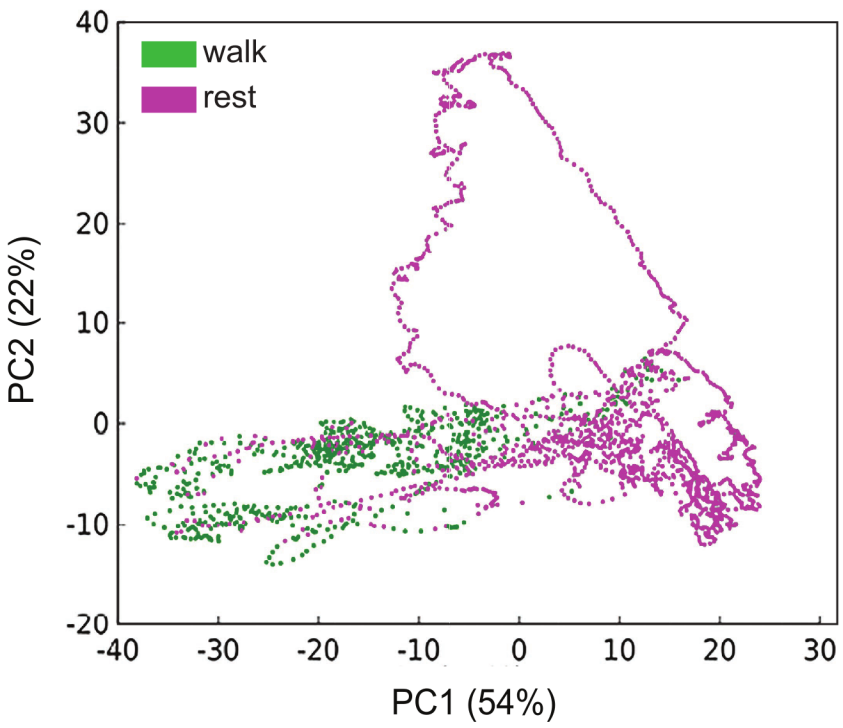

F

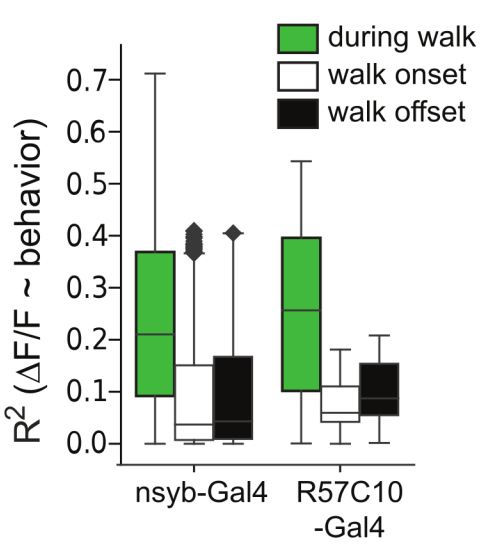

H

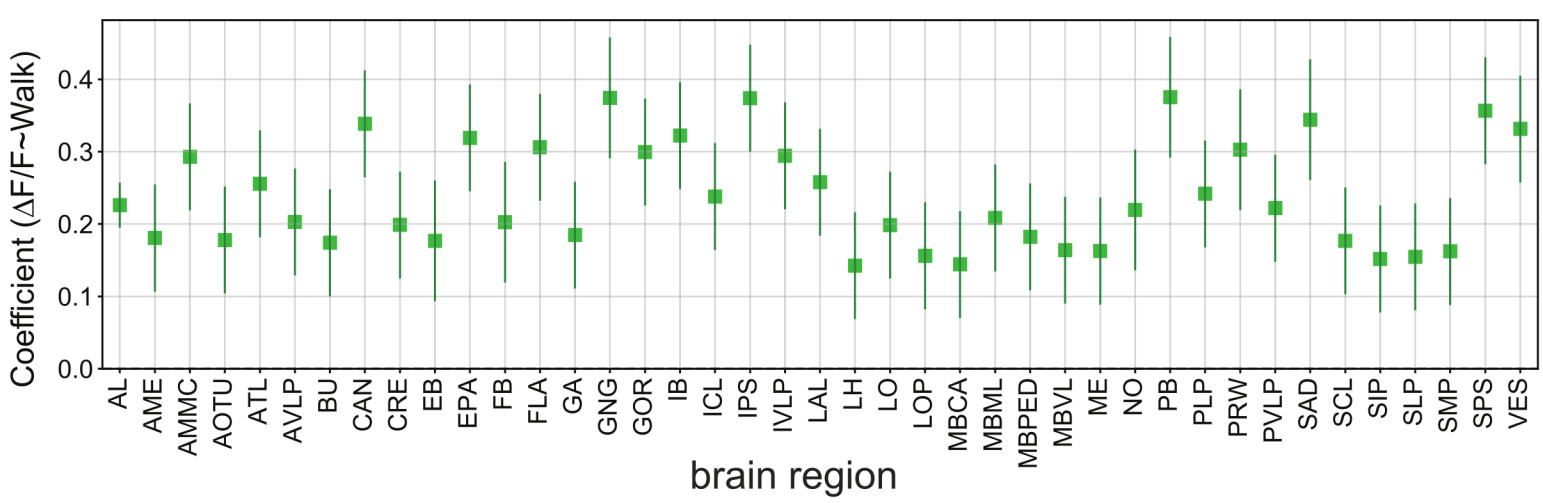

A

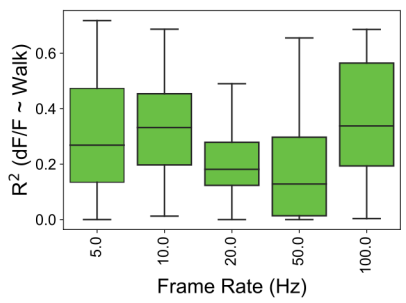

B

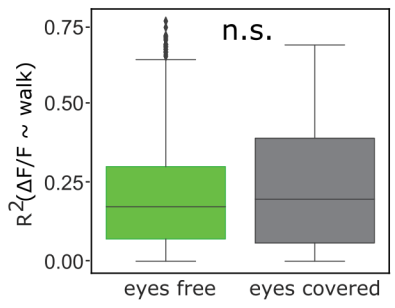

C

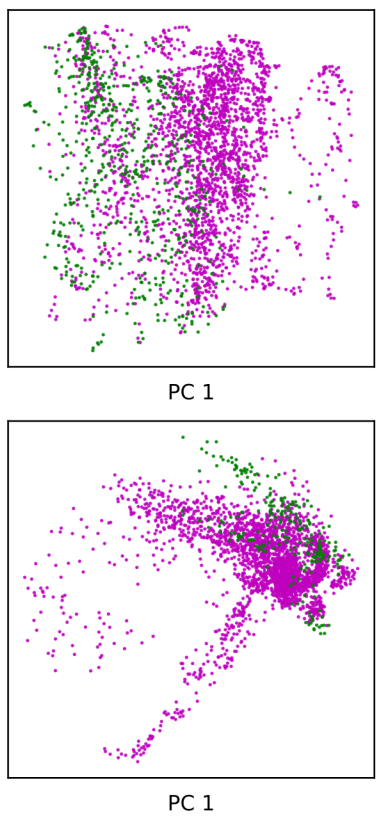

D

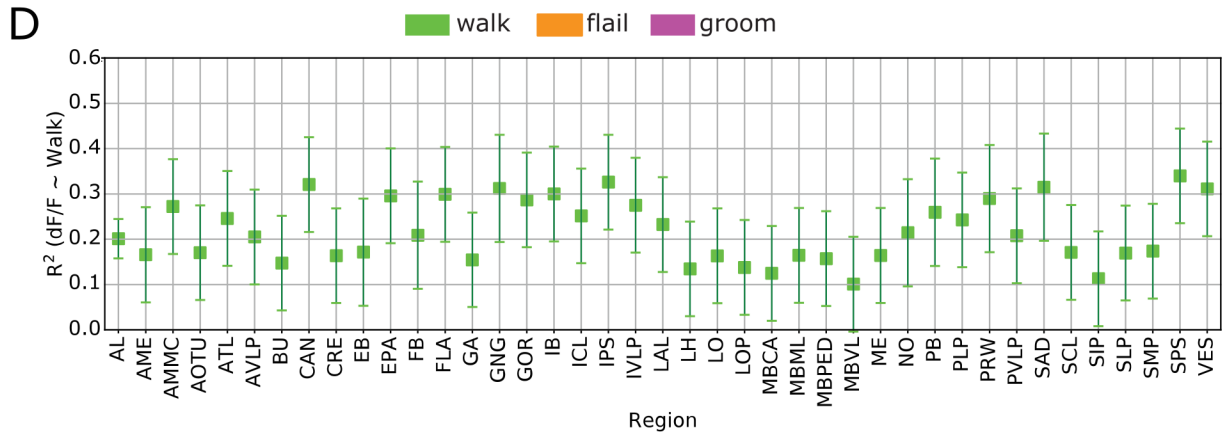

E

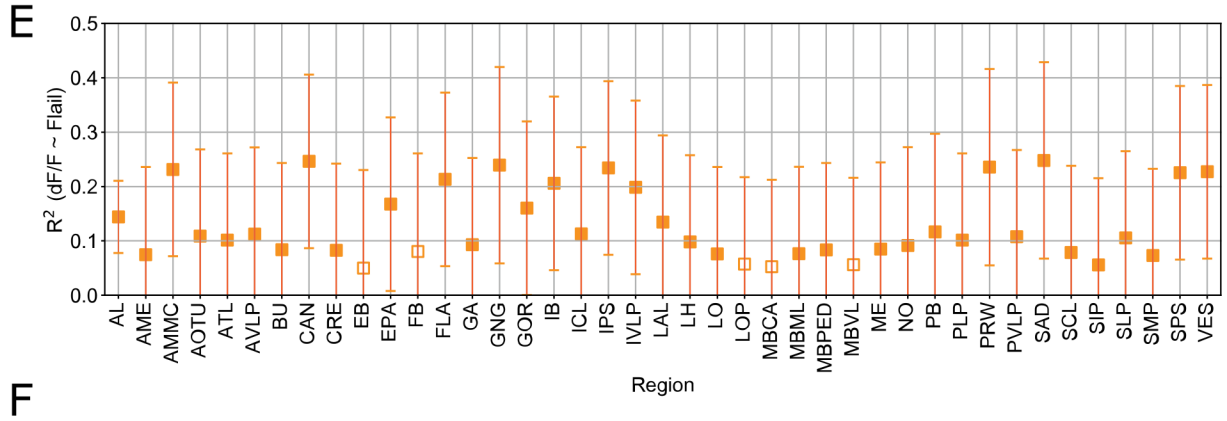

F

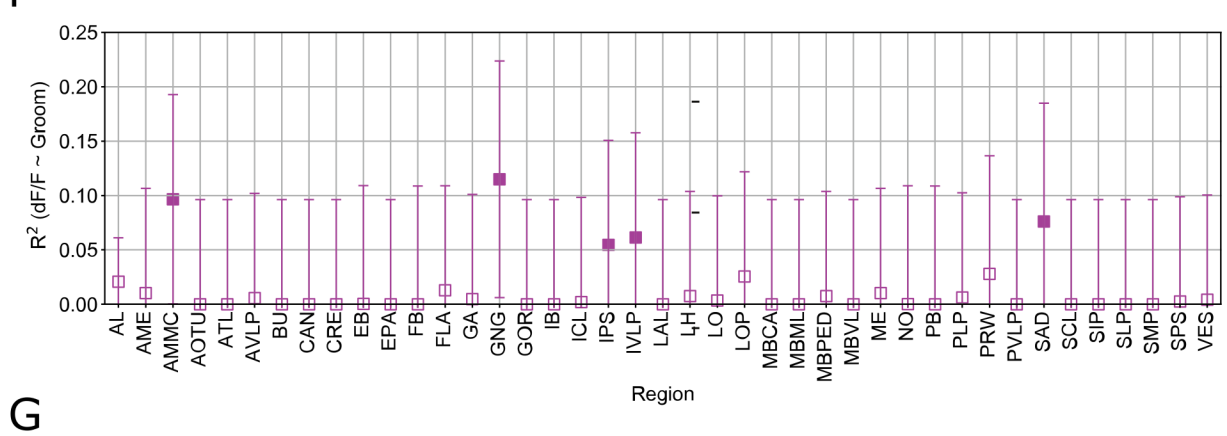

G

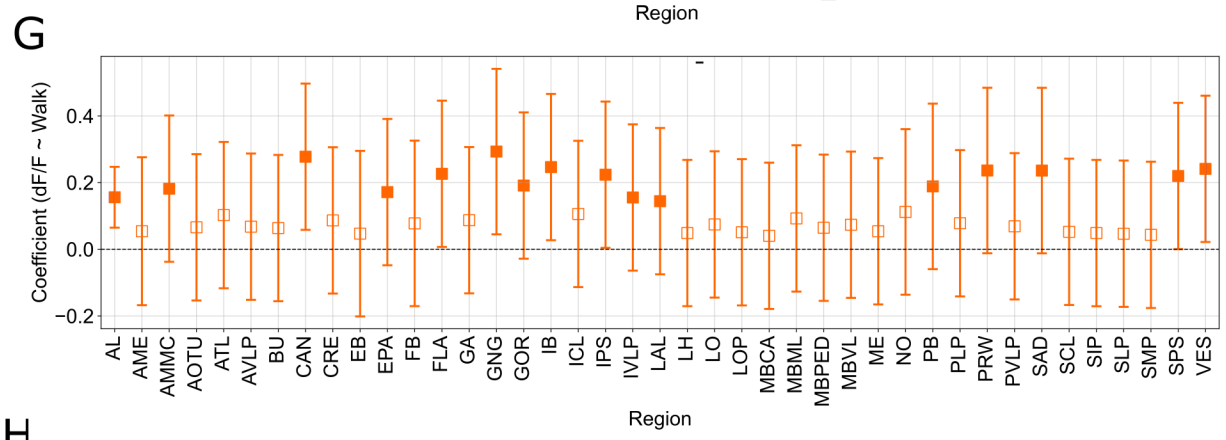

H

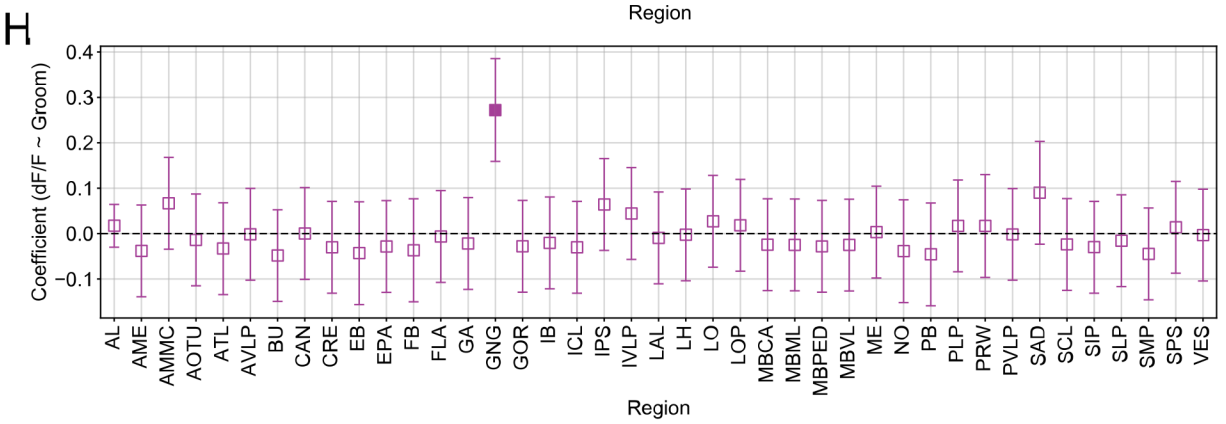

I

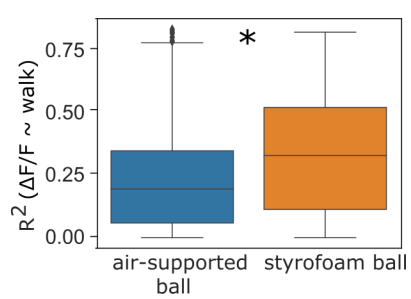

J

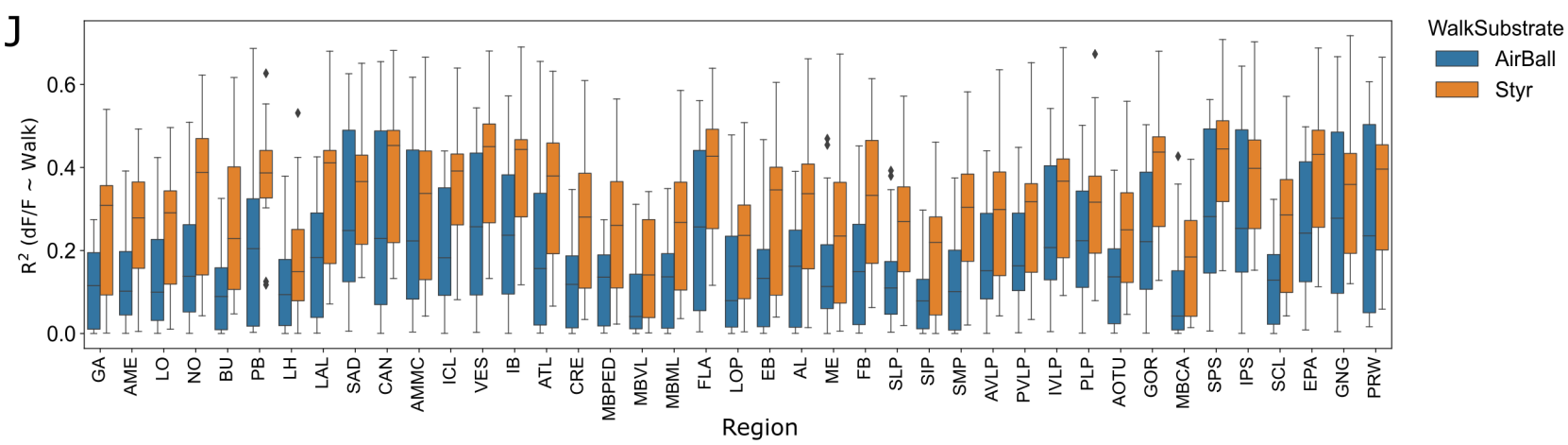

K

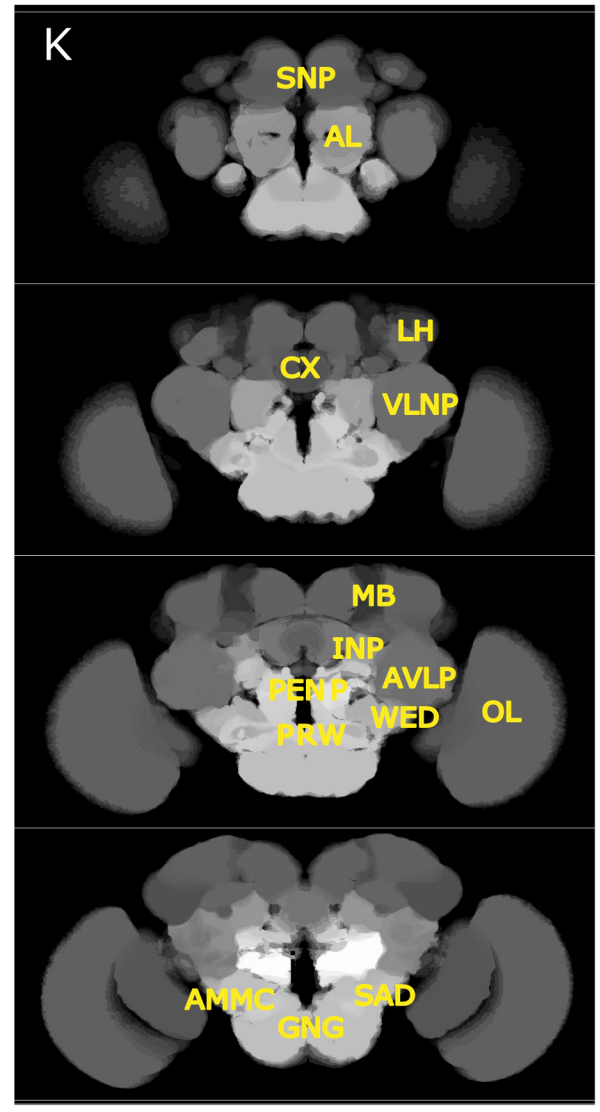

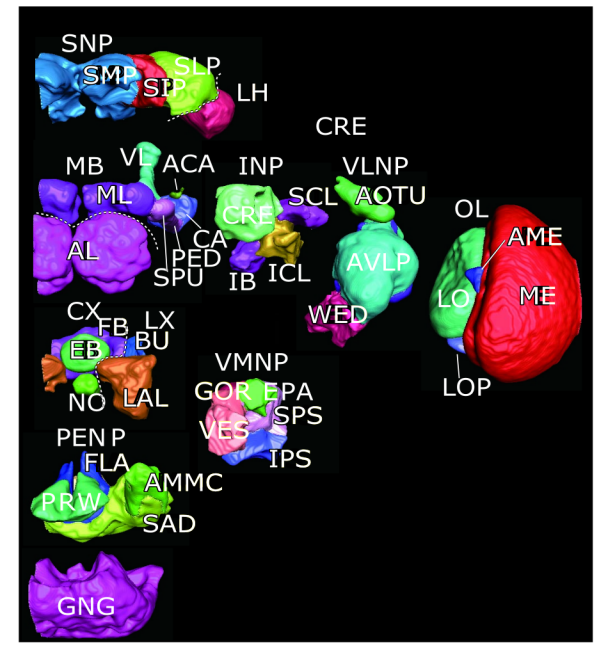

A

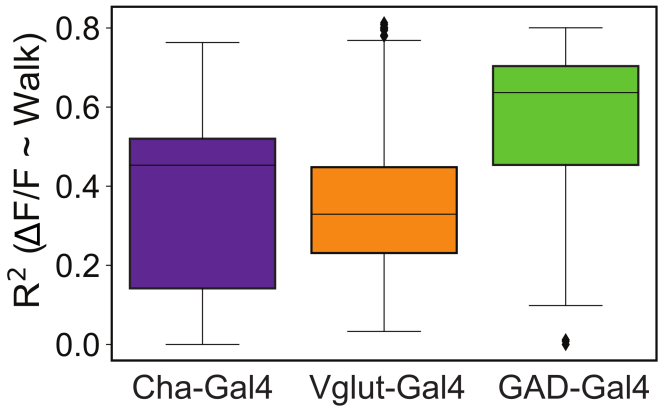
R^2 (ΔF/F ~ Walk)
0.0
0.2
0.4
0.6
0.8
Cha-Gal4
Vglut-Gal4
GAD-Gal4

B

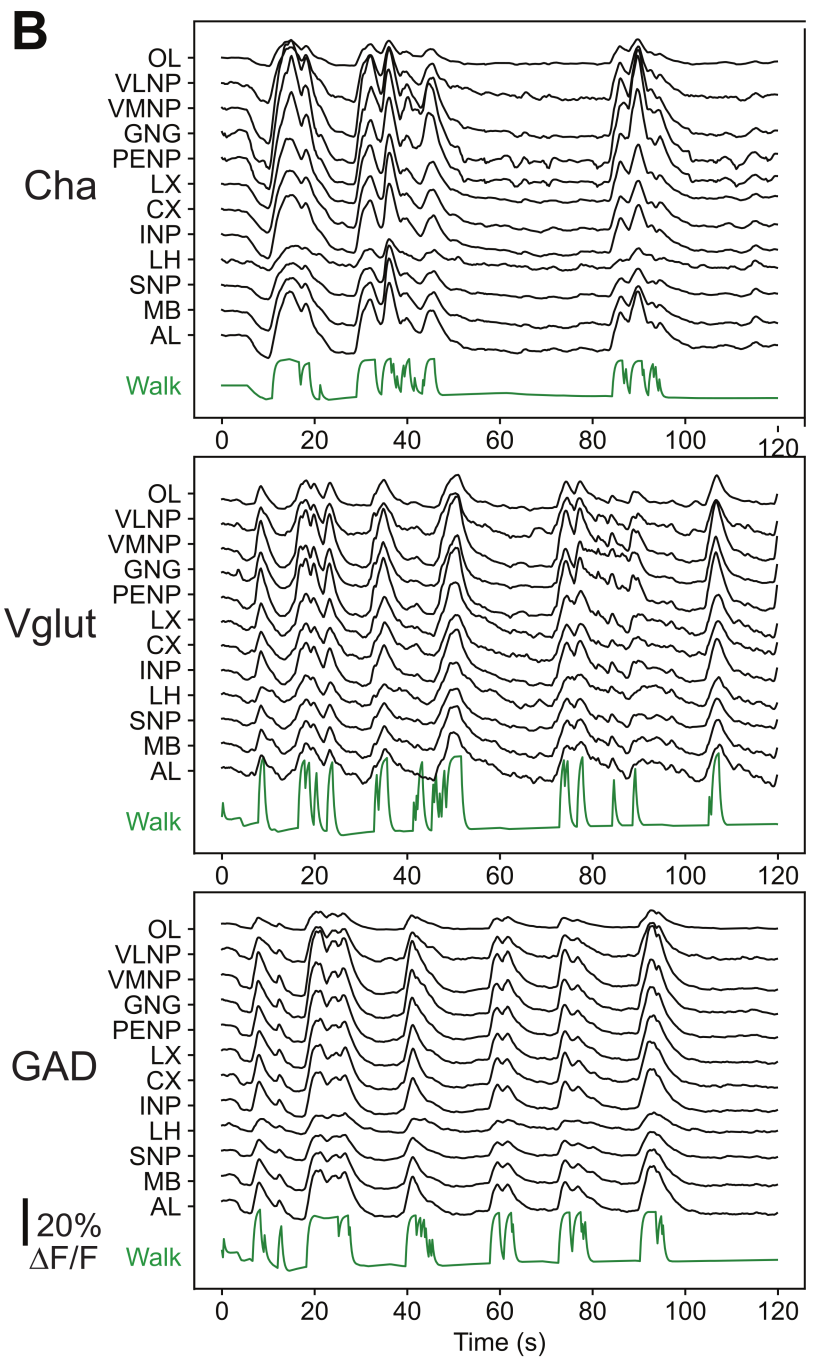
Cha
Vglut
GAD
OL
VLNP
VMNP
GNG
PENP
LX
CX
INP
LH
SNP
MB
AL
Walk
0
20
40
60
80
100
120
20%
ΔF/F
Time (s)

C

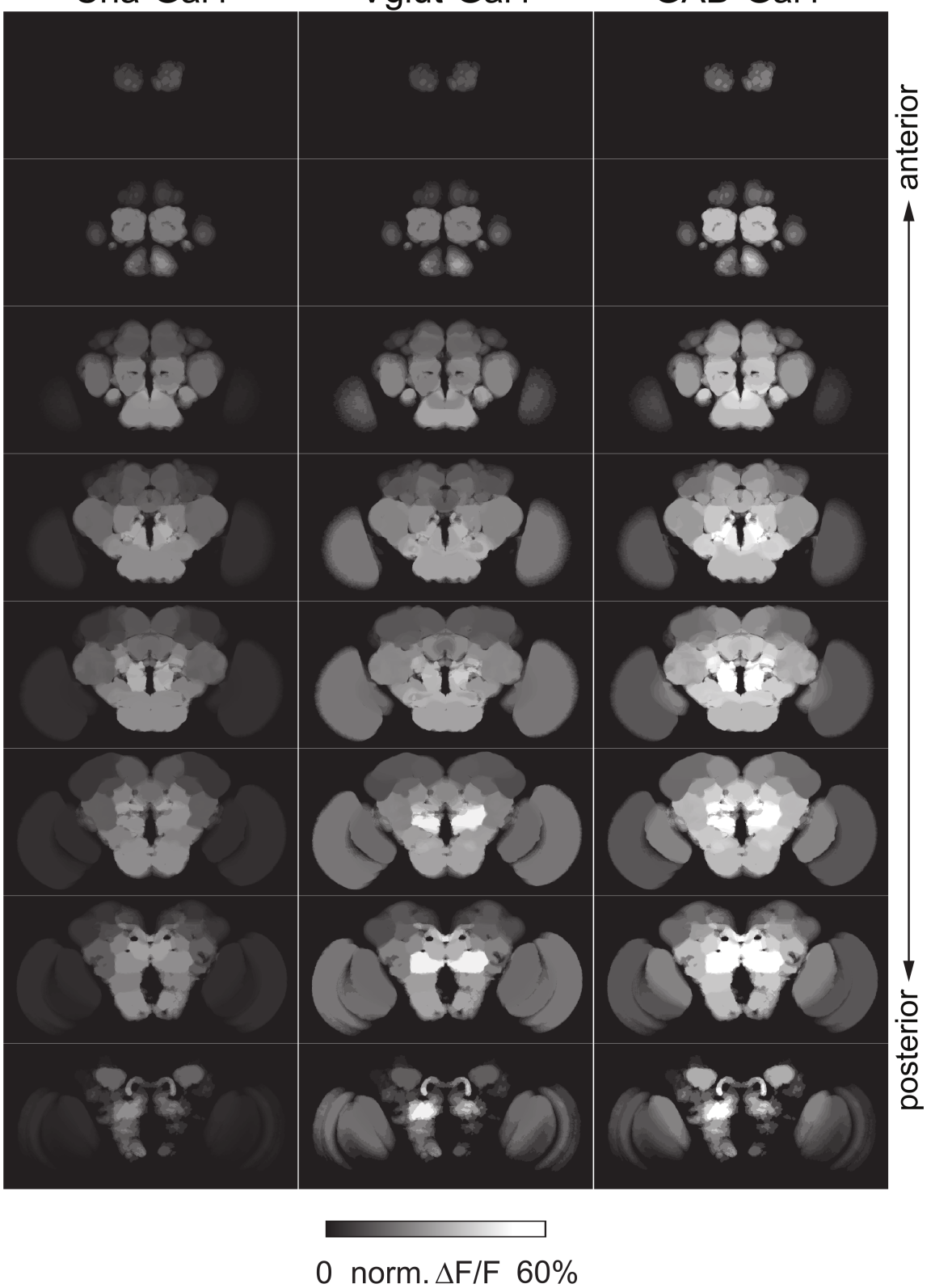
Cha-Gal4
Vglut-Gal4
GAD-Gal4
anterior
posterior
0 norm. ΔF/F 60%

D

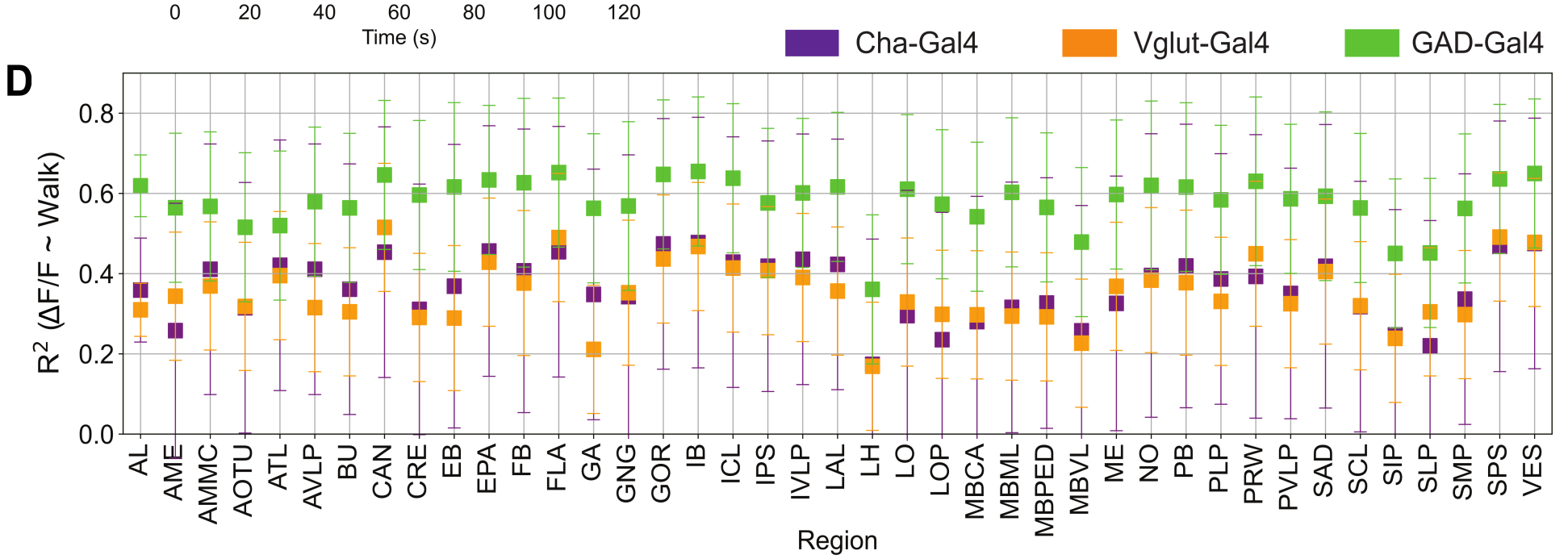
Cha-Gal4
Vglut-Gal4
GAD-Gal4
R^2 (ΔF/F ~ Walk)
0.0
0.2
0.4
0.6
0.8
AL
AME
AMMC
AOTU
ATL
AVLP
BU
CAN
CRE
EB
EPA
FB
FLA
GA
GNG
GOR
IB
ICL
IPS
IVLP
LAL
LH
LO
LOP
MBCA
MBML
MBPED
MBVL
ME
NO
PB
PLP
PRW
PVLP
SAD
SCL
SIP
SLP
SMP
SPS
VES
Region

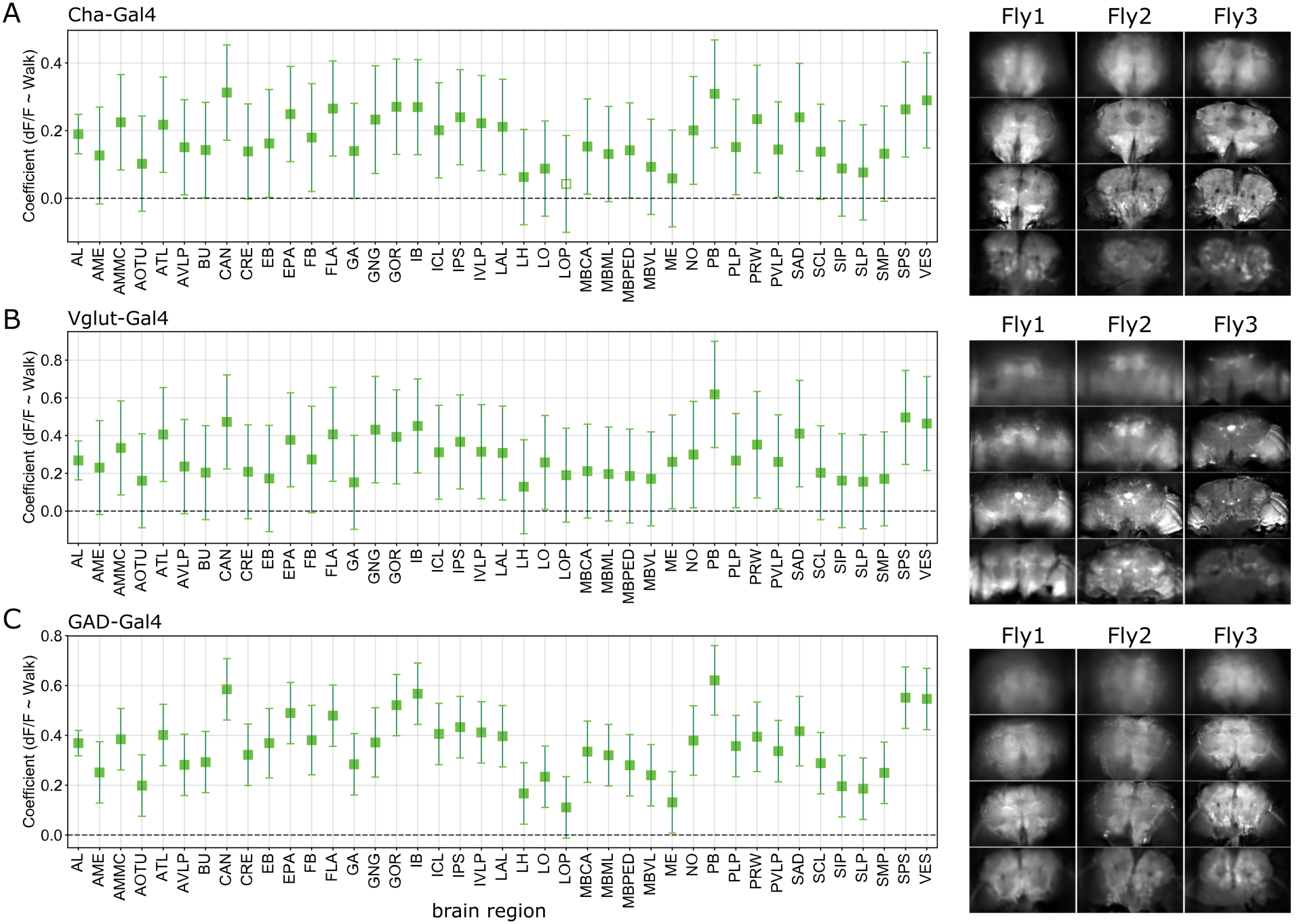
A
Cha-Gal4
B
Vglut-Gal4
C
GAD-Gal4
Coefficient (dF/F ~ Walk)
0.0
0.2
0.4
0.6
0.8
AL AME AMMC AOTU ATL AVLP BU CAN CRE EB EPA FB FLA GA GNG GOR IB ICL IPS IVLP LAL LH LO LOP MBCA MBML MBPED MBVL ME NO PB PLP PRW PVLP SAD SCL SIP SLP SMP SPS VES
brain region
Fly1
Fly2
Fly3

A

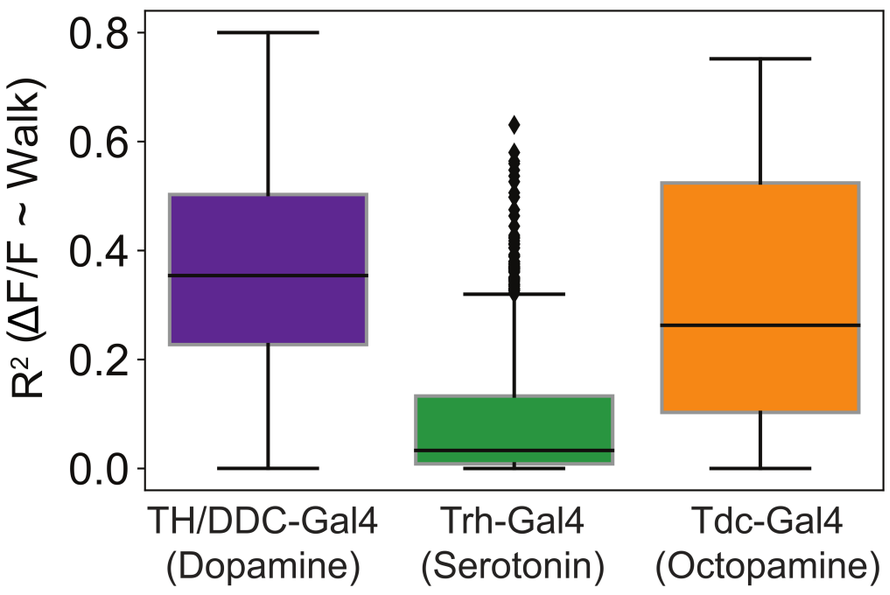
0.8
0.6
0.4
0.2
0.0
R² (ΔF/F ~ Walk)
TH/DDC-Gal4
(Dopamine)
Trh-Gal4
(Serotonin)
Tdc-Gal4
(Octopamine)

B

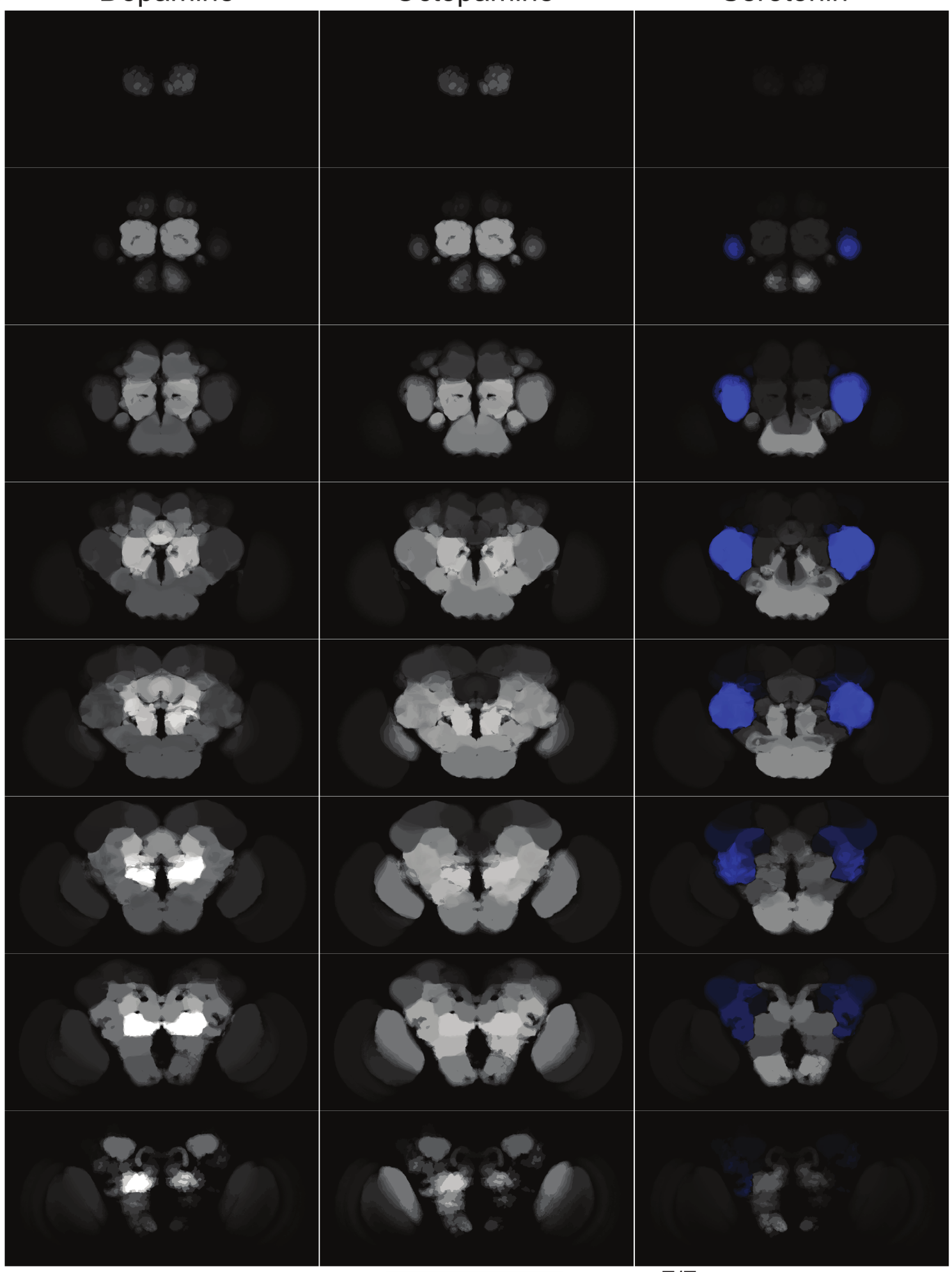
Dopamine
Octopamine
Serotonin
anterior
posterior
norm. ΔF/F
-20%
0
40%

C

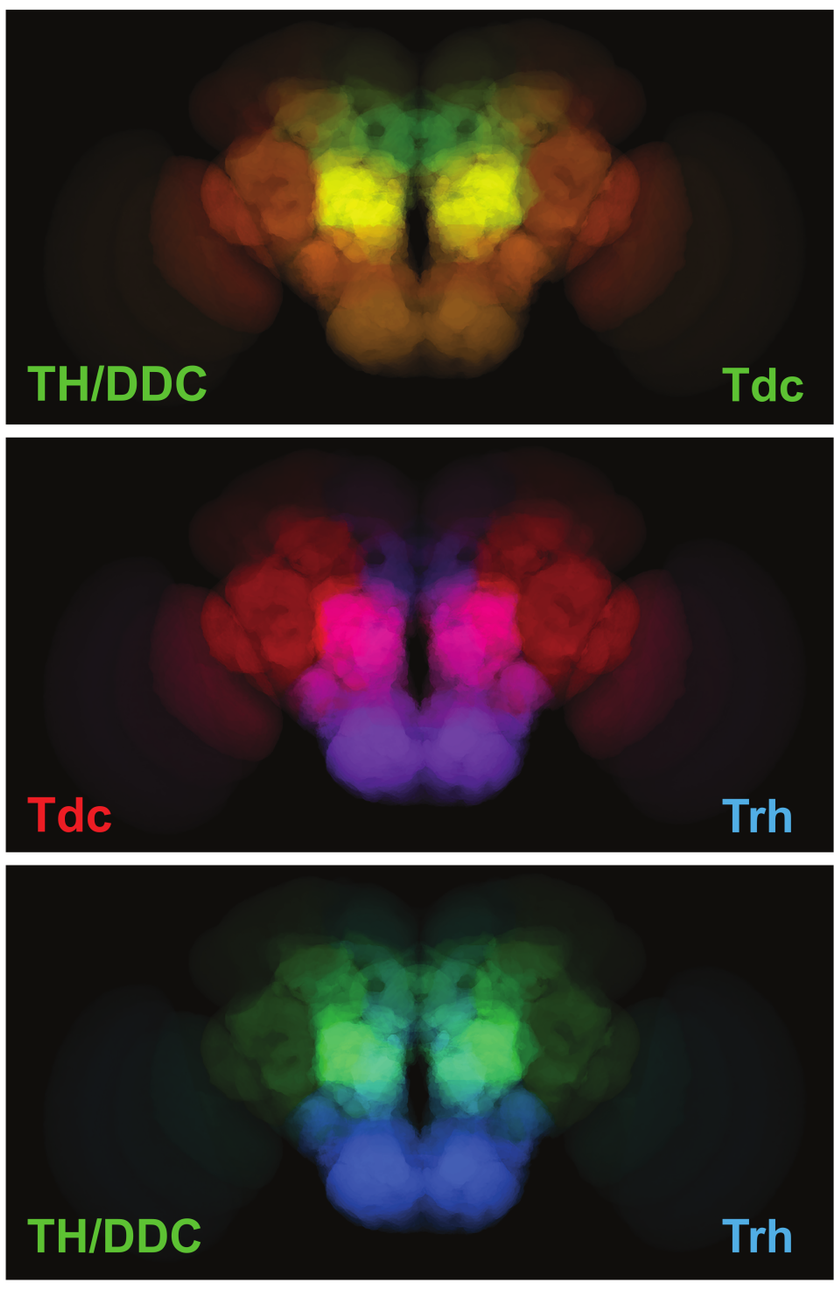
TH/DDC
Tdc
Tdc
Trh
TH/DDC
Trh

D

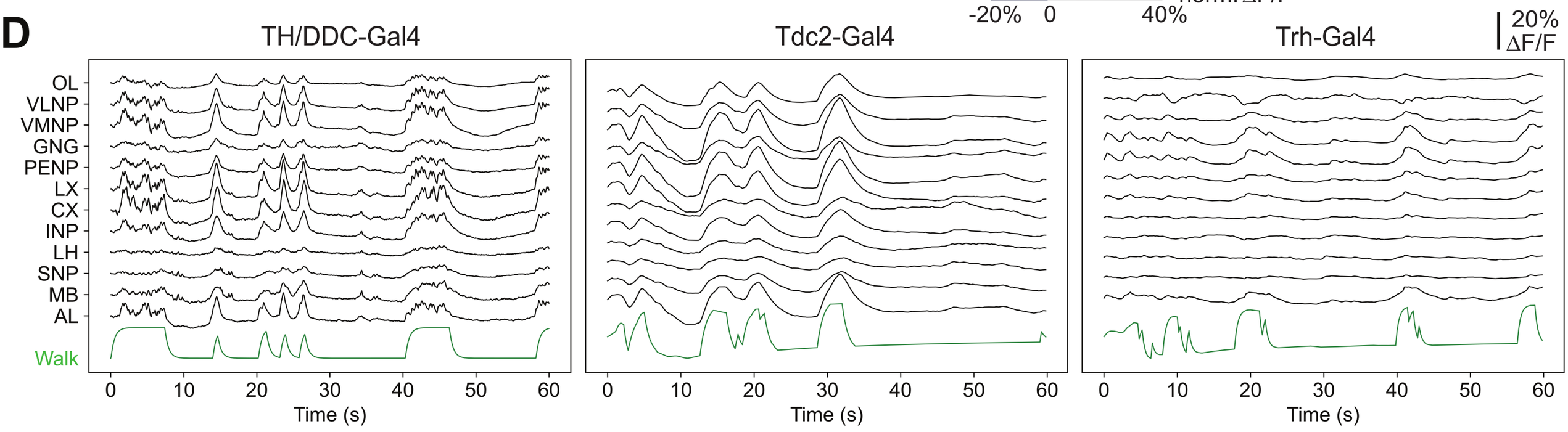
TH/DDC-Gal4
Tdc2-Gal4
Trh-Gal4
20%
ΔF/F
OL
VLNP
VMNP
GNG
PENP
LX
CX
INP
LH
SNP
MB
AL
Walk
0
10
20
30
40
50
60
Time (s)

E

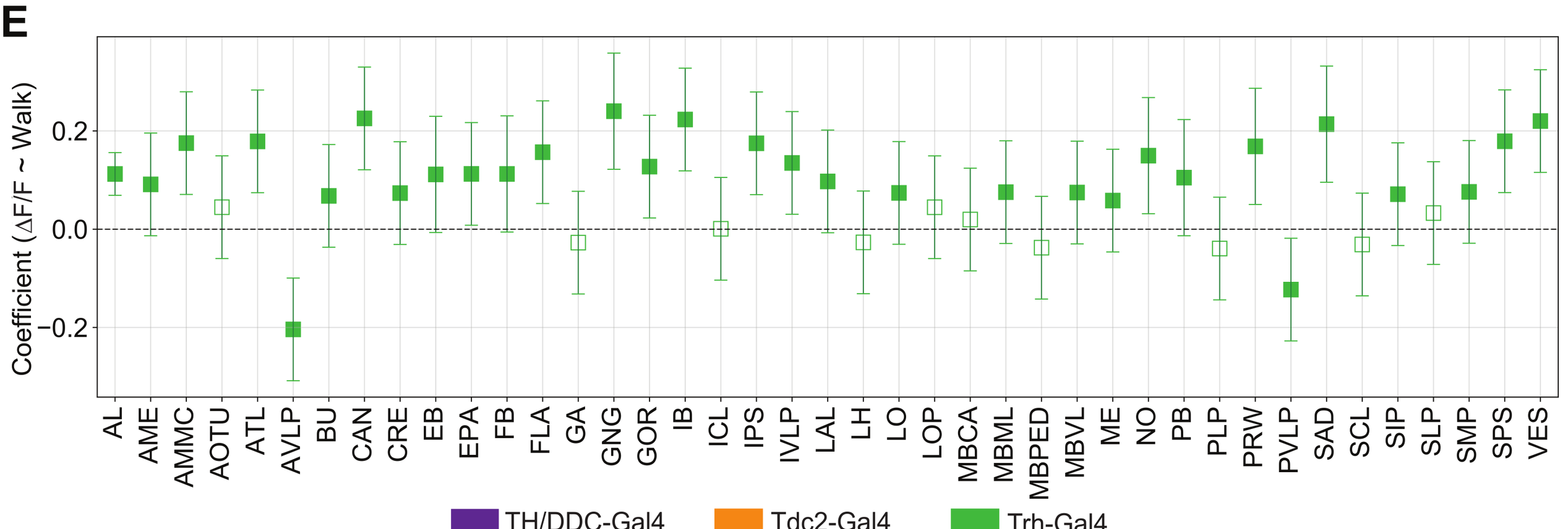
Coefficient (ΔF/F ~ Walk)
0.2
0.0
−0.2
AL
AME
AMMC
AOTU
ATL
AVLP
BU
CAN
CRE
EB
EPA
FB
FLA
GA
GNG
GOR
IB
ICL
IPS
IVLP
LAL
LH
LO
LOP
MBCA
MBML
MBPED
MBVL
ME
NO
PB
PLP
PRW
PVLP
SAD
SCL
SIP
SLP
SMP
SPS
VES

F

TH/DDC-Gal4
Tdc2-Gal4
Trh-Gal4
R² (ΔF/F ~ Walk)
0.8
0.6
0.4
0.2
0.0
AL
AME
AMMC
AOTU
ATL
AVLP
BU
CAN
CRE
EB
EPA
FB
FLA
GA
GNG
GOR
IB
ICL
IPS
IVLP
LAL
LH
LO
LOP
MBCA
MBML
MBPED
MBVL
ME
NO
PB
PLP
PRW
PVLP
SAD
SCL
SIP
SLP
SMP
SPS
VES
brain region

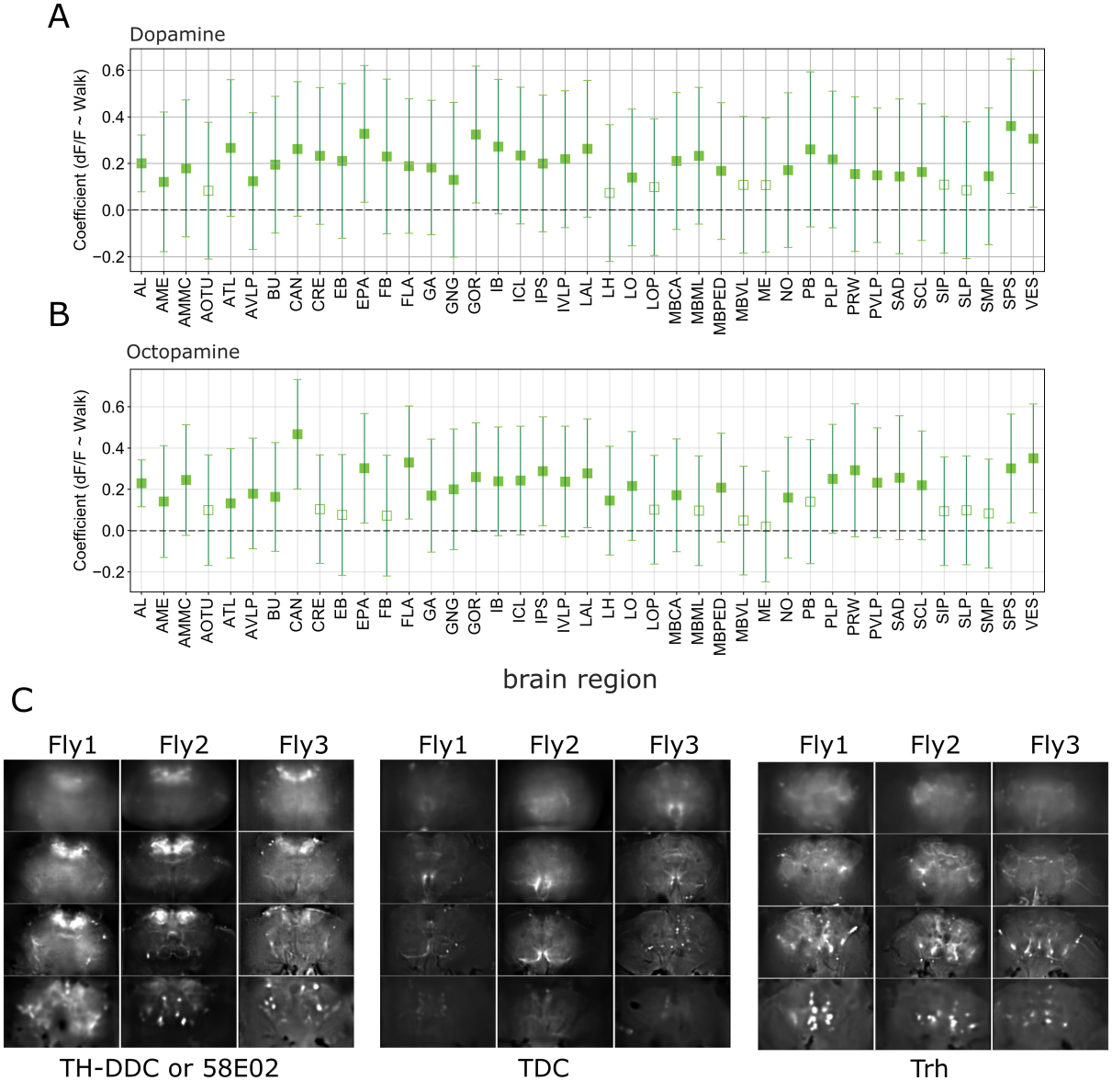
A
Dopamine
Coefficient (dF/F ~ Walk)
0.6
0.4
0.2
0.0
−0.2
AL AME AMMC AOTU ATL AVLP BU CAN CRE EB EPA FB FLA GA GNG GOR IB ICL IPS IVLP LAL LH LO LOP MBCA MBML MBPED MBVL ME NO PB PLP PRW PVLP SAD SCL SIP SLP SMP SPS VES
B
Octopamine
Coefficient (dF/F ~ Walk)
0.6
0.4
0.2
0.0
−0.2
AL AME AMMC AOTU ATL AVLP BU CAN CRE EB EPA FB FLA GA GNG GOR IB ICL IPS IVLP LAL LH LO LOP MBCA MBML MBPED MBVL ME NO PB PLP PRW PVLP SAD SCL SIP SLP SMP SPS VES
brain region
C
Fly1 Fly2 Fly3
Fly1 Fly2 Fly3
Fly1 Fly2 Fly3
TH-DDC or 58E02
TDC
Trh

A

pan neuronal

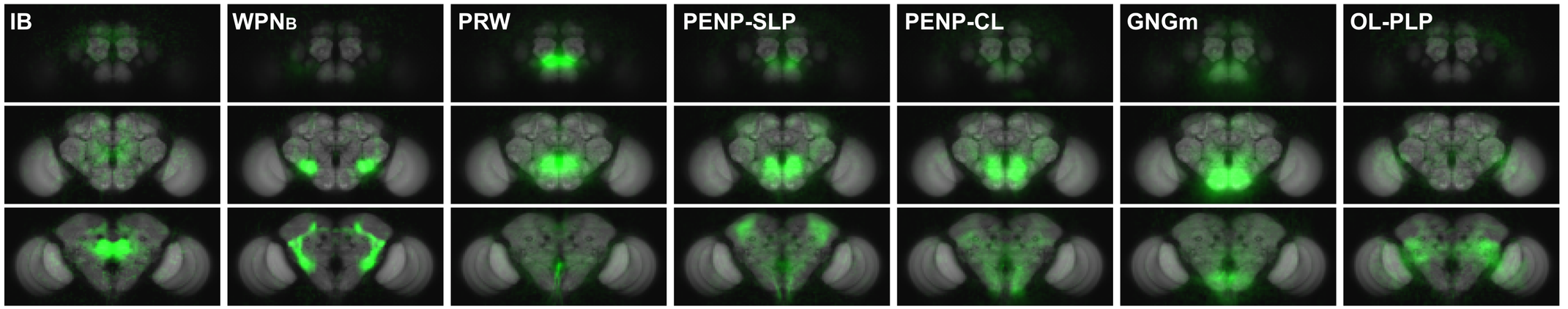

Octopamine

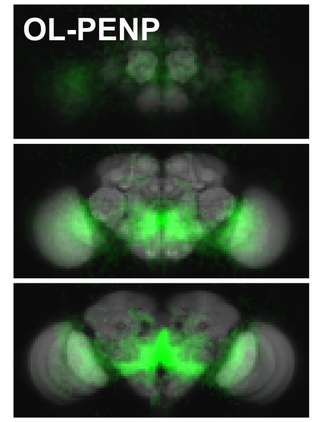

Dopamine

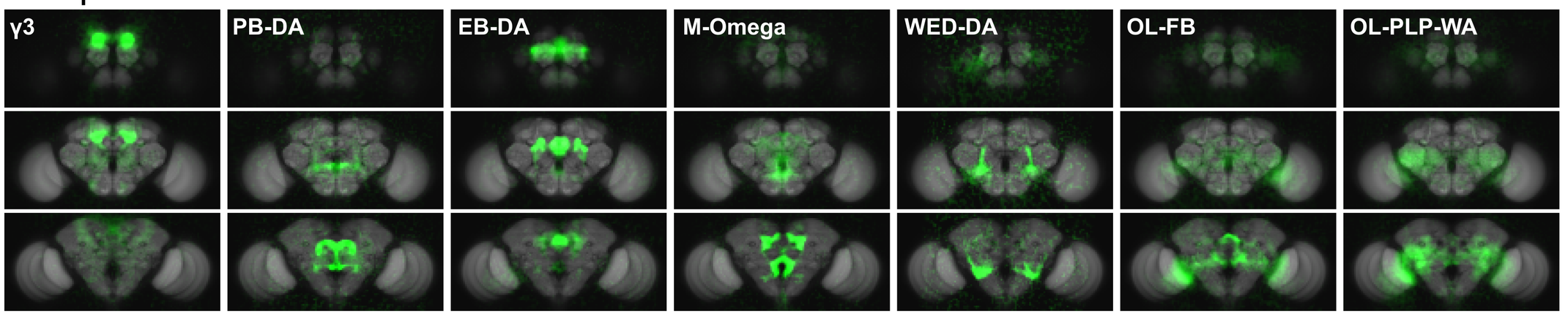

Serotonin

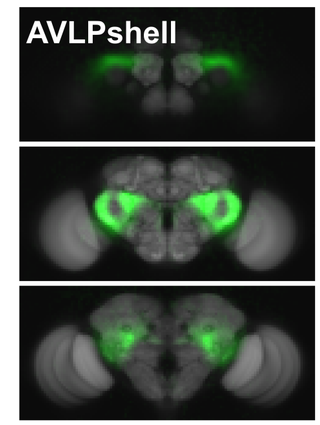

B

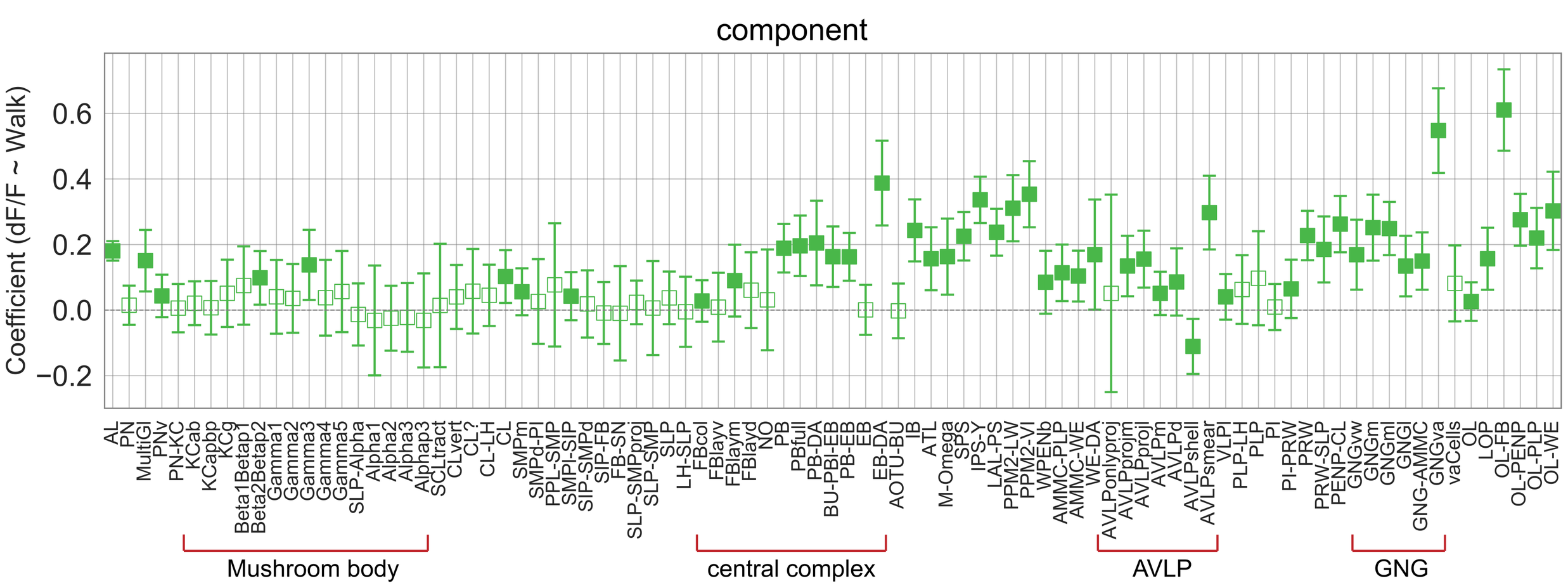

A

superior neuropils
mushroom body
olfactory system
central complex
posterior neuropils
lateral neuropils
ventral neuropils
optic lobes

B

AL
PN
MultiGl
PNv
PN-KC
KCab
KCapbp
KCg
Beta1Betap1
Beta2Betap2
Gamma1
Gamma2
Gamma3
Gamma4
Gamma5
SLP-Alpha
Alpha1
Alpha2
Alpha3
Alphap3
SCLtract
CLvert
CL?
CL-LH
CL
SMPm
SMPd-PI
PPL-SMP
SMPI-SIP
SIP-SMPd
SIP-FB
FB-SN
SLP-SMPproj
SLP-SMP
SLP
LH-SLP
FBcol
FBlaym
FBlayd
NO
PB
PBfull
PB-DA
BU-PBI-EB
PB-EB
EB
EB-DA
AOTU-BU
IB
ATL
M-Omega
SPS
IPS-Y
LAL-PS
PPM2-LW
PPM2-VI
WPENb
AMMC-PLP
AMMC-WE
WE-DA
AVLPonlyproj
AVLPprojm
AVLPproji
AVLPm
AVLPd
AVLPshell
AVLPsmear
VLPl
PLP-LH
PLP
PI
PI-PRW
PRW
PRW-SLP
PENP-CL
GNGvw
GNGm
GNGml
GNGl
GNG-AMMC
GNGva
vaCells
OL
LOP
OL-FB
OL-PENP
OL-PLP
OL-WE

C

R^2 (dF/F ~ Walk)

0.0
0.2
0.4
0.6
0.8

component

Mushroom body
central complex
AVLP
GNG

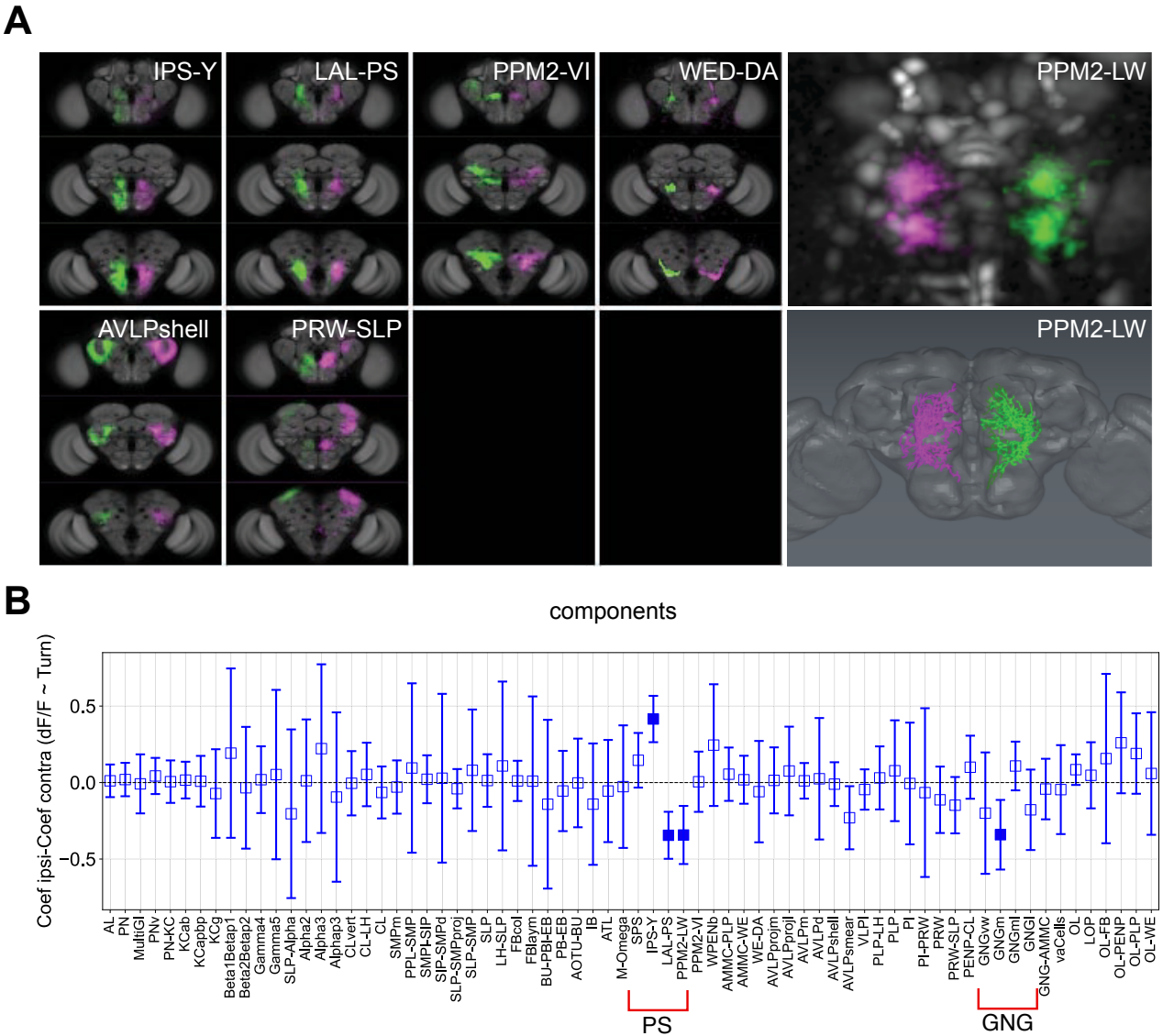
A
IPS-Y
LAL-PS
PPM2-VI
WED-DA
PPM2-LW
AVLPshell
PRW-SLP
PPM2-LW
B
components
Coef ipsi-Coef contra (dF/F ~ Turn)
0.5
0.0
−0.5
AL
PN
MultiGl
PNv
PN-KC
KCab
KCapbp
KCg
Beta1Betap1
Beta2Betap2
Gamma4
Gamma5
SLP-Alpha
Alpha2
Alpha3
Alphap3
CLvert
CL-LH
CL
SMPm
PPL-SMP
SMPl-SIP
SIP-SMPd
SLP-SMPproj
SLP-SMP
SLP
LH-SLP
FBcol
FBlaym
BU-PBl-EB
PB-EB
AOTU-BU
IB
ATL
M-Omega
SPS
IPS-Y
LAL-PS
PPM2-LW
PPM2-VI
WPENb
AMMC-PLP
AMMC-WE
WE-DA
AVLPprojm
AVLPprojl
AVLPm
AVLPd
AVLPshell
AVLPsmear
VLPl
PLP-LH
PLP
Pl
Pl-PRW
PRW
PRW-SLP
PENP-CL
GNGvw
GNGm
GNGml
GNGl
GNG-AMMC
vaCells
OL
LOP
OL-FB
OL-PENP
OL-PLP
OL-WE
PS
GNG

A

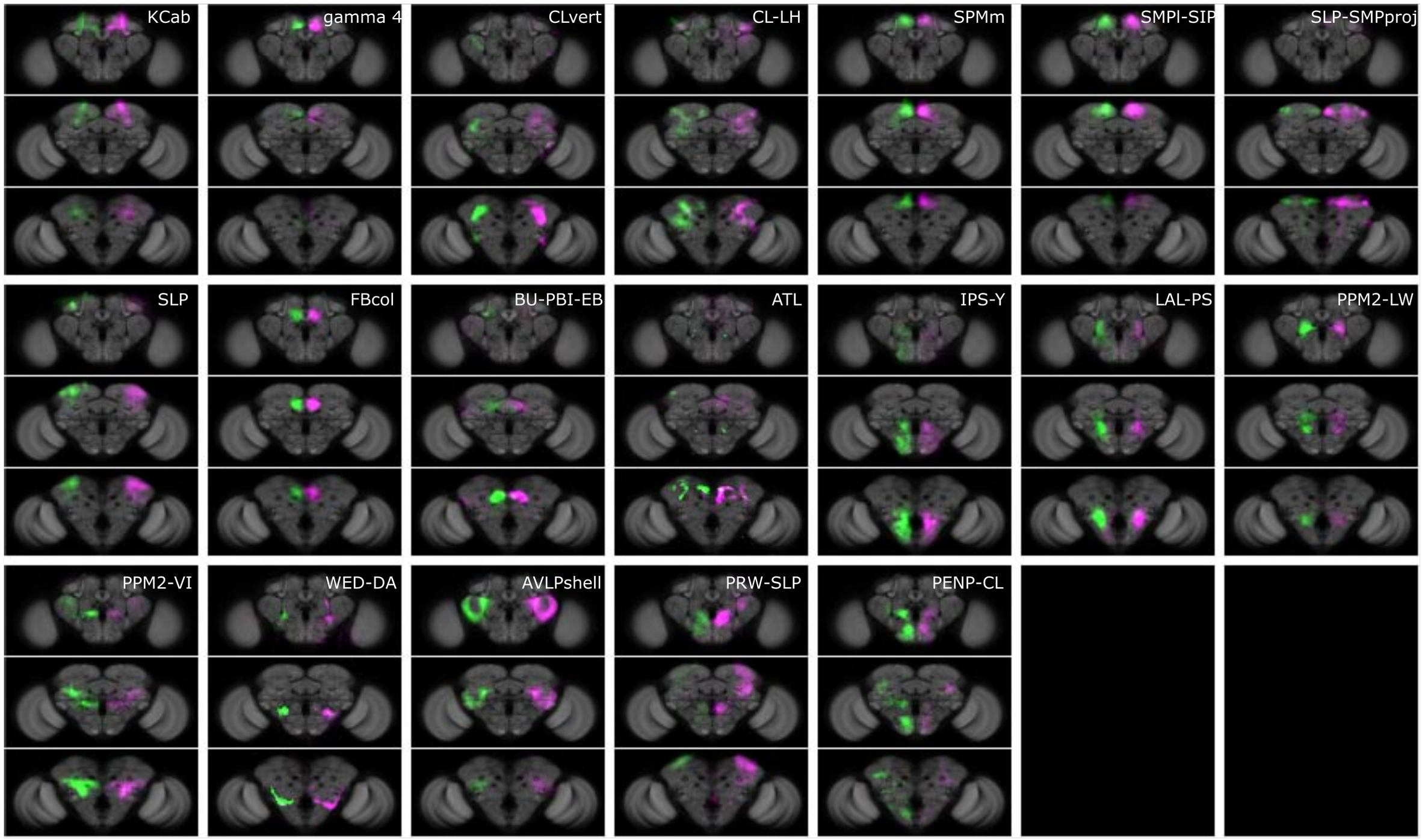

components

B

olfactory system

AL
MultiGl
PNv

mushroom body

β1β'1
γ1
γ2
γ3
γ4

superior proto-cerebrum

SMPl-SIP
SIP-FB
SLP
LH-SLP
SLP-SMPproj

central complex

FBlaym
FBlayd
PB-EB
EB
EB-DA

posterior regions

IB
M-Omega
SPS
IPS-Y
LAL-PS

lateral proto-cerebrum

AVLPprojm
AVLPm
AVLPshell
AVLPsmear
WE-DA

ventral regions

PRW
PRW-SLP
PENP-CL
GNGm
GNGml

visual system

OL
OL-FB
OL-PENP
OL-PLP
OL-PLP-WE

- Tdc2
- Trh
- TH/DDC
- Gad
- Vglut
- Cha
- Pan-neuronal

AL PN MultiGl PNv PN-KC KCab KCapbp KCg

Beta1Betap1 Beta2Betap2 Gamma1 Gamma2 Gamma3 Gamma4 Gamma5 SLP-Alpha

Alpha1 Alpha2 Alpha3 Alphap3 SCLtract CLvert CLint CL-LH

CL SMPm PPL-SMP SMPl-SIP SIP-SMPd SIP-FB FB-SN SLP-SMPproj

SLP-SMP SLP LH-SLP FBcol FBlayv FBlaym FBlayd NO

PB PBfull PB-DA BU-PBl-EB PB-EB EB EB-DA AOTU-BU

IB ATL M-Omega SPS IPS-Y LAL-PS PPM2-LW PPM2-VI

WPENb AMMC-PLP AMMC-WE WE-DA AVLPonlyproj AVLPprojm AVLPprojl AVLPm

AVLPd AVLPshell AVLPsmear VLPl PLP-LH PLP PI PI-PRW

PRW PRW-SLP PENP-CL GNGvw GNGm GNGml GNGl GNG-AMMC

GNGva vaCells OL LOP OL-FB OL-PENP OL-PLP OL-WE

Corr. ΔF/F
0.8
0
-0.8
-1
0
1
Time (s)

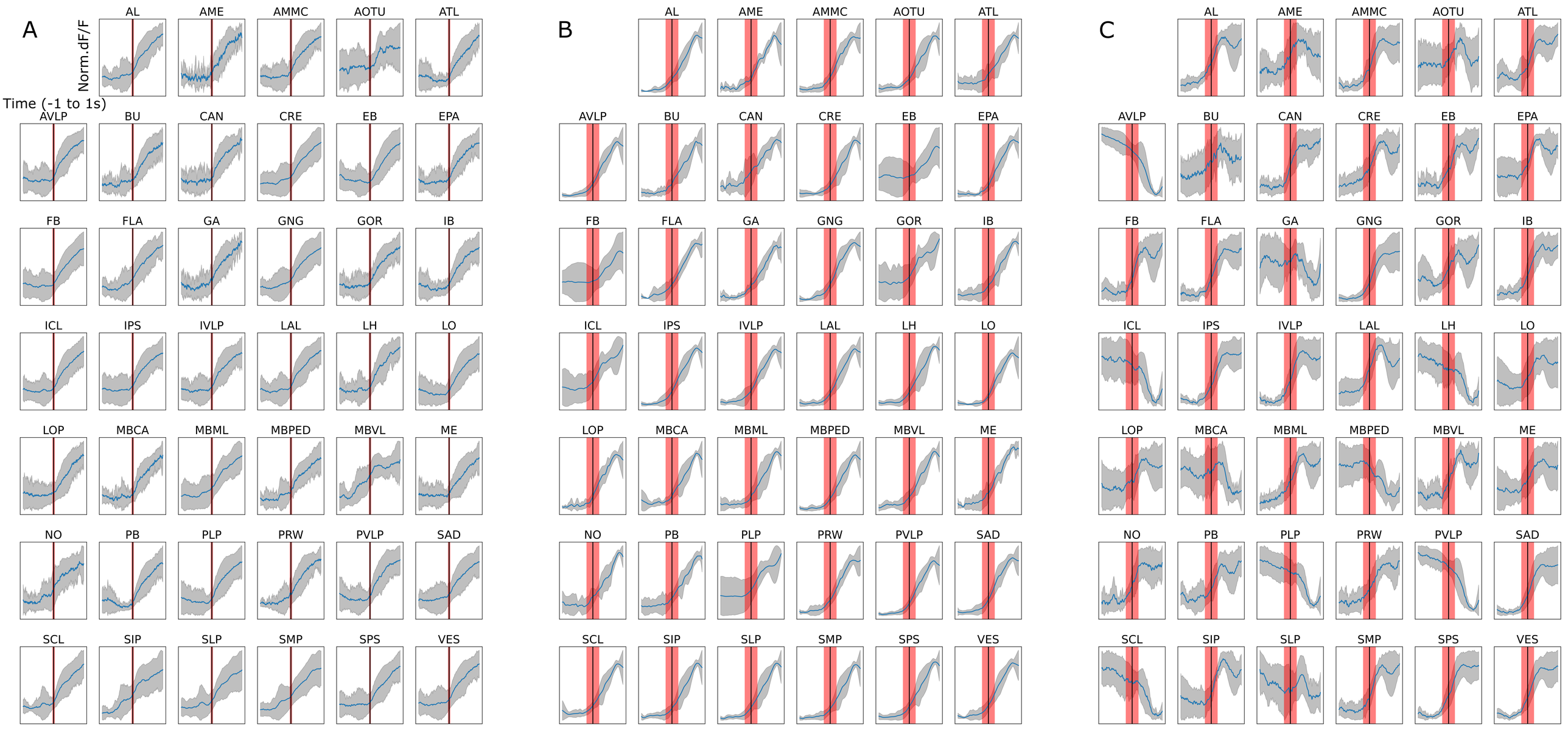
A
B
C
Norm.dF/F
Time (-1 to 1s)
AL
AME
AMMC
AOTU
ATL
AVLP
BU
CAN
CRE
EB
EPA
FB
FLA
GA
GNG
GOR
IB
ICL
IPS
IVLP
LAL
LH
LO
LOP
MBCA
MBML
MBPED
MBVL
ME
NO
PB
PLP
PRW
PVLP
SAD
SCL
SIP
SLP
SMP
SPS
VES

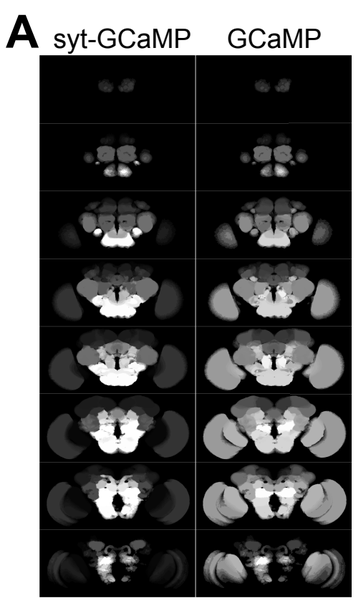
A
syt-GCaMP
GCaMP

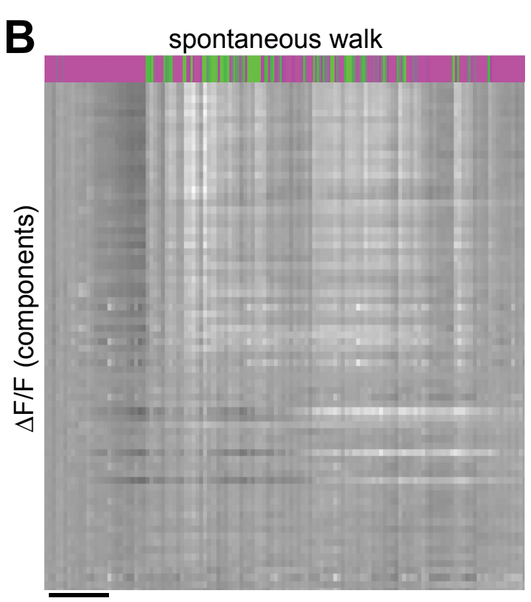
B
spontaneous walk
ΔF/F (components)

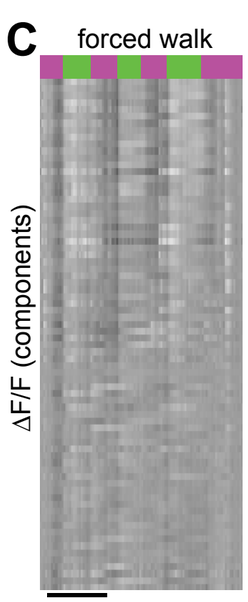
C
forced walk
ΔF/F (components)

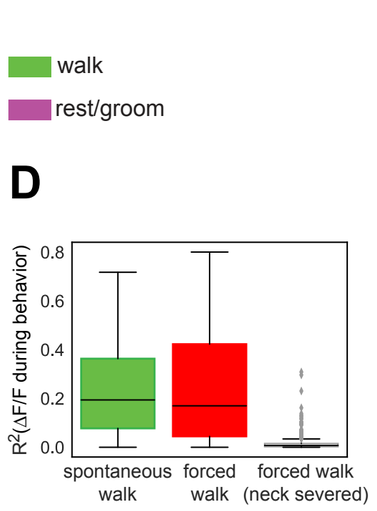
walk
rest/groom
D
R²(ΔF/F during behavior)
0.0
0.2
0.4
0.6
0.8
spontaneous walk
forced walk
forced walk (neck severed)

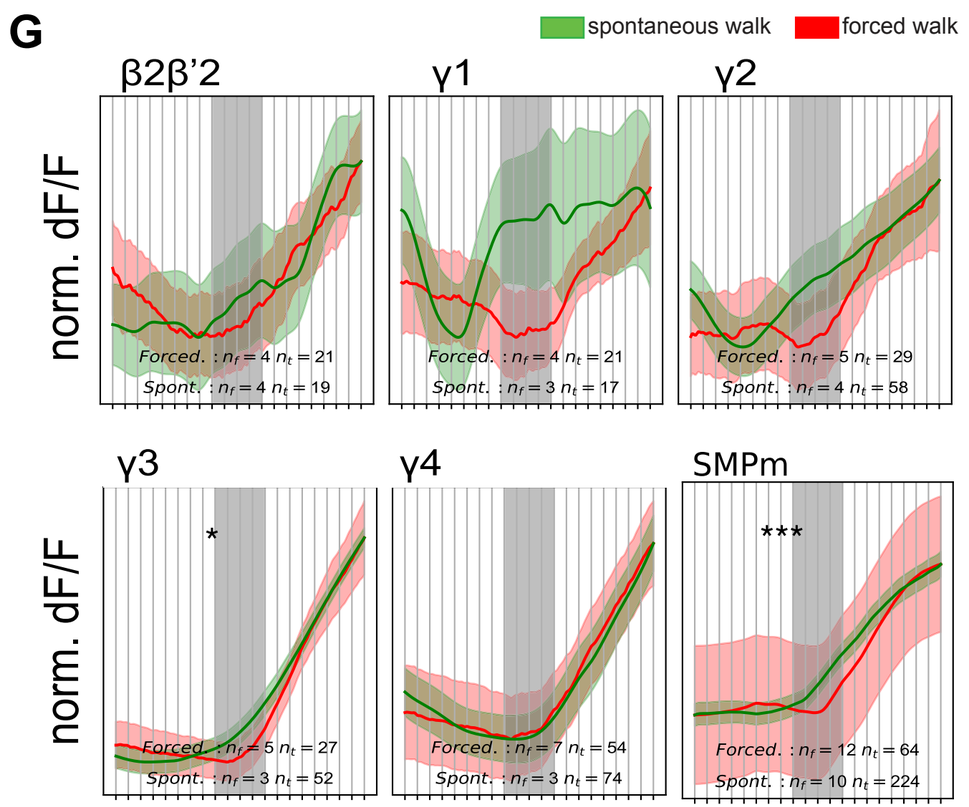
G
spontaneous walk
forced walk
β2β'2
γ1
γ2
γ3
γ4
SMPm
SPS
IPS-Y
PRW
PENP-CL
GNGva
norm. dF/F
Forced. : n_f = 4 n_t = 21
Spont. : n_f = 4 n_t = 19
Forced. : n_f = 4 n_t = 21
Spont. : n_f = 3 n_t = 17
Forced. : n_f = 5 n_t = 29
Spont. : n_f = 4 n_t = 58
Forced. : n_f = 5 n_t = 27
Spont. : n_f = 3 n_t = 52
Forced. : n_f = 7 n_t = 54
Spont. : n_f = 3 n_t = 74
Forced. : n_f = 12 n_t = 64
Spont. : n_f = 10 n_t = 224
Forced. : n_f = 9 n_t = 76
Spont. : n_f = 5 n_t = 63
Forced. : n_f = 7 n_t = 80
Spont. : n_f = 6 n_t = 68
Forced. : n_f = 10 n_t = 58
Spont. : n_f = 9 n_t = 188
Forced. : n_f = 6 n_t = 22
Spont. : n_f = 3 n_t = 60
Forced. : n_f = 4 n_t = 16
Spont. : n_f = 3 n_t = 26
t [sec]

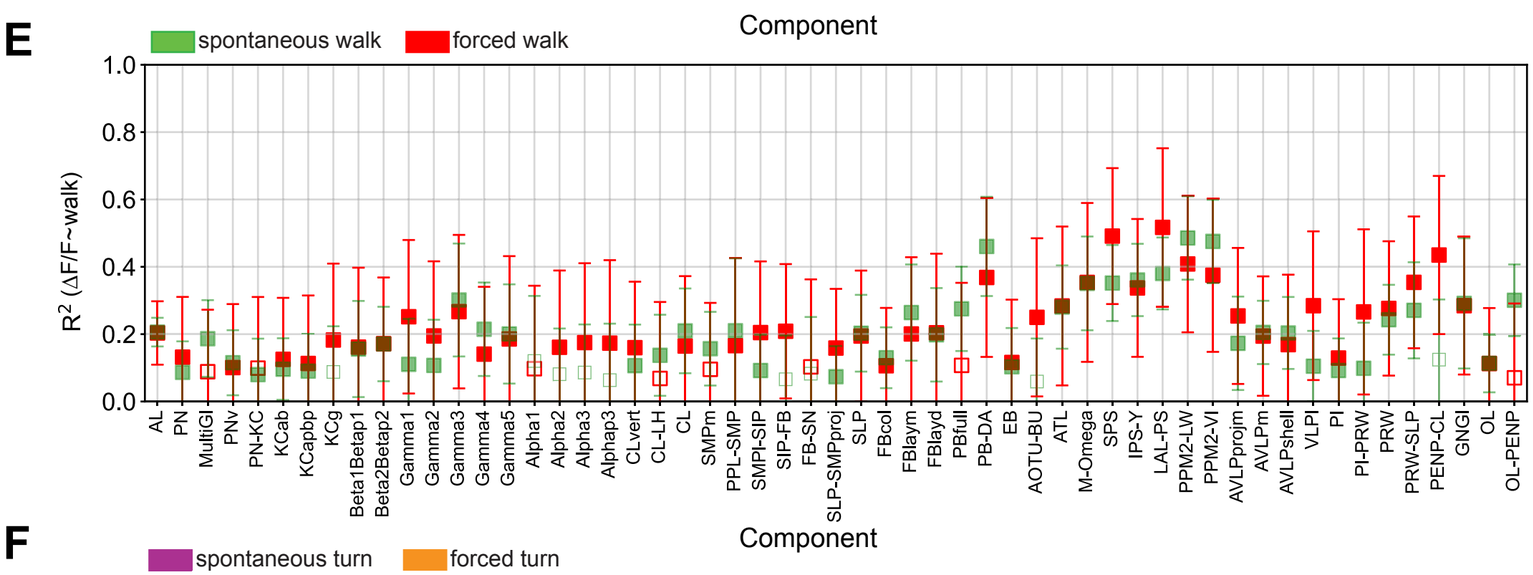
E
spontaneous walk
forced walk
Component
R² (ΔF/F~walk)
AL
PN
MultiGl
PNv
PN-KC
KCab
KCapbp
KCg
Beta1Betap1
Beta2Betap2
Gamma1
Gamma2
Gamma3
Gamma4
Gamma5
Alpha1
Alpha2
Alpha3
Alphap3
CLvert
CL-LH
CL
SMPm
PPL-SMP
SMPI-SIP
SIP-FB
FB-SN
SLP-SMPproj
SLP
FBcol
FBlaym
FBlayd
PBfull
PB-DA
EB
AOTU-BU
ATL
M-Omega
SPS
IPS-Y
LAL-PS
PPM2-LW
PPM2-VI
AVLPprojm
AVLPm
AVLPshell
VLPl
PI
PI-PRW
PRW
PRW-SLP
PENP-CL
GNGl
OL
OL-PENP

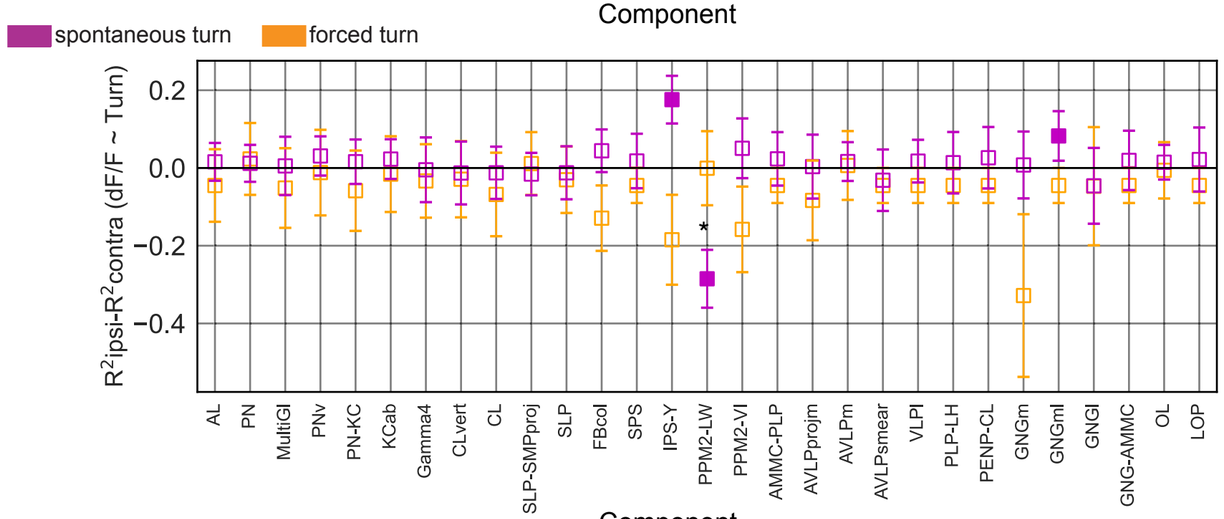
F
spontaneous turn
forced turn
R²ipsi-R²contra (dF/F ~ Turn)
Component
AL
PN
MultiGl
PNv
PN-KC
KCab
Gamma4
CLvert
CL
SLP-SMPproj
SLP
FBcol
SPS
IPS-Y
PPM2-LW
PPM2-VI
AMMC-PLP
AVLPprojm
AVLPm
AVLPsmear
VLPl
PLP-LH
PENP-CL
GNGm
GNGml
GNGl
GNG-AMMC
OL
LOP

A

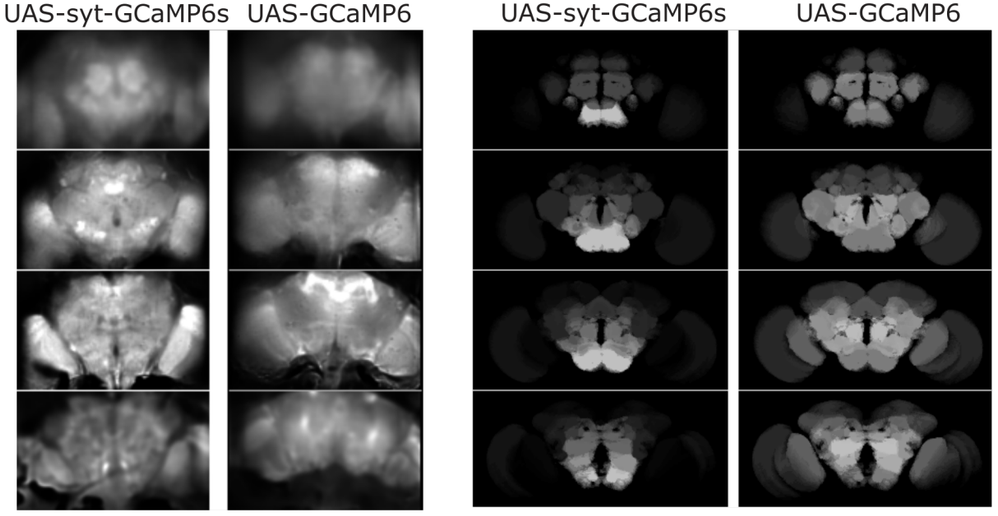
UAS-syt-GCaMP6s
UAS-GCaMP6
UAS-syt-GCaMP6s
UAS-GCaMP6

B

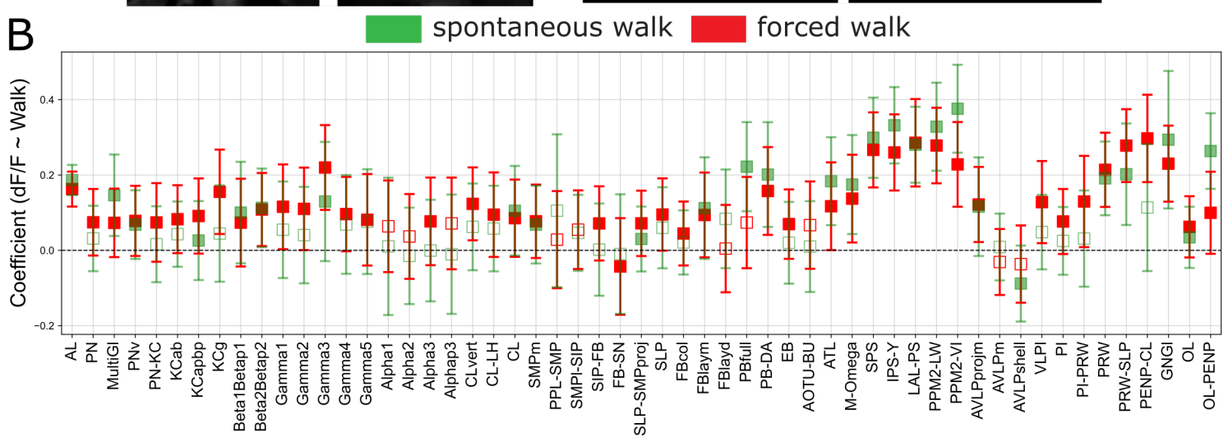
spontaneous walk
forced walk
Coefficient (dF/F ~ Walk)
AL PN MultiGl PNv PN-KC KCab KCapbp KCg Beta1Betap1 Beta2Betap2 Gamma1 Gamma2 Gamma3 Gamma4 Gamma5 Alpha1 Alpha2 Alpha3 Alphap3 CLvert CL-LH CL SMPm PPL-SMP SMPl-SIP SIP-FB FB-SN SLP-SMPproj SLP FBcol FBlaym FBlayd PBfull PB-DA EB AOTU-BU ATL M-Omega SPS IPS-Y LAL-PS PPM2-LW PPM2-VI AVLPprojm AVLPm AVLPshell VLPl PI PI-PRW PRW PRW-SLP PENP-CL GNGl OL OL-PENP

C

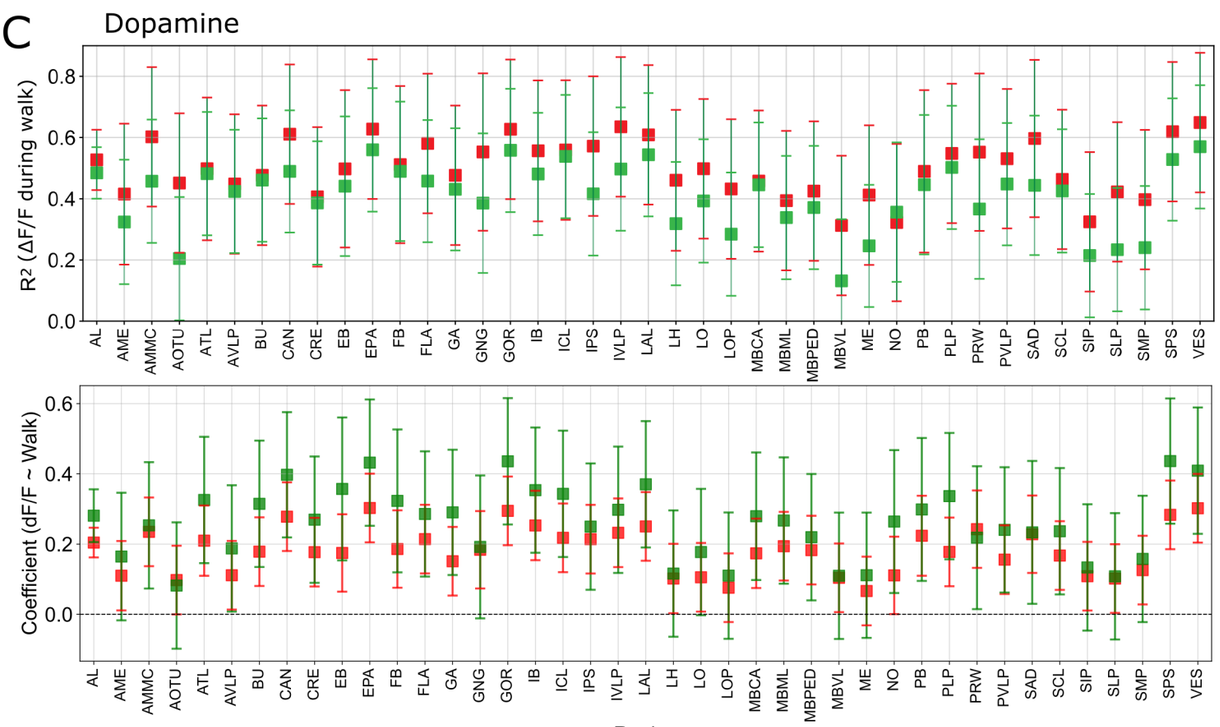
Dopamine
R² (ΔF/F during walk)
Coefficient (dF/F ~ Walk)
Region

D

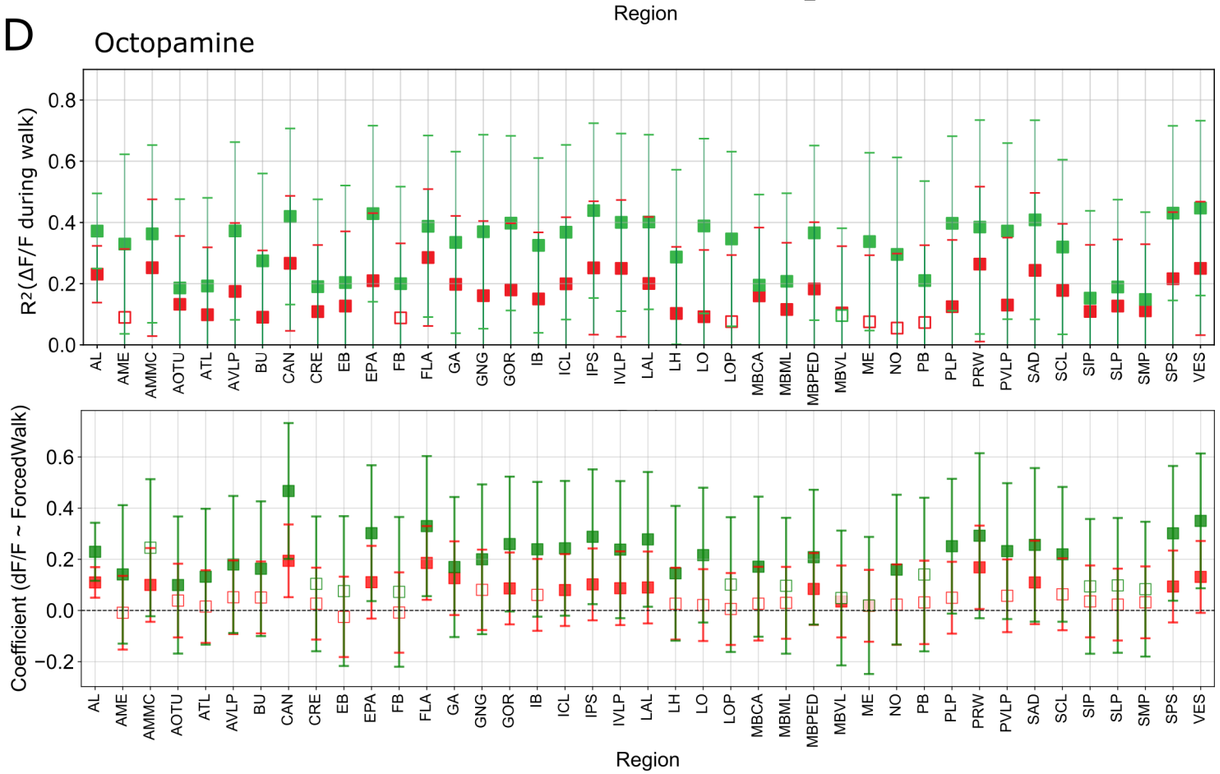
Octopamine
R2(ΔF/F during walk)
Coefficient (dF/F ~ ForcedWalk)
Region

E

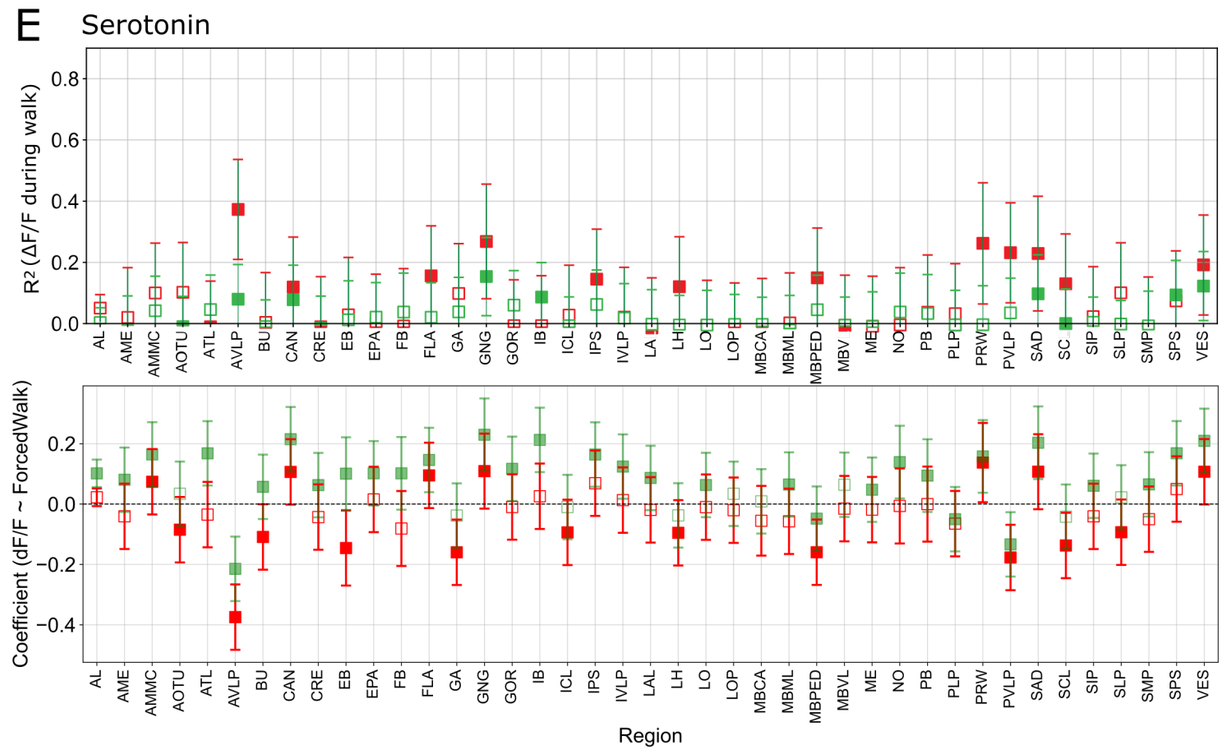
Serotonin
R² (ΔF/F during walk)
Coefficient (dF/F ~ ForcedWalk)
Region

F

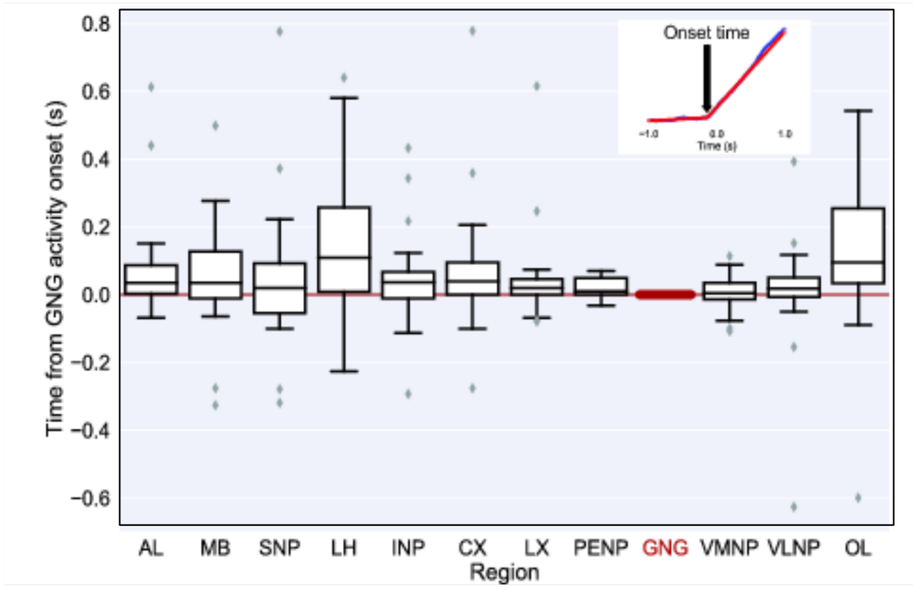
Onset time
Time from GNG activity onset (s)
AL MB SNP LH INP CX LX PENP GNG VMNP VLNP OL
Region

G

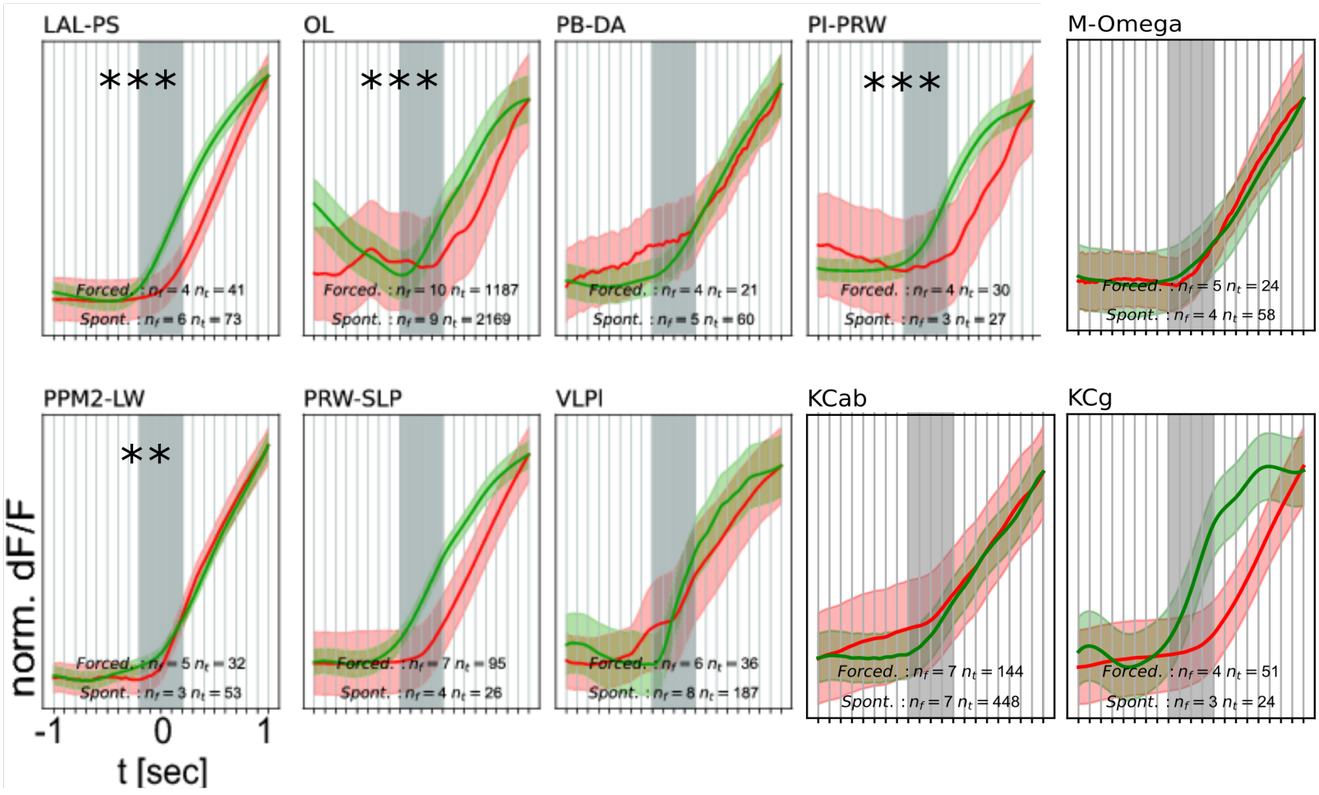
LAL-PS
OL
PB-DA
PI-PRW
M-Omega
PPM2-LW
PRW-SLP
VLPl
KCab
KCg
norm. dF/F
t [sec]